Functional Multilayer Organic Thin Films Fabricated by Layer-by-Layer Sequential Adsorption Technique

by

Dongsik Yoo

Bachelor of Science in Engineering
Seoul National University (1991)

Submitted to the Department of Materials Science and Engineering and
the Program in Polymer Science and Technology
in Partial Fulfillment of the Requirements for the Degree of

DOCTOR OF PHILOSOPHY

at the

MASSACHUSETTS INSTITUTE OF TECHNOLOGY

June 1997

Signature of Author _____
Department of Materials Science and Engineering
May 2, 1997

Certified by _____
Michael F. Rubner
TDK Professor of Polymer Science
Thesis Supervisor

Accepted by _____
Linn W. Hobbs
John F. Elliott Professor of Materials
Chair, Departmental Committee on Graduate Students

Functional Multilayer Organic Thin Films Fabricated by Layer-by-Layer Sequential Adsorption Technique

Dongsik Yoo

Submitted to the Department of Materials Science and Engineering and the Program in Polymer Science and Technology on May 2, 1997 in Partial Fulfillment of the Requirements for the Degree of Doctor of Philosophy in Polymer Science.

ABSTRACT

A novel layer-by-layer sequential adsorption technique based on electrostatic interaction is a powerful way to fabricate multilayer organic thin films. The advantages of this technique include control over the number of layers, the architecture of the multilayers, and their ease of fabrication. By controlling the conditions of the polyion dipping solutions, such as salt concentration, solution pH, and polymer concentration, the thickness of an individual layer in the multilayer can be systematically manipulated. Solution pH and salt content affect the degree of ionization and the repulsive forces between the same charged segments of the polyion, respectively. The technique has been used to modify surface properties of various substrates on a molecular level. Contact angle measurements show that the surface wettability can be manipulated in a layer-by-layer manner to produce very stable surfaces with characteristics ranging from hydrophobic to hydrophilic. The sequential adsorption of a number of different functional dye molecules has been accomplished via the alternate spontaneous adsorption of polyelectrolytes and ionic dyes from dilute solutions. Multilayer thin films containing such functional dyes as pH indicator dyes, infrared absorbing dyes, porphyrin dyes, and various fluorescent dyes have been successfully fabricated and their electrical and optical properties examined. Newly synthesized ionic ruthenium based polypyridyl dye and polymer have been utilized to fabricate light emitting devices with high brightness (ca. 100 cd/m^2) at voltages in the range of 5 - 7 volts. Multilayers containing the synthesized ruthenium based polypyridyl polymer produce highly efficient (ca. 2 % quantum efficiency) and reversible electrochemiluminescent devices. The fabrication and device evaluation of new heterostructure thin films based on this new light emitting dye and polymer are presented. The bilayer thickness and composition as well as the total thickness of the heterostructure strongly affect the functional properties of these multilayer films.

Thesis Supervisor : Michael F. Rubner
Title : TDK Professor of Polymer Science

TABLE OF CONTENTS

Page

Title Page....1

Abstract....2

Table of Contents....3

List of Figures....8

List of Tables....12

CHAPTER 1 : INTRODUCTION AND BACKGROUND

1. Introduction....13

1.1 Motivation....13

1.2 Applications of Functional Organic Thin Film....15

1.3 Sequential Layer-by-Layer Adsorption Technique....17

2. Background....21

2.1 Polyelectrolytes in Solution....21

2.2 Interaction Forces between Polyelectrolyte and Substrate....23

2.3 Structure of Adsorbed Polyelectrolyte....24

2.4 Polyelectrolyte Adsorption....25

A. Polyelectrolyte Adsorption on Surface with Opposite Charges....26

A.1 Strong Polyelectrolytes....26

A.2 Weak Polyelectrolytes....27

B. Polyelectrolyte Adsorption on Uncharged Surfaces....29

C. Neutral Polymer Adsorption on Polyelectrolyte Deposited Surface....30

2.5 Linear Growth of Sequentially Adsorbed Multilayer Film....31

2.6 Concentration of Dipping Solutions....32

2.7 Multilayer Films of Polyelectrolytes and Small Dye Molecules 32

REFERENCES 35

CHAPTER 2 : EXPERIMENTAL PROCEDURES

1. Materials 39

1.1 Polyelectrolyte Solution Preparation 39

A. Poly(aniline) Solution 39

B. Poly(thiophene-3-acetic acid) Solution 40

C. Other Polyelectrolyte Solutions 40

1.2 Dye Solution Preparation 40

1.3 Sulfonated tris(phenanthroline)ruthenium (II) dication complex, $[Ru(phen')_3]^{+2}$ Synthesis 41

1.4 Poly(tris(bipyridine)ruthenium(II)dication complex), poly($[Ru(bpy)_3]^{+2}$)ester Synthesis 42

2. Substrate Preparation 43

2.1 Hydrophilic Slide Substrate 43

2.2 Hydrophobic Slide Substrate 43

2.3 Positively Charged Slide Substrate 43

3. Layer-by-Layer Sequential Adsorption Technique 44

3.1 Hand Dipping Procedure 44

3.2 Automatic Dipping Procedure 44

4. Characterization Methods 45

4.1 Contact Angle Measurement 45

4.2 Thickness Measurement 46

A. Profilometry 47

B. Ellipsometry 47

4.3 Visible and Near ultraviolet Spectroscopy 48

4.4 Infrared Spectroscopy 49
4.5 Fluorescence and Electroluminescence Spectroscopy 50
5. Light Emitting Device Fabrication.....51
5.1 Indium tin oxide (ITO) Substrate.....51
5.2 Film Fabrication on ITO substrates.....51
5.3 Al Evaporation.....52
5.4 Current-Voltage and Light-Voltage Measurement 52
5.5 Device Lifetime Testing.....53
5.6 Efficiency of Device Performance.....53
REFERENCES.....55

CHAPTER 3 : SURFACE MODIFICATIONS AND LAYER STRUCTURES OF LAYER-BY-LAYER SEQUENTIAL ADSORBED MULTILAYERS

1. Introduction.....56
2. Contact Angle and Wettability.....58
2.1 Definitions 58
2.2 Sensitivity of Contact Angle Measurement.....63
2.3 Surface Roughness Effect on Contact Angles.....63
3. Surface Modification by Layer-by-Layer Sequential Adsorption Technique 64
3.1 Surface Properties of 1 Bilayer of Several Polyelectrolytes.....64
3.2 Surface Properties of PAH/PAA and PAH/PTAA Multilayer Films.....68
3.3 Acid-Base Interaction in Wetting.....71
3.4 Fabrication of Completely Wettable Surface.....73
4. PAH/PAA Multilayer Film Fabrication 75
5. Contact Angles of PAH/PAA multilayer films.....80
5.1 Salt Effect.....80
5.2 Solution pH Effect.....82

5.3 Concentration Effect 85
5.4 Infrared Spectra of PAH/PAA Films 86
5.5 Aging Behavior of PAH/PAA Multilayer Films 88
6. Discussion 90
7. Conclusion 96
REFERENCES 97

CHAPTER 4 : MULTILAYERS OF FUNCTIONAL DYE MOLECULES AND POLYELECTROLYTES

1. Introduction 100
2. Structural Aspects of Dye Multilayer Film 101
2.1 Fluorescein Complexion Multilayer Film 102
2.2 Bordeaux R and Crystal Violet Dyes 104
3. Functionalized Multilayer Films 105
3.1 pH indicating Azo dye Films 105
3.2 Porphyrin dye Multilayer Films 108
3.3 Infrared Absorbing Dye Multilayer Films 112
4. Ru complex Multilayer Films 114
4.1 Sulfonated $[Ru(phen')_3]^{+2}$ / Polyelectrolyte Multilayer Film 116
4.2 poly($[Ru(bpy)_3]^{+2}$) ester / Polyelectrolyte Multilayer Film 117
4.3 Sulfonated $[Ru(phen')_3]^{+2}$ / Poly($[Ru(bpy)_3]^{+2}$)ester Film 118
5. Conclusion 120
REFERENCES 121

CHAPTER 5 : NOVEL RUTHENIUM POLYPYRIDYL COMPLEXES FOR LIGHT EMITTING DEVICES

1. Introduction 123

1.1 Organic Light Emitting Devices 123
1.2 Structure of Organic LEDs 125
1.3 Fabrication Methods for Organic LEDs 127
2. Ru Polypyridyl Complexes as Light-Emitting Materials 129
2.1 Characteristics of Ruthenium Polypyridyl Complexes 129
2.2 Single Layer Devices of Sulfonated $[Ru(phen')_3]^{+2}$ and
Poly($[Ru(bpy)_3]^{+2}$)ester 132
3. Sulfonated $[Ru(phen')_3]^{+2}$ and Polyelectrolyte Multilayer Films 137
4. Poly($[Ru(bpy)_3]^{+2}$)ester and Polyelectrolyte Multilayer Films 140
4.1 Poly($[Ru(bpy)_3]^{+2}$)ester and Poly(acrylic acid) Devices 140
A. Charging Effect 143
B. Thickness-Dependence Behavior 145
4.2 Poly($[Ru(bpy)_3]^{+2}$)ester and Sulfonated poly(styrene) Devices 147
5. Poly($[Ru(bpy)_3]^{+2}$)ester and Sulfonated $[Ru(phen')_3]^{+2}$ Multilayer Films 148
6. Disscussion of Ru complexes Based LEDs 149
7. Conclusion 151
REFERENCES 153

CHAPTER 6 : CONCLUSION, SUMMARY, AND FUTURE WORK 157

Acknowledgments 163

LISTS OF FIGURES

Chapter 1

Figure 1.1. A simple model of the layer-by-layer sequential adsorption technique. 18

Figure 1.2. Examples of several materials for the layer-by-layer deposition technique. 20

Figure 1.3. Structure of an adsorbed polymer. 25

Chapter 2

Figure 2.1. Sulfonated $Ru(phen')_3^{+2}Cl_2$ (I) synthesis scheme. 41

Figure 2.2. Poly($[Ru(bpy)_3]^{+2}$)ester (II) synthesis scheme. 42

Figure 2.3. Chemical structures of (a) hexamethyl disilazane (HMDS) and (b) N-(2-aminoethyl-3-aminopropyl) trimethoxysilane (TMS) 44

Chapter 3

Figure 3.1. A sessile liquid drop on a flat surface indicating contact angle. 59

Figure 3.2. Chemical structures of polyelectrolytes used to construct multilayer thin films. 65

Figure 3.3. Contact angles of PAH/PTAA layers on hydrophilic slide glasses and PAH/PAA layers on hydrophobic slide glasses 69

Figure 3.4. Contact angles of (a) hydrophobic slide glass and (b) 1 bilayer of PAH/PAA on hydrophobic slide glass. 70

Figure 3.5. Contact angle titrations of 3 bilayers of PAH/PAA with PAA as outermost layers 72

Figure 3.6. Aging effect on contact angles of PAH/PAA layers in the air. 74

Figure 3.7. Aging effect on contact angles of PAH/PAA layers at 90 °C. 74

Figure 3.8. Linear growth of several sequentially adsorbed PAH/PAA films. 76

Figure 3.9. The amount of methylene blue dye adsorption onto PAH/PAA layers fabricated by pH 2.5, 10^{-2} M of PAH with $MgCl_2$ 0.4 M and pH 2.5, 10^{-2} M of PAA solutions....78

Figure 3.10. Salt in PAH solution effect on contact angles of PAH/PAA layers fabricated by pH 2.5, 10^{-2} M of solutions....81

Figure 3.11. Contact angles of PAH/PAA layers fabricated by pH 4.5 of 10^{-2} M solutions....82

Figure 3.12. Contact angles of PAH/PAA layers fabricated by pH 2.5, 10^{-2} M of PAH and pH 4.5, 10^{-2} M of PAA solutions....83

Figure 3.13. Contact angles of PAH/PAA fabricated by pH 4.5, 10^{-2} M of PAH and pH 2.5, 10^{-2} M of PAA solutions....84

Figure 3.14. Contact angles of PAH/PAA fabricated by pH 2.5 of 10^{-3} M PAH and PAA solutions....86

Figure 3.15. Infrared spectra of PAH/PAA films on Znse....87

Figure 3.16. Aging effects on contact angles of PAH/PAA multilayer films fabricated by pH 2.5 of 10^{-2} M PAH and PAA solutions....89

Figure 3.17. Aging effects on contact angles of PAH/PAA multilayer films fabricated by pH 2.5, 10^{-2} M of PAH with $MgCl_2$ 0.4 M and pH 2.5, 10^{-2} M of PAA.solutions....89

Figure 3.18. A proposed model of the layer-by-layer deposition....91

Figure 3.19. Mechanism of PAH/PAA layer adsorption....93

Chapter 4

Figure 4.1. Chemical structures of used polyelectrolytes....102

Figure 4.2. Chemical structure of fluorescent complexion dye....102

Figure 4.3. Linear deposition of fluorescein complexion/PAH film....103

Figure 4.4. Chemical structures of (a) Crystal Violet and (b) Bordeaux R....104

Figure 4.5. Linear deposition of Bordeaux R and PAH film....105

Figure 4.6. Chemical structure of Congo red dye....105

Figure 4.7. Amounts of UV/Vis absorption of Congo red dye/polyelectrolyte films....106

Figure 4.8. pH color change of a PAH/Congo red dye multilayer film. 107

Figure 4.9. Chemical structures of porphyrin dyes 108

Figure 4.10. Layer-by-layer growth of a) a cationic porphyrin dye/PMA multilayer and b) an anionic porphyrin dye/PEI multilayer 109

Figure 4.11. Chemical structure of tetraphenyl porphine tetrasulfonic acid, tetrasodium salt....110

Figure 4.12. UV/Vis spectra of anionic porphyrin/PAH multilayer film (420 nm peak) and with Iron in the ring (370 nm peak)....111

Figure 4.13. Chemical structure of infrared absorbing dye....112

Figure 4.14. Linear growth of infrared absorbing dye/PAH multilayer....113

Figure 4.15. UV/Vis spectra of a multilayer film containing 5 layers of Ponceau S (510 nm) and Infrared dye 125 (810 nm)....114

Figure 4.16. The chemical structures of (a) $[Ru(bpy)_3]^{+2}$ and (b) sulfonated $[Ru(phen')_3]^{+2}$....115

Figure 4.17. UV/Vis absorption of the poly($[Ru(bpy)_3]^{+2}$)ester/PAA and the poly($[Ru(bpy)_3]^{+2}$)ester/SPS films (20 bilayers)....118

Figure 4.18. The amount of Ru complex adsorption at pH 2.5 and pH 4.5 of $[Ru(phen')_3]^{+2}$ and poly($[Ru(bpy)_3]^{+2}$)ester solutions 119

Figure 4.19. UV/Vis absorbance of sulfonated $[Ru(phen')_3]^{+2}$ and poly($[Ru(bpy)_3]^{+2}$)ester films....120

Chapter 5

Figure 5.1. Absorbance and photoluminescence (PL) spectra of sulfonated $[Ru(phen')_3]^{+2}$....130

Figure 5.2. Absorbance and photoluminescence (PL) spectra of poly($[Ru(bpy)_3]^{+2}$)ester....131

Figure 5.3. Current-voltage and light-voltage behavior of spin-cast sulfonated $[Ru(phen')_3]^{+2}$ device 133

Figure 5.4. Current-voltage and light-voltage behavior of spin-cast poly($[Ru(bpy)_3]^{+2}$)ester device 133

Figure 5.5. EL spectra of sulfonated $[Ru(phen')_3]^{+2}$ and poly($[Ru(bpy)_3]^{+2}$)ester 134

Figure 5.6. Stability data of (a) $[Ru(phen')_3]^{+2}$ single-layer device and (b) poly($[Ru(bpy)_3]^{+2}$)ester single-layer device at 6 V 136

Figure 5.7. Current-voltage and light-voltage curves of PEI/$[Ru(phen')_3]^{+2}$ multilayer film. 137

Figure 5.8. Stability of 30 bilayer PEI/$[Ru(phen')_3]^{+2}$ LEDs 138

Figure 5.9. Current-voltage and light-voltage curves of PAH/$[Ru(phen')_3]^{+2}$ multilayer film. 139

Figure 5.10. Current-voltage and light-voltage curves of poly($[Ru(bpy)_3]^{+2}$) ester/PAA multilayer film. 141

Figure 5.11. Current-voltage and light-voltage curves of PAA/ poly($[Ru(bpy)_3]^{+2}$)ester generated by applying forward bias first. 144

Figure 5.12. Current-voltage and light-voltage curves of PAA/ poly($[Ru(bpy)_3]^{+2}$)ester generated by applying reverse bias first 144

Figure 5.13. Thickness dependence on Light-voltage curves of PAA/poly($[Ru(bpy)_3]^{+2}$)ester. 145

Figure 5.14. Efficiency and maximum light output of 15, 25, 30, 35 bilayers of PAA/poly($[Ru(bpy)_3]^{+2}$)ester devices 146

Figure 5.15. Thickness dependence of poly($[Ru(bpy)_3]^{+2}$)ester/SPS multilayer devices. 148

Figure 5.16. Current-voltage and light-voltage curves of poly($[Ru(bpy)_3]^{+2}$) ester/$[Ru(phen')_3]^{+2}$ LED 149

LIST OF TABLES

Chapter 3

Table 3.1. Different surface properties by changing polyanionic layers 67

Table 3.2. Layer thickness of PAH/PAA with different solution conditions.....77

Table 3.3. UV/Vis intensity of methylene blue absorbance peaks (at 600 nm).....79

Table 3.4. Relative amount of Infrared peaks at 1560 and 1700 cm^{-1} 88

Chapter 4

Table 4.1. Intensity of UV/Vis absorbance peaks of PAH/$[Ru(phen')_3]^{+2}$ films 116

Functional Multilayer Organic Thin Films Fabricated by Layer-by-Layer Sequential Adsorption Technique

CHAPTER 1

INTRODUCTION AND BACKGROUND

1. Introduction

1.1 Motivation

Organic materials show considerable promise for such applications as optoelectronics, molecular electronics, and bioengineering. Through relatively simple chemistry, organic materials can be synthesized and then functionalized to give the system its novel properties. Thin films containing the organic materials typically have a thickness ranging from a few nanometers (i.e. a monolayer) to several thousand. Such organic thin films are known to have great potential for integrated optics, sensors, friction-reducing coatings, surface modification, biological substrates, and patternable materials [1.1 - 1.2].

One of the primary barriers to wide-spread use of organic thin films is a fabrication method to build up individual organic molecules into uniform and heterostructure architectures. The use of organic thin films has also been hindered by the presence of chemical impurities and defects in the uniform film that adversely affect mechanical and thermal properties as well as chemical stability. The investigation of a technique for producing ordered heterostructures and limiting the impurities and the defects is very important to the utilization of the organic materials.

Various attempts to make uniform multilayer organic thin films have been investigated for several decades [1.3]. These include Langmuir-Blodgett deposition, spin-casting, and chemisorption. The Langmuir-Blodgett method [1.3 - 1.6] is based on the use of surface-active molecules called amphiphiles which do not dissolve in water but have hydrophilic groups at the end. A well-organized monolayer film forms at the water interface as the amphiphilic molecules attempt to minimize the repulsive forces between water and the non-polar hydrophobic groups. Monolayers can be transferred onto a substrate by dipping it into a Langmuir-Blodgett trough that contains the amphiphiles floating on water. This technique has been used to form ordered multilayered films [1.7]. However, one problem associated with this technique is their weak adhesion and interactive forces between layers. These weak interactions easily lead to misalignment of the layers and unstable structures after long periods of time. Several other problems exist, including limitations on functional groups that can be used and restrictions on substrate shape.

In comparison, spin-casting methods [1.8] are simple and widely applied techniques for producing a single layer. With spin-casting, organic materials with a wide variety of functional groups can be rapidly made. In general, small dye molecules are mixed in a binding polymer solution to prohibit the crystallization of the small molecules in the solid state. Unfortunately, this technique has not been used to fabricate ordered multilayered structures.

Chemisorption methods [1.9 - 1.11] have been investigated as a way of building multilayer films on various substrates. Successive chemical reactions graft each layer to form multilayer films. Various functional materials are often incorporated into a multilayer film with chemical reactions between layers. The problems in chemisorption methods lie in that only specialized functional reactions are possible for the application and that some difficulties occur in limiting the reaction only to the surface. It requires a reaction yield of about 100 % in order to keep the same amount of material on the surface from layer to layer.

These methods either have limitations in fabricating multilayer films or in building up organized thin multilayer films. Our group and others recently developed a novel "layer-by-layer sequential adsorption" technique, that overcomes many of the problems associated with the aforementioned techniques. It uses ionic interactions to make multilayer films [1.12 - 1.21]. In contrast to other organic thin film fabrication methods, the sequential adsorption technique is a very versatile means of fabricating multilayer thin films. There are several advantages that the sequential adsorption method offers. First, a wide array of functional materials can be used. The only requirement is that the functional polymers or dye molecules have at least two ionic charge groups. A second and very important advantage is that the method has no substrate shape, size, or treatment requirements. Therefore, this will make it possible to use multilayer organic thin films for a much wider variety of applications than ever before.

This work has focused on several fundamental issues associated with this new technique. The first part of this thesis examines the mechanism by which the adsorbed multilayers modify the surface properties of various substrates. The second part of the thesis shows the feasibility of using small functional dye molecules in the adsorbed film. Finally, the third section describes the fabrication of electrical and optical devices containing a ruthenium polypyridyl complex based dye and polymer molecules.

1.2 Applications of Functional Organic Thin Film

As mentioned earlier, organic materials have been developed for electrical, biological, and optoelectrical applications. In the future, successful application of these materials in electrical and optical devices and replacements of sensor components will require uniform and ordered films. Precise designs and arrays of organic layers will be necessary for producing reliable high-quality devices. Some of the most promising applications [1.1 - 1.3, 1.22] can be summarized as follows:

1) Organic based displays: Organic based light-emitting devices have been of considerable interest for use in large area displays. These devices have a wide color range from red to blue. Processing methods are extremely important in order to produce uniform devices. At this point, liquid crystal displays using organic materials as passive polarizers are the type of material used for this particular application.

2) Patternability of thin films: Organic thin films have also been used extensively for development of photoresist patterns. As an easier way is developed to produce thinner and more uniform patterns, we could fabricate dense and more complicated circuits. The use of organic films in recording media is also an attractive project. Several different light responsive organic materials are being considered for this application because of their higher storage density compared with magnetic recording devices.

3) Packaging and insulating layers for integrated circuits: Insulating layers (i.e., epoxy resin, polyimide resin) are sealed on top of a silicon crystal surface and packaged with a semiconductor chip with attached electrical connections. As chip designs become smaller and more complicated, organic thin films for faster dissipation of heat and lower thermal expansion are required.

4) Surface Functionalization: Adhesion, wetting, friction, biocompatibility, and chemical reactivity are dramatically altered by the attachment of one or more layers of organic functional groups at the material surface. Vastly different functional groups such as $-SO_3^-$, $-NO_2$, $-CF_3$, $-CO_2H$, and -OH, can be grafted and adsorbed onto various substrates for a wide variety of applications. Since organic polymers generally have low surface energies and are rather stable in air, they are often used for protective coatings. The highly tailorable functionality that polymers can have then makes it possible to develop coatings for different applications.

5) Sensor and optic application: Chemical response, photoelectronic, piezoelectrolic, and electrochemical materials have been investigated for sensor applications. Uniform multilayer film is important for their functional behavior. Impurities and defects in the uniform films are detrimental for these applications. In thin-film optics, nonlinear optical effects (second and third harmonic generation) are of particular interest. In organic materials, the nonlinear effects depend on the intrinsic polarizability of the molecules as well as the ordering of the organic materials.

The next section will briefly describe the unique features of the sequential layer-by-layer adsorption technique.

1.3 Sequential Layer-by-Layer Adsorption Technique

Recently, Decher and co-workers introduced a novel technique known as "layer-by-layer sequential adsorption" [For review papers on the technique, see 1.23 - 1.24]. This technique is based on the spontaneous adsorption of polyelectrolytes onto an oppositely charged surface. A simplified model of the technique is depicted in Figure 1.1. The electrostatic interactions are what hold the layers together and provide stable strong interaction. To build a multilayer structure, sequential dippings are performed using positively and negatively charged chemical species in alternating layers. The substrate is generally charged with either silane species or cationic polyelectrolytes. This makes it possible to adsorb polyions from a solution of oppositely charged (i.e., anionic) molecules.

Since the process is done by dipping a substrate in solutions, there are no size or shape limitations. After the first layer is adsorbed, the sample is rinsed several times and then immersed in the oppositely charged solution. This procedure is then repeated until the required number of layers have been deposited. One of the remarkable properties of this technique is the feasibility of controlling the thickness and the structure of a layer through changes in pH, salt quantity, and polyelectrolyte concentration. The thickness of a

deposited layer can be controlled from a few Å to several 10-Å units by changing the conditions of the solution. These effects will be discussed in the section 2.

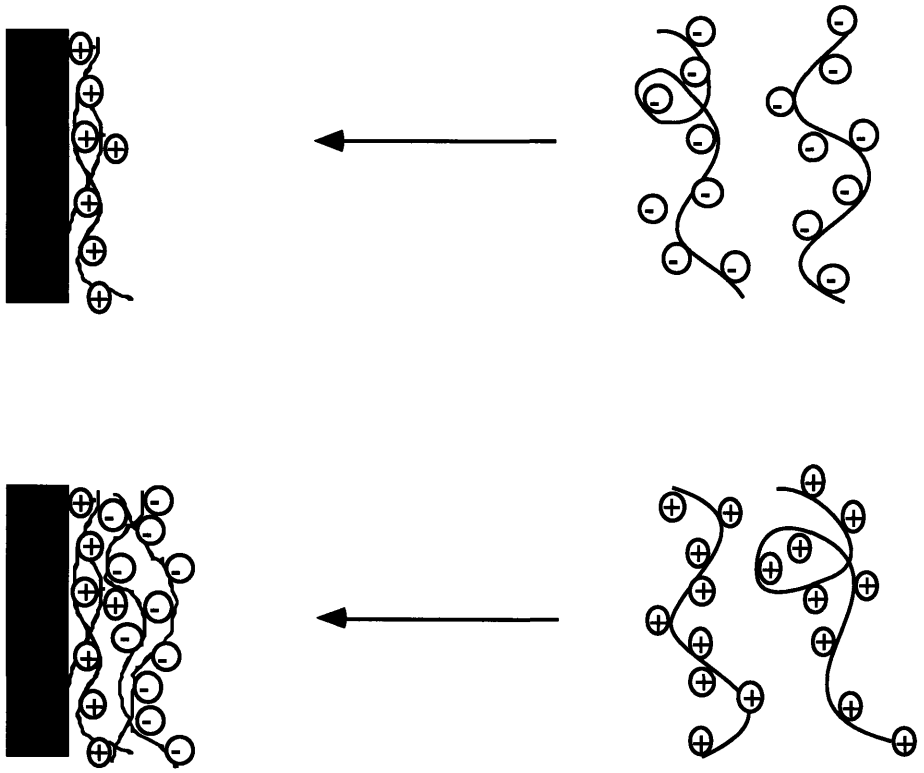

Figure 1.1. A simple model of the layer-by-layer sequential adsorption technique.

Another advantage of this technique is the precise control that it offers. By simply changing the order in which the layers are applied, the multilayered structures can be controlled in a precise way. This technique provides a way to create new thin film heterostructures with novel optical, electrical, and biological properties. For example, our group have recently demonstrated that such layer-by-layer deposited multilayers can be used to create semi-transparent and electrically conducting coatings as well as thin film light emitting diodes [1.17 - 20, 1.25 - 1.27]. The heterostructures of poly(*p* - phenylene vinylene) (PPV) light emitting devices [1.25] are an interesting case because their

properties are affected by the surrounding layers. By changing the polyelectrolyte layers and the order of the layers, the device showed the different performances.

One important aspect of this method is the deposition speed, which is relatively fast. Polyelectrolytes have very steep isotherms and reach the plateau region within a few minutes. This is a result of a high affinity type adsorption of polyelectrolytes. The adsorption process that occurs at the interface between the deposited polyelectrolyte and the counter charged polyelectrolytes in solutions may be producing kinetically determined structures [1.28, 1.29].

The sequential adsorption process can be used with many different materials. Decher et al [1.12 - 1.13] first used this technique with a combination of a polyelectrolyte and a bolaform material (Figure 1.2). The latter is a rigid rod molecule with two cationic or anionic functional end groups. Several researchers expanded upon this technique by incorporating various polyelectrolytes such as poly(allylamine), poly(acrylic acid), sulfonated poly(styrene), poly(methacrylic acid) in the multilayers [1.30]. Recently, our group succeeded in forming multilayered structures based on conducting polymers such as poly(aniline), and poly(thiophene-3-acetic acid) [1.17 - 1.19]. The conductivity of these films can be as high as 40 S cm^{-1}. Multilayered structures based on in-situ polymerization of poly(pyrrole) were also developed by our group [1.32]. Another important achievement in our group has been the incorporation of various precursor types of polymers [1.25, 1.33]. The precursor form of polymers, such as PPV and poly(imide) were multilayered with oppositely charged polyelectrolytes. After the multilayer film was fabricated, the precursor layers were converted to PPV or poly(imide) layer. Fullerenes ("Bucky Ball") fitted with ionizable surface groups were formed to multilayer films with the help of several polyelectrolytes. Other groups introduced the technique for the biological application. Proteins or polypeptides were ionically layer-by-layer deposited to form multiprotein

systems [1.34,1.35]. The multilayer film of polyelectrolytes and DNA were reported for possible applications in ecological system. Simple charged metal particles were also recently reported to be incorporated into a multilayer film [1.36, 1.37]. Figure 1.2

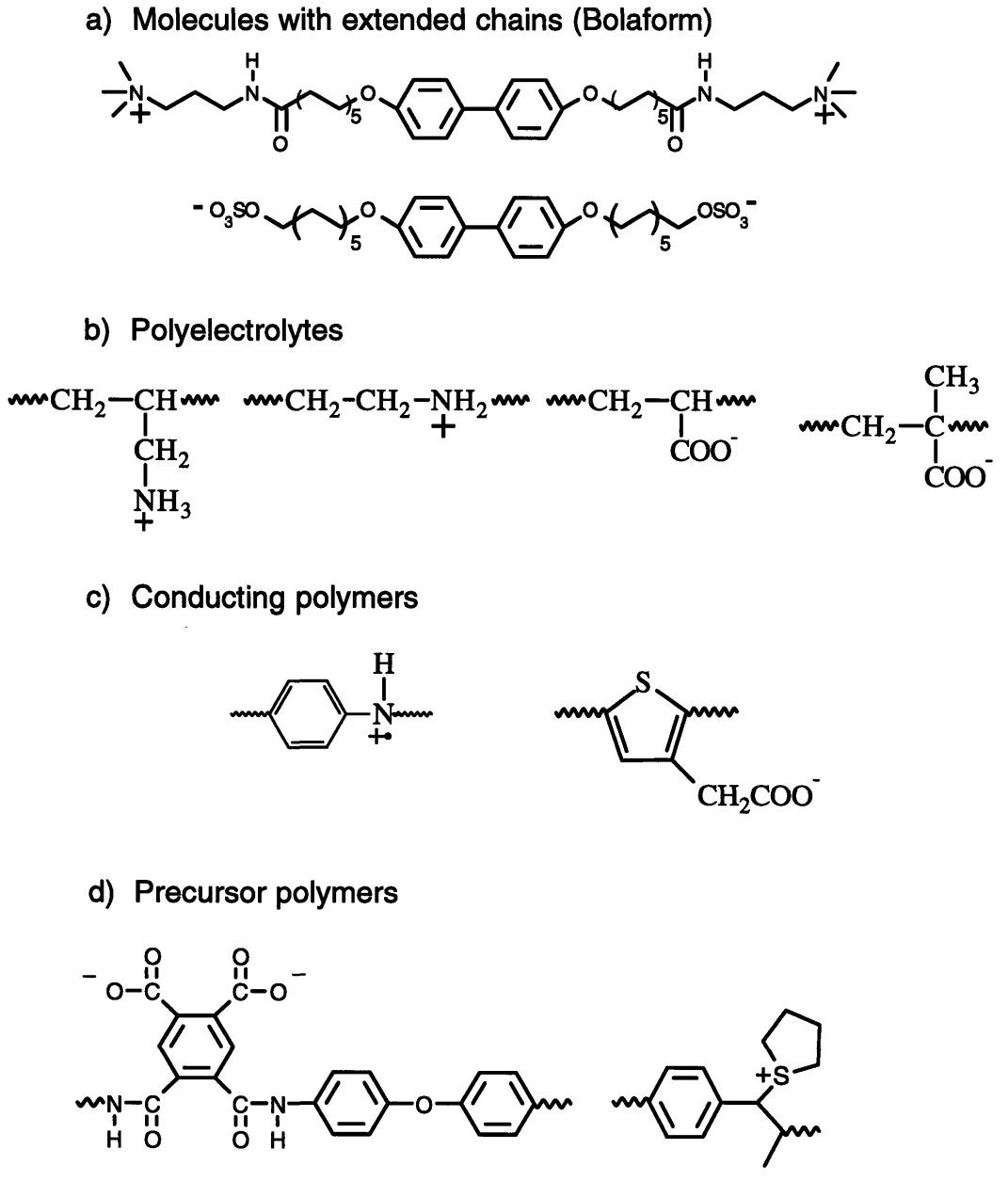

Figure 1.2. Examples of several materials for the layer-by-layer deposition technique.

summarizes several different materials applied for the layer-by-layer deposition technique.

I expanded this technique to form layer-by-layer deposited multilayer films using small dye molecules, which have only a few charges in the chemical structure. Several different examples of the multilayer films of functional dye molecules and polyelectrolytes will be discussed in chapter 4.

2. Background

Understanding polyelectrolyte behavior in solution and adsorption phenomena at interfaces is important for obtaining precise control of multilayer structures. Several aspects of this new technique will be described in the following sections.

2.1 Polyelectrolytes in Solution

When a polymer dissolves in a solvent, the conformation of the polymer chain and the associated energy states are determined by the nature of the polymer and the quality of the solvent. The end-to-end distance, or the radius of gyration, is generally used to characterize the chain conformation in solution. For 'good' solvents, the radius of gyration would be larger than for 'poor' solvents. Solvent quality can also be expressed as the size of the excluded volume of the polymer chain. This quantity refers to the effective size of a monomer or unit size of a polymer chain in solution [1.38].

In a good solvent, the polymer chains expand to increase contacts with the solvent and adopt a self-avoiding random walk. As the solvent becomes poor, we reach the theta state, where the excluded volume decreases to zero. In this case, the statistical behavior of the polymer becomes a random walk as opposed to a self-avoiding one. As the quality of the solvent decreases below the theta state, the chains attempt to exclude the solvent in order to increase polymer-polymer interactions. In concentrated solutions where the solvent is a poor one, the polymer will eventually precipitate. A polymer in poor solvent

has more tendency to adsorb onto a surface. This indicates that polymer adsorption would be much more favorable in poor solvents due to the instability of the polymer in the solution.

A polyelectrolyte is defined as a polymer that has many ionizable groups either on the main chain or in pendant groups. The strength of the ionic charge groups determines the strength of the polyelectrolyte. If the polyelectrolyte is a strong one, then pH of the solution will not change the nature of the charged species. On the other hand, if the polyelectrolyte is a weak one, then a change of pH can affect the charge density of the polyelectrolyte. This is an important issue because the interaction of a polyvalent macroion and counter ion is the source of repulsive forces that give polyelectrolytes some of their unique characteristics.

The number of dissociated groups or repulsive forces between charge groups will depend on the amount of salt in the solution as well as pH of the solution. In weak polyelectrolytes, such as poly(acrylic acid) (PAA) and poly(methacrylic acid) (PMA), the degree of dissociation is highly dependent on the pH of the solution. The dissociation constant (pK_a) of the electrolyte groups represents the equilibrium between an acid and a conjugated base. At pH below pK_a, the low degree of dissociation of charge groups in PAA and PMA makes the chain take on a coiled conformation. At pH above pK_a, the system may take on an extended chain conformation as a result of the repulsive forces between charges. When this happens, the polyelectrolyte solubility in water is also increased due to a result of the ionization of charge groups on the polymer. According to Oosawa [1.39], poly(acrylic acid) with a degree of polymerization=1000 forms a spherical random coil with a radius of gyration of 200 Å at a low pH. However, at a high pH, the radius of gyration increases up to 2500 Å. The free acid form (-COOH) decreases the solubility of PAA and makes it less soluble in water. The carboxylate group ($-COO^-$) on the other hand increases the solubility in water and makes the system behave like a polymer

in good solvent. The following equation shows the relationship between pH, pK_a and degree of dissociation, α [1.40].

$$pH = pK_a + \log(\alpha / (1-\alpha)) + f(I) \qquad (1.1)$$

where f(I) is small correction factor depending on the ionic strength (I). α is the ratio of the base forms (dissociated forms) to number of electrolyte groups. If pH is low, α will decrease which means that most of the electrolyte groups will remain in a neutral state. If pH is higher than pK_a, α would increase with this high charge group population, the repulsion forces make polyelectrolytes take on extended chain conformations. Addition of salt will also change the behavior of the polyelectrolyte, even at high pH values. The bound counterions of the salt will shield the charge of the polyelectrolyte and make it take on a coiled conformation due to the apparent reduction in repulsive forces. It is in this way that chain conformations of polyelectrolytes are strongly affected by the conditions of the solutions.

2.2 Interaction Forces between Polyelectrolyte and Substrate

After a polymer adsorbs onto a substrate, there are fewer possible conformational states. As a result, the entropy decreases when the molecules are adsorbed onto a substrate. The overall entropy change at the adsorption is the negative value of ΔS.

$$\Delta G = \Delta H - T\Delta S \qquad (1.2)$$

Through the fundamental equation of thermodynamics, a spontaneous reaction occurs when ΔG is negative. Only in cases when the strength of the enthalpic term of the free energy expression has a larger value to overcome the positive value of the entropy term, then adsorption will be the spontaneous reaction. During adsorption, if the polymer decreases the value of the entropy term, or increases enthalpy term of the interaction strength, then deposition of the chain onto the surface is favored. [1.41 - 1.42].

The interaction between substrates and polyelectrolytes is the major factor to consider because the entropic term is generally always negative and does not change appreciably as the chemistry of the system is changed. In the sequential adsorption technique, the ionic interaction forces between a substrate and the polyelectrolytes are strong enough to cause adsorption to occur. The strength of these binding forces are enhanced by the multiple sites of charges along the polyelectrolyte. Even if the segmental binding energy is very small, the large number of segments along a polymer chain lead to a strong overall binding force. Even certain types of uncharged polymers can adsorb onto a variety of surfaces. This happens because most polymers have a large number of either electron donating or electron withdrawing groups. Polymer adsorption is defined as a high affinity between a polymer and a surface. The poor solvent also facilitates polymer adsorption, but the attractive forces at interface still dominate the adsorption.

According to the result reported by Fowkes [1.43], the acidic polymer (poly(vinyl chloride)) only adsorbed onto the basic substrate (calcium carbonate) and did not adsorb onto the acidic substrate (silica). Whereas the basic polymer (poly(methyl methacrylate)) only adsorbed onto the acidic substrate (silica). These results proved that the interaction forces at interfaces are important sources of polymer adsorption. The strength of surface interactions is crucial for the polymer adsorption.

2.3 Structure of Adsorbed Polyelectrolyte

The rate of polyelectrolyte adsorption is so fast that the morphology of polyelectrolyte layer is kinetically determined at the first stage of adsorption [1.41 - 1.42]. The number of bound and unbound sites is determined by the dipping conditions of polyelectrolyte solutions. In the sequential adsorption, it can be seen that the unbounded charges of the polyelectrolytes are dangled in the polyelectrolyte solution and ready to work as interaction sites for the additional layer of oppositely charged polyelectrolytes. The structures of adsorbed polymer chains on the solid surface are characterized by trains,

loops, and tails (see Figure 1.3). The parts of trains of the adsorbed polyelectrolytes work as bonding forces to hold the adjacent polyelectrolytes. The unbounded charge groups are interacting with the oppositely charged polyelectrolytes in the consecutive dipping solution and make a binding to hold the consecutive layer.

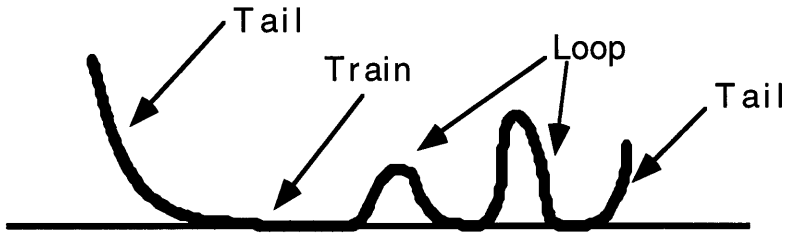

Figure 1.3. Structure of an adsorbed polymer.

The highly charged polyelectrolyte makes thin and tail layer structures, while the less charged polyelectrolyte does thick and loopy layer structures. The number of charge groups on a surface, solvent properties, and the number of charges on the polyelectrolyte are important in determining the structure of a polyelectrolyte.

2.4. Polyelectrolytes Adsorption

Polyelectrolyte adsorption is a complex process with many components such as the interactions among solvent, surface, salt and polyelectrolytes [1.44 - 1.45]. The surface charge density σ_S, the number of charges in the polyelectrolyte q_m, and the ionic strength C_s are three main factors that affect polyelectrolyte adsorption. The pH of the dipping solution changes the degree of ionization of electrolyte groups in polyelectrolytes and the charge density of a substrate or a deposited layer. Monovalent or divalent salts, such as NaCl, $MgCl_2$ and $MnCl_2$ are dissolved in the polyelectrolyte solution to increase ionic strength. The salts work to screen the charges on a substrate and polyelectrolyte. In the layer-by-layer adsorption technique, the number of charge sites of a polyelectrolyte and

a surface determine the strength of the interactions and the amount of adsorption. The strong interaction between layers is required to maintain multilayers that do not dissolve in the oppositely charged solution.

A. Polyelectrolyte Adsorption on Surface with Opposite Charges

As discussed in the previous section, electrostatic forces drive polyelectrolyte adsorption. The strong interaction between a polyelectrolyte and a substrate is responsible for the rapid adsorption and the steep isotherm. When strong acids or bases are incorporated into the system, most of the functional groups are ionized for a wide range of pH values. However, when weak acids and bases are used, the ionization of charge groups is strongly dependent on the pH of the solution. Both cases will be discussed in detail in subsequent sections.

A.1 Strong Polyelectrolytes

In this section, it is assumed that the charge groups of polyelectrolytes are fully ionized at the pH level of the dipping solution. In this case of high charge density in the polyelectrolyte, the electrostatic forces are the strong driving force for adsorption. As the density of surface charges increases, the amount of polyelectrolyte adsorption also increases to balance the surface charge. The increase, however, is not linear because the accumulation of like charges on the surface hinders additional adsorption.

When salt dissolves into the solution, i.e., ionic strength is enhanced, two opposing forces are introduced. The ionic repulsions between the deposited polyelectrolytes and those still in solution as well as the intrasegmental repulsions within a polymer chain can be reduced. In addition, the counterions of the salts can shield the charges on the surface and reduce the interaction forces at the surface. However, the interaction forces at interface are still strong enough to overcome the screened charges on a surface.

The enhanced ionic strength that the salt provided was responsible for increasing the thickness of the adsorbed layers. The charge screening is interesting from a structural point of view because this process can increase the number of loops and tails in the structure of the adsorbed layers. The charge screening at the interface also decreases the repulsive forces between the same charged polyelectrolytes in the solution and on the surface. The additional polyelectrolytes are facilitated to attach to the surface. Several research groups have reported the use of salts to produce thick layers [1.44 - 1.47]. At low salt concentration, the polymer adsorbs as an extended structure due to the strong repulsive forces.

In highly charged polyelectrolytes, molecular weight does not change the thickness of adsorbed layers. Stockton [1.48] studied the molecular weight dependence using the strong polyelectrolyte of poly(sulfonated styrene) (SPS) by changing the molecular weight of SPS from 5 to 990k. The thickness per bilayer was not varied to the different molecular weight of SPS. The highly charged SPS formed thin and train structures where the long chain or the short chain is fully extended.

In conclusion, the charge compensation is the principal factor in binding the strong polyelectrolytes to the oppositely charged substrate. The strong dependence of the ionic strength was observed with the strong polyelectrolytes.

A.2 Weak Polyelectrolytes

The charge dissociation of the weak polyelectrolytes is a function of the local pH. Not only are charges of already adsorbed weak polyelectrolytes affected but so are the charges of polyelectrolytes in solution. The interaction forces at the interface are also rather weak, but still sufficient for adsorption to occur. Adsorption behavior of weak acid polyelectrolyte can be classified into two groups. Those where the pH of the polyelectrolyte solution is above the pK_a (acid dissociation constant) of the polyelectrolyte and those where it is below the pK_a. In the former case, the fully charged

polyelectrolytes, which are similar to strong polyelectrolytes, have strong electrostatic forces at the interface. In addition, the amount of adsorption is limited by the repulsive forces at the interface hindering a deposition of like charges. In the latter case where the pH is about or lower than the pK_a, the intrasegmental and interfacial repulsion forces both decrease. This is a result of the low fraction of charge segments on the polyelectrolytes. Both theoretical [1.49] and experimental results [1.50, 1.51] show that the maximum adsorption of weak polyelectrolytes is obtained at a pH that is lower than the pK_a by 1 or 2 units. For example, the carboxylic acid of poly(acrylic acid) or poly(methacylic acid) is a weak acid with an pK_a around 4.0. When pH is much lower than the pK_a, the neutral carboxylic acid groups are not attracted to the charged surfaces as strongly. When pH is much higher than the pK_a, the strong electrostatic forces cause the polyelectrolyte adsorption with the extended chain form. In lightly charged weak polyelectrolyte systems, layer thickness depends on molecular weight due to the increase in the probability of forming loop and tail structures. The pH of a weak polyelectrolyte solution greatly influences the thickness of the adsorbed layers.

Ionic strength in a weak polyelectrolyte solution affects the adsorption behavior in different ways according to the charge density of the weak polyelectrolyte. In the low charge density of a polyelectrolyte, the ionic strength screens the low fraction of charges and thereby the attraction force decreases. The adsorbate (deposited polyelectrolytes) is nearly neutral. Sometimes, polyelectrolyte adsorption does not occur. At the highly charged state, the ionic strength screens the repulsive forces of charge segments in the polyelectrolyte. The decreased intrasegmental repulsion enhanced the polyelectrolyte adsorption with tails and loops. The adsorbed fully charged polyelectrolytes are going to keep some net charges on the surface.

In the layer-by-layer adsorption, it is expected that the charge density of an adsorbed layer of weak polyelectrolytes varies with the pH of the dipping solutions. The high pH of a dipping solution will increase the negative charges of poly(acrylic acid)

outermost layer, while the low pH of a dipping solution will decrease the charges. The difference of charge density will affect the additional layer adsorption.

In summary, in a weak polyelectrolyte adsorption, pH and ionic strength will change the surface charge density as well as the repulsive forces in the polyelectrolyte.

B. Polyelectrolyte Adsorption on Uncharged Surface

Uncharged surfaces are frequently used as a substrate in the layer-by-layer deposition. The interaction between an uncharged surface and a polyelectrolyte is much weaker than the static ionic interaction at the charged surfaces. The interaction between solvent-polyelectrolyte and polyelectrolyte-surface determine the adsorption behavior of polyelectrolytes at an uncharged surface. When the strength of polyelectrolyte-surface interaction exceeds the strength of solvent-polyelectrolyte interaction, the polyelectrolyte deposits onto the surface. The rate of the adsorption is determined by the difference of two interaction strengths.

The electrostatic effect in this case is that the segmental repulsion between the same charges of a polyelectrolyte and electroneutrality of charge segment groups on a surface. In general, with increasing charge density in polyelectrolytes, both the interactions between solvent and polyelectrolytes and between polyelectrolytes and surfaces are enhanced. If the surface has some of electron donor or acceptor groups, the level of dissociation of electrolyte groups will enhance the polyelectrolyte adsorption.

In solutions of high salt content, i.e., ionic strength, the counterions decrease the intrasegment repulsion and electroneutrality was easily achieved at the interface. The fixed counterion to the polyelectrolyte segments will be freed at the polyelectrolyte adsorption. The polyelectrolyte tends to adsorb to most surfaces with the coiled structure at high salt content.

C. Neutral Polymer Adsorption on Polyelectrolyte Deposited Surface

The polymer adsorption on charged surfaces is very similar to polymer adsorption onto the uncharged surface except the adsorption dependence on salt in the solution. Most polymers, which have electron donor or acceptor groups, adsorb from solution onto a surface. Even though a polymer loses some of its freedom through adsorption, most of polymers gain a sufficient adsorption free energy per segment to overcome a certain minimum adsorption free energy.

The solvency parameter, as can be expressed for Flory-Huggins interaction parameter χ [1.52], is important to polymer adsorption. The parameter χ is defined as

$$\chi = z(h_{12} - \tfrac{1}{2}h_{11} - \tfrac{1}{2}h_{22}) / kT \qquad (1.3)$$

where z is coordination number and component *1* is a solvent and component *2* is a polymer. The h means the interaction enthalpy per contact. If χ is bigger than 0, the solvent becomes poor and the polymer prefers the contact of similar segments. The amount of the polymer adsorption is controllable by selecting the solvent.

The adsorption phenomena can be described as the exchange process upon adsorption of a segment, where a solvent-surface interaction is displaced by a segment-surface interaction. Through the same concept in the solvency parameter, Silberberg [1.53] introduced the adsorption enthalpy parameter χ_s which is defined as

$$\chi_s = z'(h_{s1} - h_{s2} + \tfrac{1}{2}h_{22} - \tfrac{1}{2}h_{11}) / kT \qquad (1.4)$$

where z' is contact sites at the surface and component s is the surface. If χ_s is positive, the adsorption is preferred. Those two parameters are the most important considerations in the polymer adsorption.

The adsorption, in general, increases with decreasing solvency parameters, while with increasing the adsorption enthalpy parameters. The polymers in good solvents require strong interaction for the deposition onto the surface. The poor solvent enhanced the

adsorption of polymer onto the surface. The higher molecular weight polymer has stronger tendency to adsorb onto the surface because the numbers of sites decreases the solubility of polymer. This explained why polymers are easier to adsorb onto the surface, compared with the small molecule adsorption where the entropy penalty is much lower. The polymer adsorption on charged surfaces follows the general trends of polymer adsorption with enhanced interaction forces. The ionic strength again does not influence the polymer and may seal the charges on the surface to lose the interaction forces.

The polymer adsorption is complex and is varied to the conditions of number of charges, ionic strength and surface properties. By considering several parameters, we can find the right condition to make linear growth multilayer films and tune an adsorbed layer thickness in the layer-by-layer deposition.

2.5 Linear Growth of Sequentially Adsorbed Multilayer Film

The adsorbed polymer chain links to substrates by several bound segments (n). The Boltzmann factor for desorbed states can be expressed by $exp(-nE_b/KT)$, where the E_b is the energy barrier of each segment desorption. The probability of desorption decreases as the numbers of interaction segments increase. Compared with the small molecular deposition, once deposited polymer is not likely to be depleted into the solution due to the several interactions. The unbound charges of the deposited layer work as interaction sites in the oppositely charged dipping solution. Once the dipping procedure keeps the same charge density and the same structure of the multilayered films, the amount of adsorption becomes constant and hereby the thickness increment of bilayer is sustained.

The nonlinear growth is sometimes observed in the cases where the surface charges shrink or grow as the number of layer deposition increases. Most of nonlinear adsorption is overcome by changing the dipping conditions to keep adsorbed layers from desorbing, but some materials eventually lead to non-linear growth. For example, a highly

branched polyelectrolyte like poly(ethyleneimine) would increase the charge density through the increased roughness and polyions with low charge density would lower the available charges on a surface as the number of layers increase.

2.6 Concentration of Dipping Solutions

The concentrations of polyelectrolytes in this study are maintained in the 10^{-2} to 10^{-4} M of repeat unit concentrations. This regime is still dilute solutions where polyelectrolytes do not overlap each other. In general, higher concentration can produce thicker layers in a given time due to a higher diffusion rate and concentration at the interface. The dependence of overall thickness on concentration is affected by the affinity type of the interface. A strong polyelectrolyte is less sensitive to the concentration of dipping solutions than an uncharged polymer or a weak polyelectrolyte. In the case of strong polyelectrolytes, the rate of adsorption is fast and covers the whole surface in the early stage of the adsorption with mostly train structure. The already adsorbed polyelectrolytes limit the additional adsorption of polyelectrolytes by static ionic repulsions. The tails and loops of the weak adsorbed polyelectrolytes are enhanced with the higher concentration of polyelectrolytes at interface.

2.7 Multilayer Films of Polyelectrolytes and Small Dye Molecules

Through this study, this novel layer-by-layer adsorption technique was expanded to build-up multilayer films of functional dye molecules and polyelectrolytes. Organic dyes have shown many interesting properties for the possible applications in electronics and optics [1.54]. The organic dyes, however, are hard to be used as a definite layer or multilayer structures with other functional materials. In general, the dye molecules are mixed with polymer binders and spun onto the substrates. The layer-by-layer adsorption technique may be a unique way to fabricate the heterostructure of an organic dye monolayer with other functional layers.

There are various differences between the adsorption of small dye molecules and polymers, in many aspects. The enthalpy penalty upon the adsorption in polymer is much greater than the small dye molecule upon adsorption, because no conformation change occurs at the small dye molecule adsorption. The small dye molecules are willing to be adsorbed onto the charged surface as long as the interactions exist. The adsorbed small dye molecules, however, have much higher possibilities to be depleted from the surface, because the small dye molecules have only a few charge groups bound to the layers. To build up a multilayer structure, the stronger bonds are required for the adsorption of the small dye molecules.

The organic materials for forming the individual layers in the layer-by-layer deposition on the modified surfaces are either monomeric substances having more than two ionizable functional groups of the same charge, or so-called polyelectrolyte type. Two separate charges in the dye structures are required at least to incorporate dye molecules in the multilayer structures. Unless there are sufficient interactions between dye molecules and polyelectrolytes on the surface, multilayer films cannot successfully build up. The different adsorption mechanism and layer structure could be determined by the kinds of charges in the dye structures. For example, the case of strong acid like $-SO_3^-$, is used for a wide range of pH of the dipping solutions and induce stronger bonds, but the weak acid like -COOH, has small pH ranges for the processing to hold the polyelectrolyte to build up multilayer films. The tails and loops of adsorbed polyelectrolytes work as binding sites and deter the desorption of once adsorbed dye molecules. The loopy structure of layers enhances the adsorption of dye molecules in the solution.

Up to this point, several issues in the sequential layer-by-layer deposition technique were discussed. The technique employs several complex phenomena involved in polymer adsorption and gives the possibility to fine tune the molecular structures and adsorption behavior by changing pH, concentration and ionic strength of the polyelectrolyte dipping

solution. Various kinds of materials which have some charge groups can be used to build up layer-by-layer multilayer films.

REFERENCES

[1.1] Swalen, J. D.; Allara, D. L.; Andrade, J. D.; Chandross, E. A.; Garoff, S.; Israelachivile, J.; McCarthy, T. J.; Murray, R.; Pease, R. F.; Rabolt, J. F.; Wynne, K. J. Yu, H.; *Langmuir* **1987**, *3*, 932.

[1.2] *Adv. Mater.* **1991**, *3*, Special Issue on Organic Thin Films.

[1.3] Ulman, A. "An Introduction to Ultrathin Organic Films from Langmuir-Blodgett to Self-Assembly"; Academic Press: San Diego, 1991.

[1.4] Blodgett, K. B.; Langmuir, I. *Phy. Rev.* **1937**, *57*, 964.

[1.5] Roberts, G. "Langmuir-Blodett Films"; Plenum Press: New York, 1990.

[1.6] Sagiv, J. *J. Am. Chem. Soc.* **1980**, *102*, 92.

[1.7] Kuhn, H.; Möbius, D.; Bücher, H. in "Techniques of Chemistry, Part 3B, Vol. 1", Weissberger, A. and Rossiter, B. W. Eds.; Wiley: New York, 1973, p577.

[1.8] Spangler, L. L.; Torkelson, J. M.; Scot Royal, J. *Poly. Eng. and Sci.* **1990**, *30*, 644.

[1.9] Tillman, N.; Ulman, A.; Penner, T. L. *Langmuir* **1989**, *5*, 101.

[1.10] Kakkar, A. K.; Yitzchaik, S.; Roscoe, S. B.; Kubota, F.; Allan, D. S.; Marks, T. J.; Lin, W.; Wong, W. L. *Langmuir* **1993**, *9*, 388.

[1.11] Byrd, H.; Whipps, S.; Pike, J. K.; Ma, J.; Nagler, S. E.; Talham, D. R. *J. Am. Chem. Soc.* **1994**, *116*, 295.

[1.12] Decher, G.; Hong, J. D. *Ber. Bunsenges. Phys. Chem.* **1991**, *95*, 1430.

[1.13] Decher, G.; Hong, J. D. *Thin Solid Films* **1992**, *210/211*, 831.

[1.14] Lvov, Y.; Decher, G.; Möhward, H. *Langmuir* **1993**, *9*, 520.

[1.15] Lvov, Y.; Hass, H.; Decher, G.; Möhwald, H.; Kalachev A. *J. Phys. Chem.* **1993**, *97*, 12835.

[1.16] Decher, G.; Lvov, Y.; Schmitt, J. *Thin Solid Films* **1994**, *244*, 772.

[1.17] Cheung, J. H.; Fou, A. C.; Ferreira, M.; Rubner, M. F. *Polymer Preprints* **1993**, *34*, 757.

[1.18] Cheung, J. H.; Fou, A. C.; Rubner, M. F. *Thin Solid Films* **1994**, *244,* 985.

[1.19] Ferreira, M.; Cheung, J. H.; Rubner, M. F. *Thin Solid Films* **1994**, *244*, 806.

[1.20] Fou, A. C.; Ellis, D.; Ferreira, M.; Rubner, M. F. *Polymer preprints* **1994**, *35*, 221.

[1.21] Yoo, D.; Lee, J-K.; Rubner, M. F. *Mat. Res. Soc. Symp. Proc.* **1996**, *413*, 395.

[1.22] *Mat. Res. Soc. Bull.* **1995**, *20*, Special Issue on Organic Thin Films.

[1.23] Knoll, W. *Current Opinion in Colloid & Interface Sci.* **1996**, *1*, 137.

[1.24] Decher, G. in "Comprehensive Suptramolecular Chemistry Vol. 9"; Sauvage, J.-P and Hosseini, M. W. Eds.; Pergamon: Oxford, 1996, p507.

[1.25] Fou, A. C.; Onitsuka, O.; Ferreira, M.; Rubner, M. F.; Hsieh, B. R. *J. Appl. Phys.* **1996**, *79*, 1.

[1.26] Tian, J.; Wu, C-C.; Thompson, M. E.; Sturm, J. C.; Register, R. A.; Marsella, M. J.; Swager, T. M. *Adv. Mater.* **1995**, *7*, 395.

[1.27] Hong, H.; Davidov, D.; Avany Y.; Chayet H.; Faraggi, E. Z.; Neumann, R. *Adv. Mater.* **1995**, *7,* 846.

[1.28] Papenhuijzen, J.; Fleer, G. J.; Bijsterbosch, B. H. *J. Colloid Interface Sci.* **1985**, *104*, 553.

[1.29] Meadows, J.; Williams, P. A.; Garvey, M. J.; Harrop, R. A.; Phillips, G. O. *Colloids and Surfaces* **1988**, *32*, 275.

[1.30] Yoo, D.; Rubner, M. F. *SPE Proceedings,* Boston, MA, **1995**, 2568.

[1.31] Ferreira, M.; Rubner, M. F. *Macromolecules* **1995**, *28*, 7107.

[1.32] Fou, A. F.; Rubner, M. F. *Macromolecules* **1995**, *28*, 7115.

[1.33] Baur, J. : Rubner, M. F. *To be submitted.*

[1.34] Lvov, Y.; Decher, G.; Sukhorukov, G.; *Macromolecules* **1993**, *26*, 20.

[1.35] Lvov, Y.; Ariga, K.; Ichinose, I.; Kunitake, T. *J. Am. Chem. Soc.* **1995**, *117*, 22.

[1.36] Kleinfeld, E. R.; Ferguson, G. S. *Science* **1994**, *265*, 370.

[1.37] Gao, M.; Zhang, X.; Yang, Y.; Yang, B.; Shen, J. *Chem. Soc. Chem. Comm.* **1994**, 2777.

[1.38] Hiemenz, P. C. "Polymer Chemistry"; Marcel Dekker: New York, 1984.

[1.39] Oosawa, F. "Polyelectrolytes"; Marcel Dekker: New York, 1971.

[1.40] Mandel, M. in "Encyclopedia of Polymer Science and Engineering, 2nd. ed. Vol. 11."; John Wiley & Sons: New York, 1985, p739.

[1.41] Fleer, G. J.; Lyklema, J. in "Adsorption from Solutions at the Solid/Liquid Interface"; Parfitt, G. D., Rochester, C. H., Eds.; Academicn Press: London, 1983, p153

[1.42] Silberberg, A. in "Encyclopedia of Polymer Science and Engineering, 2nd. ed. Vol. 1"; John Wiley & Sons: New York, 1985, p577.

[1.43] Fowkes, F. M.; Mostafe, M. A. *IEC Prod. R&D* **1978**, *17*, 3.

[1.44] Fleer, G. J.; Cohen Stuart, M. A.; Scheutjens, J. M. H. M.; Cosgrove, T.; Vincent, B. "Polymers at Interfaces"; Chapman & Hall: London, 1993.

[1.45] Van de Steeg, H. G. M.; Cohen Stuart, M. A.; Keizer, A.; Bilsterbosch, B. H. *Langmuir* **1992**, *8*, 2538.

[1.46] Cosgrove, T.; Obey, T. M.; Vincent, B. *J. Colloid Interface Sci.* **1986**, *111*, 409.

[1.47] Decher, G.; Lvov, Y.; Schimitt, J. *Thin solid Films* **1994**, *244*, 772.

[1.48] Stockton, W. B. Ph. D. Thesis, M.I.T., 1995.

[1.49] Böhmer, M. R.; Evers, O. A.; Scheutjens, J. M. H. M. *Macromolecules* **1990**, *23*, 2288.

[1.50] Blaakmeer, J.; Böhmer, M. R.; Cohen Stuart, M. A.; Fleer, G. J. *Macromolecules* **1990**, *23*, 2301.

[1.51] Robb, I. D.; Sharple, M. *J. Colloid Interface Sci.* **1982**, *89*, 301.

[1.52] Flory, P. J. "Polymer Chemistry"; Cornell University Press: Ithaca, 1953.

[1.53] Silberberg, A. *J. Chem. Phys.* **1968**, *48*, 2835.

[1.54] Gregory, P. "High-Technology Applications of Organic Colorants"; Plenum Press: New York, 1991.

CHAPTER 2

EXPERIMENTAL PROCEDURES

This chapter provides a description of the experimental processes and techniques used in this study. Materials used to construct layer-by-layer deposited multilayer films and the synthesis of Ru complex based materials will be explained. A description of film characterization techniques is included. Finally, the fabrication and measurements of a light emitting device (LED) will be explained.

1. Materials

1.1 Polyelectrolyte Solution Preparation

A. Poly(aniline) Solution

Polyaniline (PAN) solutions (the PAN was synthesized using the procedures reported by Chaing and MacDiarmid [2.1]) were prepared by dissolving PAN in dimethyl acetamide (DMAc) at 20 mg/ml. The solution was then stirred overnight, followed by 8-10 hours of sonicating. The solution had some fine particulates which were removed by filtering through a 2μm filter, followed by a 0.45μm filter. The PAN dipping solution was prepared by slowly adding one part (by volume) of the PAN solution in DMAc with 9 parts water. The pH of the PAH solution was adjusted to about 3.0-3.5 with methane sulfonic acid (MeSA). The pH was then quickly lowered to 2.5-2.6 by adding drops of concentrated MeSA.

B. Poly(thiophene-3-acetic acid) Solution

Poly(thiophene-3-acetic acid) (PTAA) was prepared by the ferric chloride polymerization of ethyl thiophene-3-acetate (Lancaster Synthesis) followed by acid hydrolysis of the ester group [2.2]. Dipping solutions with a PTAA concentration of 0.01M (based on unit molecular weight) and a pH level of 4.8 were used with 0.4 M of NaCl.

C. Other Polyelectrolyte Solution

Poly(vinylbenzyltrimethylammonium) (PVBT) was supplied by Prof. Otto Vogl of Polytechnic University, Brooklyn, NY. Poly(methacrylic acid) (sodium salt, Mw=50,000) (PMA), Poly(acrylic acid) (Mw=90,000) (PAA), poly(diallyldimethyl ammoniumchloride) (High Mw version) (PADA) and poly(styrene-4-sulfonate) (Mw=75,000) (SPS) were obtained from Polysciences. Poly(allylamine) (Mw=28,000) (PAH) was obtained from Aldrich. All polyelectrolytes were used as received, without further purification. Those polyelectrolyte dipping solutions of 10^{-2} M were made in Millipore water and pH adjusted with HCl and NaOH. Salts, such as $MgCl_2$ and NaCl, were dissolved in the polyelectrolyte solutions to enhance polyelectrolyte adsorption.

1.2 Dye Solution Preparation

Congo red dye, Porphyrin dyes, Crystal Violet dye, Ponceau S, and Bordeaux R dye were purchased from Aldrich. Infrared absorbing dye and Fluorescein complexion were obtained from Kodak. All dyes were used without further purification. The dyes were dissolved in Millipore water to give 10^{-2} M - 10^{-3} M solution. Those dyes have at least two ionic groups in chemical structures. Again, pH was adjusted using HCl and NaOH solutions.

1.3 Sulfonated tris(phenanthroline)ruthenium (II) dication complex, ($[Ru(phen')_3]^{+2}$) Synthesis [2.3]

$[Ru(phen')_3]^{+2}Cl_2$ was prepared by slight modification of a reported method [2.4] . The reaction scheme of $[Ru(phen')_3]^{+2}Cl_2$ is shown in Figure 2.1. Commercial $RuCl_3 \cdot xH_2O$ was dried in a vacuum oven at 150°C for 3 hours. It was then ground finely in a mortar and dried in the oven for further two hours prior to use. A mixture of predried $RuCl_3$ (311 mg, 1.50 mmol) and anhydrous disodium salt of 4,7-diphenyl-1,10-phenanthrolinedisulfonic acid (2.41 g, 4.50 mmol) in 60 ml of water was then refluxed for 60 minutes in the presence of a reducing agent (NaH_2PO_2, 0.15 g, 1.66 mmol). The resulting dark-orange solution was concentrated under vacuum and the product precipitated into acetone. Yield was quantitative and the product was purified two or three more times

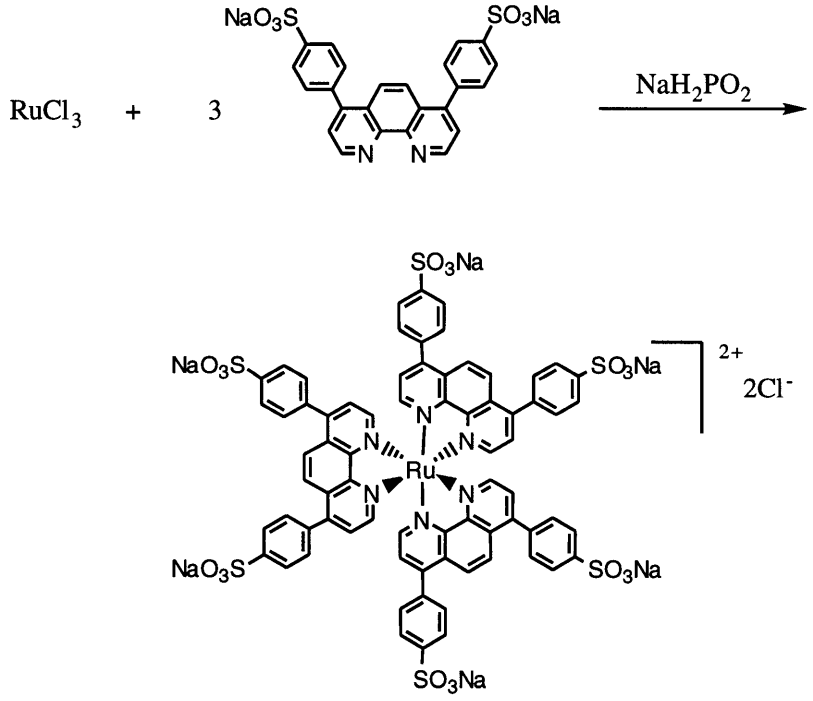

(I)

Figure 2.1. Sulfonated $Ru(phen')_3^{+2}Cl_2$ (I) synthesis scheme.

by recrystallization from methyl alcohol into acetone. The yield was more than 99% after the product was dried in air.

1.4 Poly(tris(bipyridine)ruthenium(II)dication complex), (poly($[Ru(bpy)_3]^{+2}$)ester) Synthesis

A polyester type of $Ru(bpy)_3^{+2}$ was supplied from Jin-Kye Lee in our group. The detailed synthesis of the polymer is described elsewhere [2.5]. However, the basic routes of the synthesis of poly($[Ru(bpy)_3]^{+2}$)ester include the step-polymerization of a difunctionalized Ru(II) complex, $Ru(bpy)_2[bpy(CH_2OH)_2]^{+2}$, with dodecanedioyl dichloride, $ClOC(CH_2)_{10}COCl$. The final step of the synthesis scheme is shown in Figure 2.2.

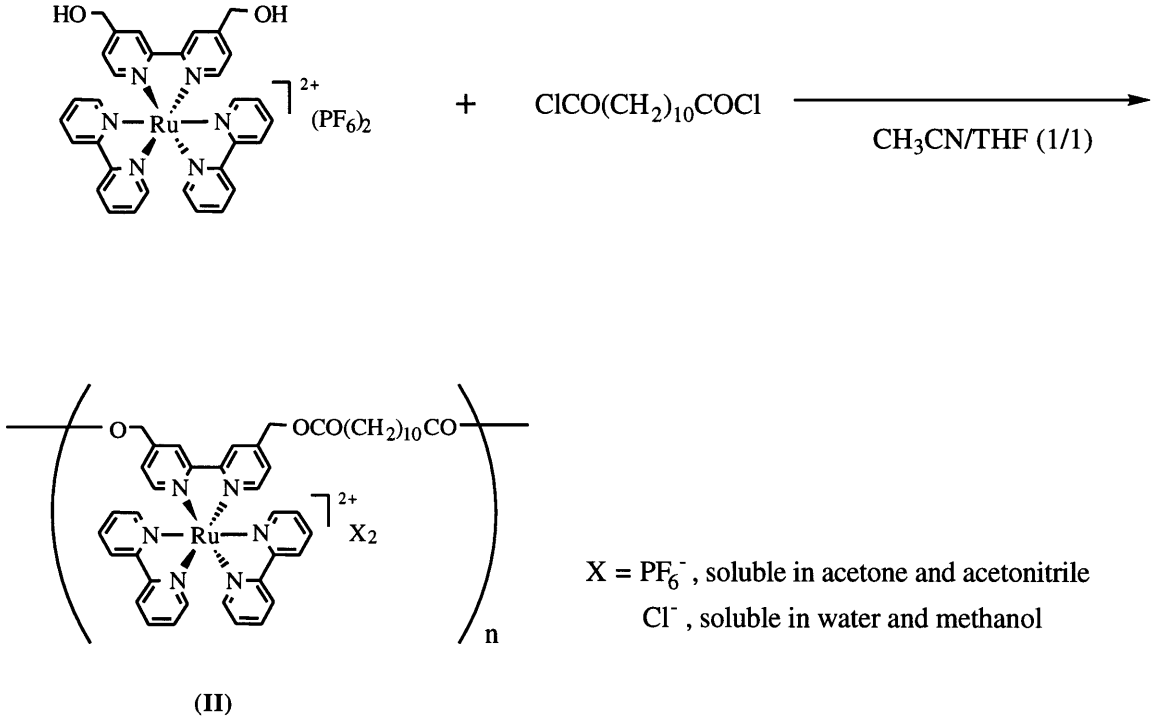

(II)

Figure 2.2. poly($[Ru(bpy)_3]^{+2}$)ester (II) synthesis scheme.

2. Substrate Preparation

The clean surface was required for uniform adsorption. Microscope glass slides treated to render their surface hydrophilic and hydrophobic were used for the dipping procedure.

2.1 Hydrophilic Slide Substrate

Commercially pre-cleaned glass substrates were first placed in a concentrated sulfuric acid (H_2SO_4)/Hydrogen peroxide (H_2O_2) (7:3) bath for 1 hour and then in a $H_2O/H_2O_2/NH_3$ (5:1:1) bath for 30 minutes. The substrates were extensively rinsed with Millipore deionized water (resisitivity $\geq$ 18MΩ) after each cleaning step. The substrates were dried with filtered compressed air and further dried at the 90°C for 1 hour. These slides were stored in a plastic case prior to use.

2.2 Hydrophobic Slide Substrate

Hydrophobic surfaces were created by a gas phase treatment of hydrophilic slides with 1,1,1,3,3,3 disilazane (HMDS) obtained from Aldrich. Its structure is shown in Figure 2.3. The cleaned slides and 1 ml of HMDS were placed in a desiccator which was then evacuated and maintained at a static vacuum (200 mTorr) for 36 hours. The liquid disilazane was placed into a small evaporating dish and placed inside a vacuum dessicator. Once the vacuum reached 200 mTorr, the chamber was sealed to keep a static vacuum for 36 hours. After the disilazane treatment, the slides were rinsed with Millipore water and hexane to remove residual HMDS. The contact angle of the hydrophobic substrates was around 65 degrees.

2.3 Positively Charged Slide Substrate

Positively charged surfaces were fabricated by a solution treatment of the cleaned hydrophilic slides with (N-2-aminoethyl-3-aminopropyl)trimethoxysilane (TMS) which

was supplied by Huls America, Inc. The cleaned slides were immersed for 10 minutes each into the following solvents: methanol (HPLC grade, Mallinckrodt), 1:1 methanol/toluene, toluene (analytic reagent grade, Mallinckrodt). After rinsing with methanol and toluene, the cleaned slides were exposed to a 5 volume% solution of TMS in toluene for 15 hours. After silazation, the slides were immersed in fresh boiling toluene for 1 hour. Then they were immersed for 10 minutes each in toluene, 1:1 to toluene/methanol, and methanol. Finally, they were extensively rinsed with Millipore water to remove residual TMS and dried. This produced a surface with covalently anchored amine functionalities; these functionalities were protonated in the low-pH solutions.

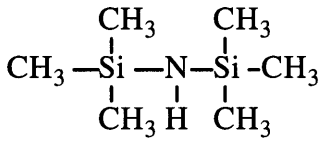

(a) 1,1,1,3,3,3 hexamethyl disilazane

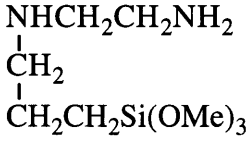

(b) N-(2-aminoethyl-3-aminopropyl) trimethoxysilane

Figure 2.3. Chemical structures of (a) hexamethyl disilazane (HMDS) and (b) N-(2-aminoethyl-3-aminopropyl) trimethoxysilane (TMS).

3. Layer-by-Layer Sequential Adsorption Technique

The layer-by-layer deposition technique used to create alternating multilayer thin films involves repeated dipping of a substrate into dilute polycation and polyanion solutions.

3.1 Hand Dipping Procedure

Films were deposited by alternately dipping substrates into polyelectrolyte solutions. The substrates were dipped in the polyelectrolyte solution for 15 minutes and subsequently rinsed with pH 2-4 solutions, which was adjusted to be the same pH of the

dipping solutions, until most non-adsorbed material was removed. After each deposition and rinsing, the samples were blown dry with a flow of compressed, filtered air. The substrate was then dipped in the oppositely charged solution, for an equal amount of time followed by the rinsing and drying procedures. The deposition was performed at room temperature.

3.2 Automatic Dipping Procedure

The layer-by-layer fabrication of multilayer thin films was carried out via the use of an automatic dipping machine in the form of a programmable slide stainer (HMS programmable slide stainer/Zeiss Inc.). This dipping machine was programmed to immerse substrates (glass or patterned ITO) into a series of up to twenty different solutions. The substrates were dipped into a polyelectrolyte solution followed by three agitated rinses in three separate bins of pH adjusted water. The substrate was then dipped into the oppositely charged polyelectrolyte solutions followed by these 3 separate rinses with pH adjusted water. The dipping time in polyionic solutions was controlled for 15 minutes, and the rinsing times were 2 minutes for the first two rinses and 1 minute for the third rinse. No drying step was used in the automatic dipping procedure.

4. Characterization Methods

4.1 Contact Angle Measurement

An Advanced Surface Technology video contact angle measuring device was used to measure the contact angle of water on deposited layer films. The contact angles presented in this thesis are advancing contact angles which were measured with the sessile drop technique [2.6 - 2.8]. An advancing contact angle (θ_A) is the kinetically stationary angle formed on the surface after a water drop have advanced on the surface. A water drop was made on the tip of a syringe and placed on a sample by moving the substrate vertically

until contact was made between the water drop and the sample. The subsequent addition of a small amount of water to the water drop on the surface produced the static advancing angle with the surface in a few seconds. The contact point of the syringe was kept at the same position on the water drop. The needle was raised very slowly to prevent deformation of the water drop. An image of the droplet was taken though the CCD camera and enlarged. The right and left contact angles of the droplet were then measured using an enlarged image transmitted to the computer screen. The size of water droplets was maintained constant at 1μl. (when the surface is homogenous, the size of the water drops should not affect the value of the contact angles [2.6 - 2.8]) Before measurement of the contact angle, the samples were dried at 90°C for 1 hour and stored in ambient air for 2 days. When the contact angles of consecutively deposited layers were measured, 12 separate samples were prepared where the total number of layers per sample varied from 1 to 12. Four separate locations (2 measurements each) on the sample were measured to ensure a representative value of the contact angle. The average value of the measured contact angles was used to represent the wetting characteristics of the sample.

4.2 Thickness Measurement

Multilayer films with 10, 20, 25 and 30 bilayers were built up on silicon wafers and hydrophilic glass slide substrates. The films on the silicon wafers were used to measure the total thickness of the films via ellipsometry because the smooth surface reduces the noise in the light reflected from the substrate surface. Films on glass slides were scratched for profilometry measurement. The depth of the scratch was then measured.

Thickness increment measurement was based on the consecutive layer depositions onto the 10 and 11 layered samples. After each layer deposition, the thickness was measured with 477 and 633 nm laser sources. Three additional layers were deposited onto the 10 and 11 layered samples. The averaged values were then chosen to represent the incremental thickness of the film.

A. Profilometry

Profilometry is a mechanical contact method. The thickness of a film is measured by scanning a scratched in depth profile with a diamond stylus. The films were scratched with a razor blade to form approximately 1000 Å lines. By profiling the scored line, the depth of the line was measured. The average value of five measurements was chosen to represent the thickness of the film. A Sloan Dektak 8000 profilometer was used and the stylus was set to the pressure of 10 mg to minimize error and noise. The Dektak profilometer was used to measure films of 200 Å and thicker.

B. Ellipsometry

Ellipsometry is a sensitive and non-destructive method for measuring the thickness of thin films. Ellipsometry can be used to give direct measurements of the thickness and refractive index of thin films on various surfaces, including metals, semiconductors, insulators, and polymers [2.9 - 2.10]. The technique is based on the measurement of changes in the ellipticity of polarized light caused by reflection at an interface. These changes are strongly influenced by the presence of a film on a smooth reflecting surface. The ellipticity can be described by the ratio and phase difference of two plane waves. The light wave can be viewed as a superposition of two plane waves, one of which has the electric vector in the plane containing the wave vectors of the incident light and the other with the electric vector at right angle to this plane. These two components change as a function of the refractive index and the film thickness.

Ellipsometry is suitable for the measurement of films whose thickness is much less than the wavelength of light. In a typical ellipsometer, monochromatic light is plane polarized (P = angle of polarization) and reflected on the film surface. A reflected beam enters the compensator and is elliptically polarized to plane-polarized (A = angle of polarization). The angle A is determined by the analyzer. These two angles (P, A) give the phase shift between the parallel and perpendicular components (Δ), and the changes in the

ratio of the amplitudes of the two components (tan ψ). The differential values of Δ, ψ are related to the ratio of the reflection coefficients of parallel (r_p) and polarized (r_s) light, respectively,

$$\frac{r_p}{r_s} = \tan\psi \cdot \exp(i\Delta) \qquad (2.1)$$

As the films have different refractive indices from the substrate, the film thickness is measured by calculating the difference between the clean substrate surface and the substrate with films. In principle, for thickness > 50 Å, ellipsometry can determine both the thickness and reflective index. At least five points were measured and averaged for the value of thickness. The data variance was within 10 Å. At least two different wavelengths of light were examined to measure the thickness of a sample.

4.3 Visible and Near ultraviolet Spectroscopy

Visible and near ultraviolet (UV/Vis) spectra were generated on an Oriel Multispec spectrophotometer. Since PAN, PTAA and the dye molecules have distinctive colors, UV/Vis spectroscopy is a powerful tool to check the amount of adsorption, proof of linear adsorption, and chain orientation. Upon checking the UV/Vis spectral peaks of each layer, the amount of adsorption was correlated with the number of functional groups on the surface.

The chain orientation of molecules in films can be determined by using polarized light spectroscopy. By comparing the absorption of light parallel (P) to the plane of incidence with that of light perpendicular (S) to the plane of incidence, the average orientation of a chromophore is determined [2,11,2.12]. The relations of the ratio of P absorption (A_p) to S absorption (A_s) is given in the below equation (2.2).

$$\frac{A_P}{A_S} = \frac{n_1 \cdot \cos i + n_3 \cdot \cos r}{n_1 \cdot \cos r + n_3 \cdot \cos i}(\cos i \cdot \cos r + \frac{{n_1}^3 n_3 \cdot \sin^2 i}{{n_2}^4 \tan^2 \theta}) \qquad (2.2)$$

where n_p is the refractive index of phase P (1=air, 2=polymer film, 3=glass substrate), i is the angle of incidence at the air-film interface, and r is the angle of refraction at the film-glass interface. The dichro ratio is useful for making relative comparisons among different conditions.

In order to check amount of carboxylic acid groups on a PAH/PAA multilayer film structure, positively charged methylene blue dye (obtained from Aldrich) was applied to dye multilayer films. The methylene blue did not deposit on bare slides. The amount of the methylene blue adsorption was traced with the UV/Vis spectroscopy. The PAH / PAA films with different number of layers were immersed in 10^{-3} M methylene blue solutions for 10 minutes. After the dye immersion, the dyed multilayer films were soaked in water (pH=4.0) for 1 minute and dried with a mild air flow.

4.4 Infrared Spectroscopy

Infrared spectroscopy was performed to study interactions in the polymer layers, particularly where hydrogen bonding or acid-base interactions were concerned. The vibrational energies of the polymer functional groups are changed by interactions between layers. The resulting vibration energy difference appears as shifts in the vibration peaks of the infrared spectra. If the bonds are stronger, vibrational peaks move to lower wave number.

There is a strong tendency for hydrogen bonds to form if a hydrogen atom attached to an adjacent atom, such as O or N, which carries a local concentration of negative charge. The most important effect is a lowering of the stretching frequency of the hydrogen bonded OH or NH group with respect to that of the 'free' groups [2.13].

The carboxylic peak in infrared spectroscopy can be used to check interactions between the layers by relative amounts of carboxylate $-COO^-NH_3^+$ and hydrogen-bonded $-COOH-NH_2$. Compositional heterogeneity was compared based on 1560 cm^{-1} of $-COO^-$ and 1700 cm^{-1} of -COOH [2.14, 2.15].

Similar to the UV/Vis spectroscopy, infrared spectroscopy is an appropriate method to check the amount of adsorption, especially for materials that do not have peaks in the UV/Vis range. A polished Zn/Se plate was used as a substrate for the layer-by-layer deposition. Distinct functional group absorptions can also determine the amount and the linearity of adsorption.

4.5 Fluorescence and Electroluminescence Spectroscopy

Photoluminescence and electroluminescence spectra of Ru complex incorporated films were measured using a SPEX 312 scanning fluorimeter with CCD detector. Photoluminescence spectra were taken by exciting the maximum absorption wavelength of Ru complex materials. The excitation wavelength of Ru complex based samples was chosen to be 470 nm. The samples were placed at the front face. The resulting photoluminescence was collected by mirrors facing the substrate. The slits were typically set to 1.0 mm for the source and the detector. The photoluminescent peak in Ru complex materials was measured at 630 nm.

The electroluminescence of the Ru complex based light emitting devices (LEDs) was measured in ambient air. The sample LEDs were positioned to face the detector. Then the wire leads from a manual extended power source was connected. The devices were turned on and the CCD carray collected the light for one second. The electroluminescence spectrum was recorded with correction factors for the CCD detector. The electroluminescent peak of Ru based LEDs was determined to be 630 nm.

5. Light Emitting Device Fabrication

5.1 Indium tin oxide (ITO) Substrate

Electroluminescent devices were fabricated on glass substrates patterned with 2 mm wide, 2000 Å thick lines of indium tin oxide (ITO) electrodes. The ITO substrates for device fabrication consisted of two or four ITO lines. The ITO substrates were received from TDK, Japan. The two point resistance of each ITO line is about 10 Ohms. These substrates were scored with a diamond cutter and broken into pieces of appropriate size. The ITO patterned substrates were sonicated in a 1:3 Lysol® (generic household cleaner): Millipore water solution for 15 minutes. Then, the substrates were rinsed with fresh Millipore water. The substrates were then placed in Millipore water and sonicated for 15 minutes. This pure water rinsing and sonication steps were repeated three more times. The substrates were sonicated in acetone and ethanol for 15 minutes each. These cleaned substrates were used immediately or stored under vacuum to maintain the clean surface.

5.2 Film Fabrication on ITO substrate

The cleaned ITO substrates were dried under vacuum at 60°C before use. The spin-casting method or the layer-by-layer deposition technique were used to build up LEDs in this study.

The spin-cast LEDs of Ru complex materials were fabricated by dissolving the Ru complexes in 2-methoxy ethanol and then filtering through a teflon coated μm syringe filter. The Ru complex solutions were dropped onto the cleaned ITO slide until the whole surface was covered. The substrates were then spun at 3000 rpm for 1 minute, allowing the solvent to evaporate. Any residual solvent was removed under vacuum.

The cleaned ITO substrates for the layer-by-layer deposition technique were pre-treated with 1 layer of a polycation, (PAH or PEI), rinsed with Millipore water, and dried with an air gun. Then a layer of polyanion was deposited onto the polycationic layer. The negative or positive charges were established on the ITO surfaces. Automatic dipping or

hand dipping methods explained in previous sections were then used to form the multilayer film.

5.3 Al Evaporation

2 mm wide lines of Al were deposited perpendicular to the ITO lines via thermal evaporation at a pressure of $2 \cdot 10^{-6}$ Torr. The size of LED cells was thereby determined to be 4 mm^2. The aluminum was evaporated at a rate of 250 Å per second onto the films by using 6 Al clips. The resultant thickness of the aluminum lines was typically between 2000 - 2500 Å. Each sample therefore has two or four ITO lines and two or four Al lines. The intersection made four or sixteen active devices that can be addressed individually by contacting the appropriate gold leads to a power source. ITO sides were connected with the positive charge and Al sides were connected with the negative charge of the power source. The samples were placed under dynamic vacuum of 100 mTorr until they were ready to be tested.

5.4 Current-Voltage and Light-Voltage Measurement

The samples were mounted onto L shaped glass slides. Gold wires were taped down on the glass slides and were electrically contacted to the ITO or Al lines by silver paste. Once the sample was tightly mounted onto the glass slides, the sample was placed in a dark, controlled, nitrogen atmosphere. Inside the dark nitrogen atmosphere, light and current were measured with a silicon photodiode (Model 1830-C from Newport Instruments) and current meter (Hewlett Packard 34401A). The operation voltage was applied to the devices using a programmable constant voltage source (Model 636 from Keithley). The typical distance between an active cell and the detector was 1 cm. A 3 mm by 3 mm mask was used to exclude unwanted light from the detector.

The current-voltage and light-voltage curves were taken automatically by a custom LabView program written by our group. The LabView program controlled a series of

commands to ramp the voltage from zero to a designated maximum voltage. The step voltage was 0.5 volt and delay per each voltage increment was 5 seconds. The delay per each voltage increment gave some time to reach equilibrium values after a new voltage was set. Once the voltage reached the designated maximum voltage, the program ramped down the voltage with the same voltage step and the same delay per step. If the designated voltage was a negative value, the program proceeded to ramp the voltage down from zero to the maximum negative bias first and then increase the voltage from the maximum negative bias to the zero with the same step. The current (mA) and the light intensity (nW) at each voltage step were recorded automatically through the program and plotted with a voltage axis. Each active light emitting cell was scanned multiple times until the light and current versus voltage curves were identical in the upward and downward scans. The hysteresis between the upward and downward scans is due to a charging effect in the Ru complex based LEDs.

5.5 Device Lifetime Testing

The life-time and stability of the device were investigated at the same voltage. The LED devices were again operated under the nitrogen gas and maintained at the designated voltage. Each measurement of current and light values were read according to a user defined "sampling time interval".

5.6 Efficiency of Device Performance

One of the most important parameters for evaluating LED behavior is the EL efficiency. The efficiency of the devices is equal to the average number of photons produced for each electron. The external and detectable light output was used to calculate an external quantum efficiency. The losses and reflected light output at the ITO and glass substrates were not observed. An internal quantum efficiency only can be calculated by using "correction factors".

The flux of photons was calculated by dividing the light power output reading by the energy per photon. The energy per photon was averaged based on the center wavelength of the electroluminescence peak of Ru complex materials (630 nm). The number of electrons per second can also be calculated by dividing the current by unit charge current. The ratio of photon flux and electron flux gives the external quantum efficiency. However, the small size of the photodiode used may not detect all the light output from LED cell. A correction factor to convert the collected light output to the real light output based on the distance and the angle between the detector and a LED cell. This was calculated by the similar method in the literature [2.16]. The calculated correction factor shows that the detector only collects about 27% of the light emitted. The refractive index of the ITO substrate was assumed to be 1.5.

$$P_c(\text{corrected light output}) = P_m(\text{measured light output}) / 0.27 \quad (\text{nW}) \qquad (2.3)$$

$$\textit{Photon Flux} = (P_c / h\upsilon) \quad (\text{Photon / second}) \qquad (2.4)$$

where h is the Frank's constant and υ is the wavelength of light output.

$$\textit{Electron Flux} = (I / e) \quad (\text{electron / second}) \qquad (2.5)$$

In this equation, I is the measured current (mA) and e is the charge current. The external quantum efficiency (EQE) is calculated as the values of photon flux and electron flux.

$$EQE(\%) = [(I / e) / (P_c / h\upsilon)] * 100 \qquad (2.6)$$

Maximum light output was a practical important parameter. The light output in nW is converted into cd/m^2 through the optometer measurement (S370 from Graseby Optronics). The approximate conversion factor for the Ru complex based devices were determined as 25 - 30 nw=1 cd/m^2.

REFERENCES

[2.1] Chiang, J. H.; MacDiarmid, A. G. *Synth. Met.* **1986**, *13*, 193.

[2.2] Royappa, A. J.; Rubner, M. F. *Langmuir* **1992**, *8*, 3168.

[2.3] Lee, J-K.; Yoo, D.; Handy, E. S.; Rubner, M. F. *Appl. Phys. Lett.* **1996**, *69*, 1686.

[2.4] *Inorganic Synthesis* **1990**, *28*, 338.

[2.5] Lee, J-K.; Yoo, D.; Rubner, M. F. Submitted in *Chem. Mater.* **1997**.

[2.6] Zisman, W. A. in "Contact Angle, Wettability, and Adhesion"; Advance in Chemistry Series No. 43; American Chemical society: Washington D.C., 1964, p1.

[2.7] Schrader, E.; Loeb, G. I. "Modern Apporach to Wettability"; Plenum Press: New York, 1992.

[2.8] Mittal, K. L. "Contact Angle, Wettability and Adhesion"; VSP: Utrecht, 1993.

[2.9] Azzam, R. M. A.; Bashara, N. M. "Ellipsometry and polarized light"; North-Holland Publishing Company: Amsterdam, 1977.

[2.10] Ulman, A. "An Introduction to Ultrathin Organic Films from Langmuir-Blodgett to Self-Assembly"; Academic Press: San Diego, 1991.

[2.11] Kawai, T.; Umemura, J.; Takenaka, T. *Langmuir* **1989**, *5*, 1378.

[2.12] Vandevyver, M.; Barraud, A.; Teixier, R.; Maillard, P.; Gianotti, C. *J. Colloid Interface Sci.* **1982**, *85*, 571.

[2.13] Eklind, H.; Hjertberg, T. *Macromolecules* **1993**, *26*, 5844.

[2.14] Bower, D. I.; Maddams, W. F. "The Vibrational Spectroscopy of Polymers"; University of Cambridge Press: Cambridge, 1989.

[2.15] Coleman, M. M.; Su, Y.; Painter, P. C. *Macromolecules* **1994**, *27*, 127.

[2.16] Greenham, N. C.; Friend, R. H.; Bradley, D. D. C. *Adv. Mater.* **1994**, *6*, 491.

CHAPTER 3

SURFACE MODIFICATIONS AND LAYER STRUCTURES OF LAYER-BY-LAYER SEQUENTIAL ADSORBED MULTILAYERS

1. Introduction

Surface properties of materials play important roles in applications such as paints and coatings, adhesives, lubrication, biocompatible materials and separation methods [3.1 - 3.5]. In these applications, high-energy solid surfaces promote the adhesion of solutes such as polymers, inks, paints, proteins, and cells, while low-energy solid surfaces provide chemically inert and non-wettable interfaces.

Several methods have been developed to modify the surfaces of polymers and siliceous surfaces [3.1]. The incorporation of surfactant onto the materials, corona discharge [3.6, 3.7] and other low-pressure plasma treatments [3.8 - 3.11], as well as chemical methods [3.12 - 3.15] have all been used to incorporate functional groups, capable of interaction with liquids, onto the surface.

The disadvantage of using common surfactants is that the hydrophilic properties rendered by such materials are easily destroyed by the surfactant being dissolved in water. The corona discharge and cold plasma treatments are currently being used in industry to implant oxidized functional groups thereby creating high energy surfaces which work to enhance coating, printing and adhesive bonding. The drawbacks of these techniques are the severe conditions required for the impingement of various ions, radicals, and electrons onto the surface. This treatment also does not produce well-defined surfaces due to various reactions at the surface. In addition, the prepared surfaces are relatively unstable due to the high concentration of functional groups at the solid-liquid or solid-gas interface. This high concentration causes the functional groups to differ away from

the interface. Therefore, the modified substrates should be used in a short time (about a few days) to maintain the modified surface properties.

Chemical methods are also possible ways to modify the wettability of a solid surface, but the problems associated with this technique lie in the severe reaction processes required to generate functional groups on the surfaces. The technique seems to be impractical for a wide range of applications. These severe chemical reactions influence not only the surface but also the bulk properties of polymeric materials. A simple technique for surface modification that can be maintained for an extended time is therefore an important topic for many researchers.

A novel layer-by-layer sequential adsorption technique has been introduced to modify surface properties. This technique makes it possible to apply to any surface (e.g., hydrophobic, hydrophilic, films with various surface groups, etc.) a thin polymer film in a layer-by-layer manner using aqueous solutions. This sequential adsorption technique was considered as a possible way to modify surface properties because of the well established fact that the surfaces of many different types of materials can be dramatically modified by the adsorption of a thin film of a polymeric material [3.16, 3.17]. In this new deposition mode, layers of polycations and polyanions are sequentially adsorbed onto a substrate surface by alternate dipping the substrate into dilute aqueous solutions of these polyelectrolytes. The ionic attractions developed between the oppositely charged polyelectrolytes promote a strong interlayer adhesion and a uniform and linear deposition process. In this dipping procedure, individual layers have their own functional groups which can be used to achieve desirable surface properties. Polyelectrolytes with strong adsorption to a surface are suitable for the first layer, while control over the desired surface property is obtained by the consecutive layers.

The first part of this chapter will show that the wettability of a surface can be systematically controlled via the deposition of suitable multilayers of polycations and polyanions. For example, the fabrication of a completely wettable surface on siliceous substrates through the use of this layer-by-layer deposition technique will be discussed. If the surface is hydrophilic enough to inhibit the creation of water droplets on the surface, anti-fogging and easy cleaning

behaviors can be obtained through the strong interactions between water and the modified surface. Polyelectrolytes are typically adsorbed onto a surface from a dilute aqueous solution with an adsorption time of about 15 minutes usually being sufficient to achieve the complete coverage. The amount and structure of the deposited polyelectrolyte in each layer is determined by the nature of the polyelectrolyte/surface interaction and the condition of the dipping solutions. We can control the adsorption to form either a more extended chain and consequently thinner layer, or to favor a more coiled chain and thicker layer.

In the second part of this chapter, the systematic changes of the layer thickness and the level of interdiffusion of layers in the layer-by-layer deposition of multilayer films will be examined. Various films of poly(allylamine hydrochloride) (PAH) and poly(acrylic acid) (PAA) were produced by controlling pH, ionic strength and concentration of the polyelectrolyte solutions. PAH and PAA layers were introduced because these two layers have distinct wettabilities and are sensitive to the dipping condition. Incremental thickness measurements and the selective adsorption of cationic dye molecules onto the multilayer films were need to probe the adsorption behavior of the PAH and PAA. The use of static water contact angles demonstrated that the surface wettability showed a layer-by-layer oscillation and the amplitude of these oscillations in the even-odd number layer pattern reflected the different levels of interdiffusion of the two layers.

2. Contact Angle and Wettability

2.1 Definitions

Contact angle measurement is one of the most convenient and most sensitive methods of characterizing a solid/liquid interface as it directly measures the fundamental energies at an interface, although it is not easy to get precise data or to interpret the experimental data. The relationship between surface tension and wetting was first discussed by Young [3.18] in 1805. A small drop of a liquid was placed onto a flat level surface of a film and an angle between the drop

and the surface at the air-liquid-surface interface was measured (depicted in Figure 3.1). The contact angle is considered to be the result of the mechanical equilibrium of the drop resting on a plain solid surface under the action of three surface tensions- γ_{lv} at the interface of the liquid and vapor phases, γ_{sl} at the interface of the solid and liquid phases, and γ_{sv} at the interface of solid and vapor phases. Hence, for a liquid drop on a solid surface, the equilibrium situation is given by Young's equation (3.1).

$$COS\theta = \frac{\gamma_{sv} - \gamma_{sl}}{\gamma_{lv}} \qquad (3.1)$$

From Young's equation, $COS\theta$ is proportional to the difference between γ_{sv} and γ_{sl}. The value of γ_{lv} does not depend on the surface. This means that the interaction between a surface and a liquid drop dominates the value of the contact angle. The lowest energy state will correspond to the liquid spreading out to cover as much of the solid surface as possible.

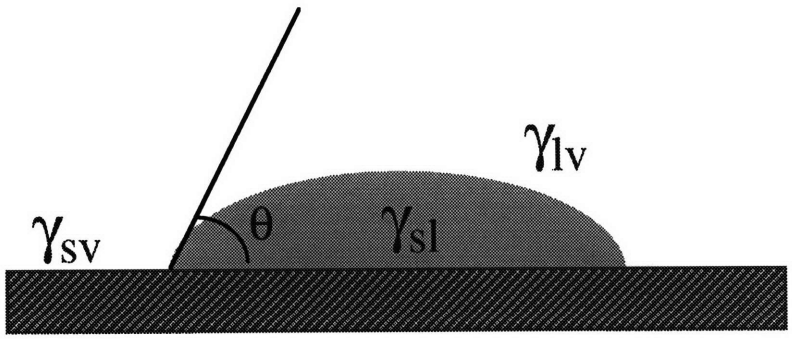

Figure 3.1. A sessile liquid drop on a flat surface indicating contact angle.

The direct measurements of the contact angle can be used to give a definition to the notion of wettability and indicate the surface parameters or interfacial tensions such as γ_{lv}, γ_{sl}, and γ_{sv}, which cannot be directly measured.

Suppose $\gamma_{sv} - \gamma_{sl} \leq \gamma_{lv}$, then Young's equation may also be written

$$COS\theta = \frac{\gamma_s - \pi_{esv} - \gamma_{sl}}{\gamma_l - \pi_{elv}} \qquad (3.2)$$

where the π terms are defined by the following equations.

$$\gamma_s \equiv \gamma_{sv} + \pi_{esv} \qquad (3.3)$$

$$\gamma_l \equiv \gamma_{lv} + \pi_{elv} \qquad (3.4)$$

Here, γ_s and γ_l are the surface free energies of the separate phases in contact only with their own vapor, and the π_e terms are the equilibrium spreading pressures. The film pressure at the liquid-vapor interface, π_{elv}, is commonly ignored because the adsorption at the liquid-vapor interface will be small if the solubility of the solid in the liquid is very low. The π_{esv} term is measured experimentally, and its value can be negligible for molecularly smooth low-energy solids, when a liquid forms non-zero contact angle. The measurement of π_e is not a simple matter on a macroscopic solid surface. The two π_e values are tacitly assumed to be negligible [3.19]. In the approximation that π_{esv} and π_{elv} can be neglected, Young's equation becomes a simplified equation (3.5).

$$COS\theta \cong \frac{\gamma_s - \gamma_{sl}}{\gamma_l} \qquad \gamma_s - \gamma_{sl} \leq \gamma_l \qquad (3.5)$$

$$\gamma_s - \gamma_{sl} \geq \gamma_l \qquad \text{if} \quad \text{COS}\,\theta = 1 \qquad (3.6)$$

Young's equation is now a function of experimental data, such as the surface tension of a liquid drop and a solid surface. In principle, we can extrapolate the data of γ_{sl} based on measured contact angles by using the known value of γ_l and measurable value of γ_s. In reality, however, it is still hard to differentiate between γ_s and γ_{sl} in the contact angle data because the heterogeneity, reorientation, solubility and interaction of the surface all affect the wetting behavior of a liquid drop.

To access the wetting behavior in terms of the surface tension of the liquid, the equation based on adhesion forces was suggested. The equilibrium energy of adhesion is the reversible

force required to separate a unit area of liquid from a solid. It is defined by the Young-Dupré equation [3.20]

$$\Delta G_{sl}^{a} = -\gamma_l(1+\cos\theta) \qquad (3.7)$$

Israelachivili and Gee suggested a more general experimental approach to the treatment of the wetting behavior based on this equation [3.21]. ΔG_{sl}^{a} may be divided into two different forces; Lifshitz-Van der Waals attraction (LW) and acid-base interaction (AB) [3.22]. Each force is defined as follows.

$$\Delta G_{sl}^{a} = \Delta G_{sl}^{aLW} + \Delta G_{sl}^{aAB} \qquad (3.8)$$

$$\Delta G_{sl}^{aLW} = -2\sqrt{\gamma_s^{LW} \cdot \gamma_l^{LW}} \qquad (3.9)$$

$$\Delta G_{sl}^{aAB} = -2\sqrt{\gamma_s^{+}\gamma_l^{-}} - 2\sqrt{\gamma_s^{-}\gamma_l^{+}} \qquad (3.10)$$

which yield the following important equation

$$\gamma_l(1+\cos\theta) = 2\sqrt{\gamma_s^{LW} \cdot \gamma_l^{LW}} + 2\sqrt{\gamma_s^{+}\gamma_l^{-}} + 2\sqrt{\gamma_s^{-}\gamma_l^{+}} \qquad (3.11)$$

If we measure γ^{LW}, γ^{-} and γ^{+}, the contact angle is then defined. We can possibly map the values of surface tensions through the several measurement of contact angles [3.23]. The values of γ^{LW} terms do not vary to a material, and is smaller than the ionic interaction parameters, γ^{-} and γ^{+}. The amount of acid-base interaction at the interface contributes the wetting behavior more strongly.

In order to obtain simple quantitative correlation between the acid-base contribution in equation (3.11) and the work of adhesion can be separated into the surface population of acidic or

basic sites, N^{ab}, and the enthalpy of the acid-base interaction, ΔH^{ab} according to the Fowkes and Mostafa equation [3.24],

$$W^{ab} = -fN^{ab} \cdot \Delta H^{ab} \qquad (3.12)$$

Here, f is a factor for converting the enthalpy to free energy. f is less than unity. The number of interaction sites between the solid and liquid is important in determining the wetting of a surface.

In the layer-by-layer deposition, there are many charged ionic groups on the surface of the multilayer films. Some of these groups are directly connected to the underlying oppositely charged layer and others are dangling and not attached to the surface. For dangling functional groups such as, sulfonic acid and amine, as the drop advances over the surface, γ_{sl} would be compensated by the relative amounts of ionized and deionized groups on the surface [3.25 - 3.27]. The work of adhesion is equivalent to the negative free energy change associated with the contacting event or adhesion of two phases, that is $W^{ab} = -\Delta G^{a}$. The free energy of spreading is strongly affected by the number of ionic groups on the surface. The extent of water wettability should depend directly on the number of ionic interaction sites at the contact area. Surfaces which have an ionic character are likely to be hydrophilic whereas surfaces of materials where covalent bonds or Van der Waals forces predominate are likely to be hydrophobic. Only weak van der Waals forces exist at the fluorocarbon surface which are the most hydrophobic of all common organic substances. The latter part of the equation (3.11) goes to zero when unpolar polymers, such as polyethylene and poly(tetraflouride), interact with liquids.

Water is considered to have the same tendency for deprotonation and protonation. γ^{+} and γ^{-} of water are defined as value of 25.5. A high concentration of charge on the surface can enhance its hydrophilic nature. In other words, the hydrophilicity of a surface is proportional to the number of charges on the surface. The hydrogen bonding and acid-base interactions at the interface are very important forces which can enhance wettability. This equation indicates that our

polyelectrolyte depositions can modify the wettability through the ionic interactions as well as the functional group at the surfaces.

2.2 Sensitivity of Contact Angle Measurement

As "interphase" is defined to be the depth sensitivity by an analytical tool. The interphase of wetting is in 5 - 10 Å of a solid from the surface. The functional groups outside this region from the surface do not influence the wetting behavior of the solid surface. In case that liquid can penetrate into solid materials or dissolve surface, the interphase is deeper than 5 - 10 Å region. Contact angle measurement is one of the most sensitive methods of analyzing surface properties.

An advancing angle is measured by slowly adding liquid from a syringe to a drop already on the surface. The advancing contact angle (θ_A) is the kinetically stationary angle formed after a drop has advanced across a surface. The accuracy of the advancing angle measurement is enhanced by the cautious addition of water onto the water drop. Agreement between different individuals measuring the same drop will be about 1 -2°. It is recommended that measurements of contact angle are often made on both sides of the several drops and the numbers averaged. A receding contact angle (θ_R) is the kinetically stationary angle formed after a drop has receded across a surface.

2.3 Surface Roughness Effect on Contact Angles

Solid surfaces are known to be inhomogenous on a molecular scale, as well as on a (sub) microscopic or even macroscopic scale, both physically and chemically. Physical inhomogeniety, i.e., surface roughness changes the area of the solid-liquid interface. One can define a true contact angle (θ_{true}), an observed contact angle (θ), and a roughness factor (r), which is defined as the ratio between the true surface area and its geometrical area ($r \geq 1$) and can be expressed by the following relationship [3.28, 3.29]

$$COS\theta = r \cdot COS\theta_{true} \qquad (3.13)$$

According to this equation, a rough surface will increase a contact angle for those that are greater than 90° and decrease those that are less than 90°.

A hysteresis, defined as the difference between the advancing and receding contact angle, is strongly related to surface roughness. A measure of surface roughness can be given by the difference between the contact angle, θ_A, observed in advancing the liquid boundary over a dry, clean surface and the angle θ_R, observed in receding the liquid boundary over the previously wetted surface. A rougher, nonpolar surface will increase the advancing contact angles and decrease the receding contact angles and as a result, the hysteresis will also increase. Although the roughening of the surface does increase the advancing angles, it is found that the effect of roughness is much more pronounced in the measurement of receding angles. The results by [3.30, 3.31], suggest that the absolute value of advancing contact angles are more accurate in determining the chemical composition of a surface [3.19]. Micron scale roughness can exhibit the observed differences in contact angles, but the roughness of our multilayer film is under 100 Å. It can be assumed that the different contact angles observed in layer-by-layer deposited films come primarily from the chemical composition on the surface. The advancing contact angles are quite reproducible and accurately measure the surface properties and the relative amounts of functional groups present. The contact angles can be interpreted in terms of the structure and composition of the outermost layers.

3. Surface Modification by Layer-by-Layer Sequential Adsorption Technique

3.1 Surface Properties of 1 Bilayer of Several Polyelectrolytes

Sequentially adsorbed films with various polycations and polyanions were fabricated on hydrophilic glass microscope slides. The adsorption process was begun by first depositing a polycationic layer, such as poly(aniline) (PAN) or poly(allylamine hydrochloride) (PAH), onto the slides to generate positive charges. Polyanions were then applied as an outermost layer to modify

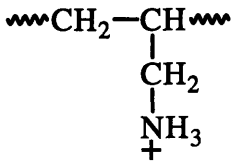

Poly(allylaminehydrochrolide) (PAH)

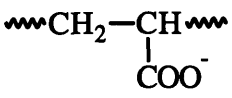

Poly(acrylic acid) (PAA)

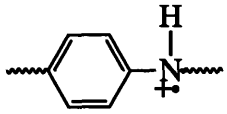

Poly(aniline) (PAN)

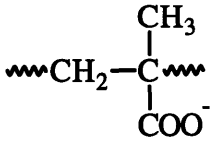

Poly(methacrylic acid) (PMA)

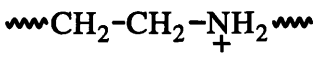

Poly(ethyleneimine) (PEI)

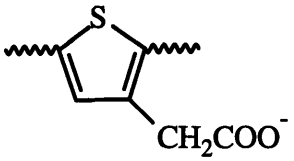

Poly(thiophene-3-acetic acid) (PTAA)

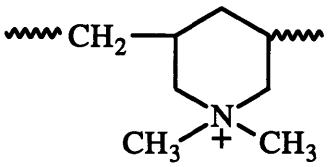

Poly(diallyldimethyl)amine (PADA)

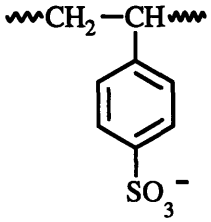

Poly(sulfonated styrene) (SPS)

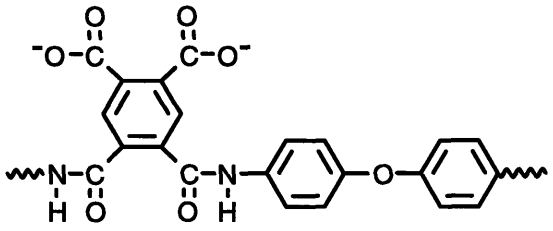

PMDA-ODA (unconverted)

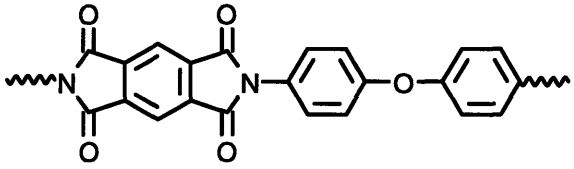

PMDA-ODA (converted)

Figure 3.2. Chemical structures of polyelectrolytes used to construct multilayer thin films.

surface properties. The structures of the polycations and polyanions used in this study are shown in Figure 3.2. We tried to determine the effect of various polyanions as the outermost layer on the wettability of the surface. To answer this question, a series of different combinations of PAH or PAN with other polymers was used for the surface modification. The surface hydrophilicity of a single bilayer was determined by measuring the advancing contact angle of water drops on the surface. The contact angle of uncoated hydrophilic glass slides was determined to be about 10° ± 2.

Table 3.1 shows that single bilayer films made from combinations of polycations and various polyanions produced different surface properties ranging from hydrophilic to hydrophobic. The contact angles in table 3.1 indicate that by simply changing the outermost layer, significantly different surfaces in terms of wettability were produced according to the chemical structure of the polyions. In addition, the surface properties of the outermost polyions are also influenced by the dipping conditions. As a result, the hydrophilic nature of the outermost layer determined the wettability of the multilayer films. The carboxylic acid groups of poly(acrylic acid) (PAA) produce completely wettable surfaces, while the aromatic groups of converted (PMDA-ODA), poly(thiophene-3-acetic acid) (PTAA) and sulfonated poly(styrene) (SPS) produce hydrophobic surfaces despite the fact that they have ionic groups in the side chains. Our group has recently shown that the contact angle of the outermost layer of poly(phenylenevinylene) (PPV) was more than 100° indicating that very hydrophobic surfaces are possible with this technique. The results in Table 3.1 suggest that this layer-by-layer deposition is a unique way to control wettability onto a surface. The different conditions of dipping solutions also changed the wettability of the 1 bilayer samples.

As will be discussed shortly, the number of unbound charged groups, and the level of interpenentration of each layer as well as the chemical structure of the polyions play important roles in generating the different surface wettabilities. The fabrication of various PAH/PAA structures by changing the conditions of PAH and PAA dipping solutions and a proposed model of the layer-by-layer deposition will be discussed in the latter part of this chapter.

Table 3.1. Different surface properties by changing polyanionic layers. Hydrophilic substrates were used. No ionic strength adjusted in polyanionic solutions.

Combination of Bilayer Films	Contact Angle (degrees)
A. PAH as cationic layer	
1. PAH / Poly(acrylic acid) pH 2.5 - Auto-dipping	‹ 5
2. PAH / Poly(acrylic acid) pH 2.5 - Hand-dipping	18 ± 5
3. PAH / Poly(methacrylic acid) pH 2.5 - Auto-dipping	11 ± 2
4. PAH / Poly(methacrylic acid) pH 2.5 - Hand-dipping	20 ± 4
5. PAH / Poly(3-thiophene acetic acid) pH 4.3	50 ± 3
6. PAH / Sulfonate Poly(styrene) pH 2.5	55 ± 2
7. PAH / PMDA-ODA (unconverted) pH 3.8	37 ± 6
8. PAH / PMDA-ODA (converted) pH 3.8	72 ± 3
B: PAN as cationic layer	
1. PAN / Poly(methacrylic acid) pH 2.5 - Hand-dipping	23 ± 3
2. PAN / Poly(vinyl pyrrolidone) pH 5.3	34 ± 3
3. PAN / Poly(vinyl alcohol) pH 5.3	35 ± 3
4. PAN / Poly(3-thiophene acetic acid) pH 4.3	51 ± 2
5. PAN / Poly(sulfonate styrene) pH 2.5	51 ± 2

* Polyaniline(PAN) Solution Conc. 10^{-3} M, pH 2.5

* Polyallylamine(PAH) Solution Conc. 10^{-2} M, pH 2.5

* Polyanionic Solution Conc. 10^{-2} M

It is also observed that different methods of dipping generate different hydrophilic surfaces of PAH/PMA and PAH/PAA. The automatic dipping method produced a completely wettable surface (contact angle ‹ 5°), while the hand-dipping method only produced a surface with a contact angle of about 18°. The automatic dipping process increased the concentration of PAA

and thereby the density of carboxylic acid groups on the surface. The completely wettable surface successfully inhibited the formation of fog by blocking water aggregation on the surface. The PMA layer showed a slightly higher contact angle as compared to the PAA layer. These experimental results show that only 1 bilayer of adsorbed material can effectively modify the surface properties and can be systematically controlled with a combination of polyelectrolytes.

In order to explore the effects of multiple layers and the subsequent layer dependence, samples having from 1 to 12 layers of PAH/PTAA and PAH/PAA were built up and the wettability of the samples measured. The contact angle data of these consecutive layers can give us some information about the contribution of each layer to the wettability of the surface.

3.2 Surface Properties of PAH/PAA and PAH/PTAA Multilayer Films

The sequentially adsorbed layers of PAH/PAA on hydrophobic slide substrates and PAH/PTAA on hydrophilic slide substrates were fabricated with a PAH solution (pH 2.5 , 10^{-2} M), a PAA solution (pH 2.5, 10^{-2} M) and a PTAA solution (pH 4.3, 10^{-3} M, NaCl 0.4 M) using both the automatic dipping and the hand dipping method.

Figure 3.3 shows that these deposited multilayers can be used to alter the surface wettability of both hydrophilic and hydrophobic substrates. An odd number of layers indicates a PAH as the outermost layer, whereas an even number of layers indicates PAA or PTAA as the outermost layer. It can be seen in the PAH/PAA adsorbed layers that the contact angle systematically alternates between a completely wettable surface to one with a contact angle around 28°, depending upon the outermost layer (the polycation or the polyanion). The oscillation continues to about the same degree even after 12 layers have been deposited onto the surface. These results clearly show that each individual layer distinctly affects the wettability of the surface. After only one bilayer of polyelectrolyte deposition, the surface of the substrate was modified to be completely wettable. This oscillation in contact angle, however, is seen to be much less for the case of the PAH/PTAA system as opposed to the PAH/PAA system. The small oscillation observed suggest that the surface properties do not depend much on the outermost layer in the

PAH/PTAA system. It is believed that the reasons for the small contact angle oscillation are that the two layers are heavily interdiffused and also have similar wettabilities. The thickness per bilayer of the PAH/PTAA system was about 22 Å and that of PAH/PAA (automatic dipping method) was about 42Å.

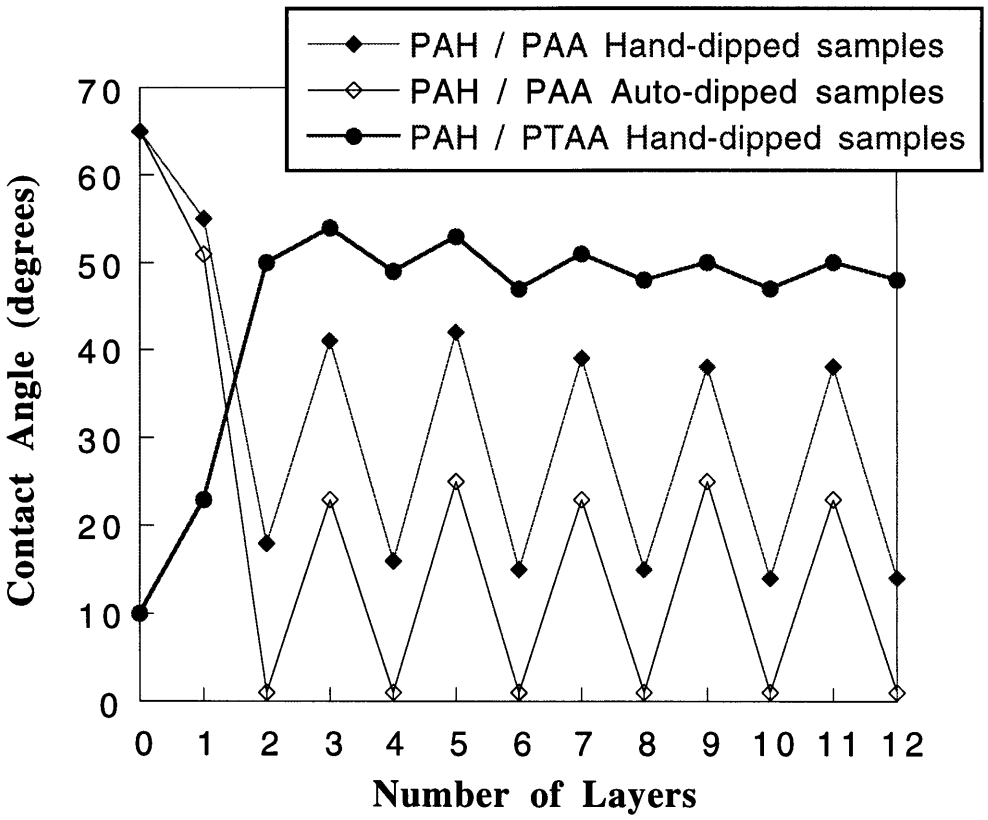

Figure 3.3. Contact angles of PAH/PTAA layers on hydrophilic slide glasses and PAH/PAA layers on hydrophobic slide glasses.

For the hydrophilic substrate, it only takes 1 bilayer of the PAH/PTAA system to change the contact angle from 10 to about 50, thereby rendering the surface less wettable. Similarly, a hydrophobic surface can be modified to be a completely wettable by depositing 1 bilayer of the PAH/PAA (10^{-2} M, pH 2.5 / 10^{-2} M, pH 2.5) system through the automatic dipping method.

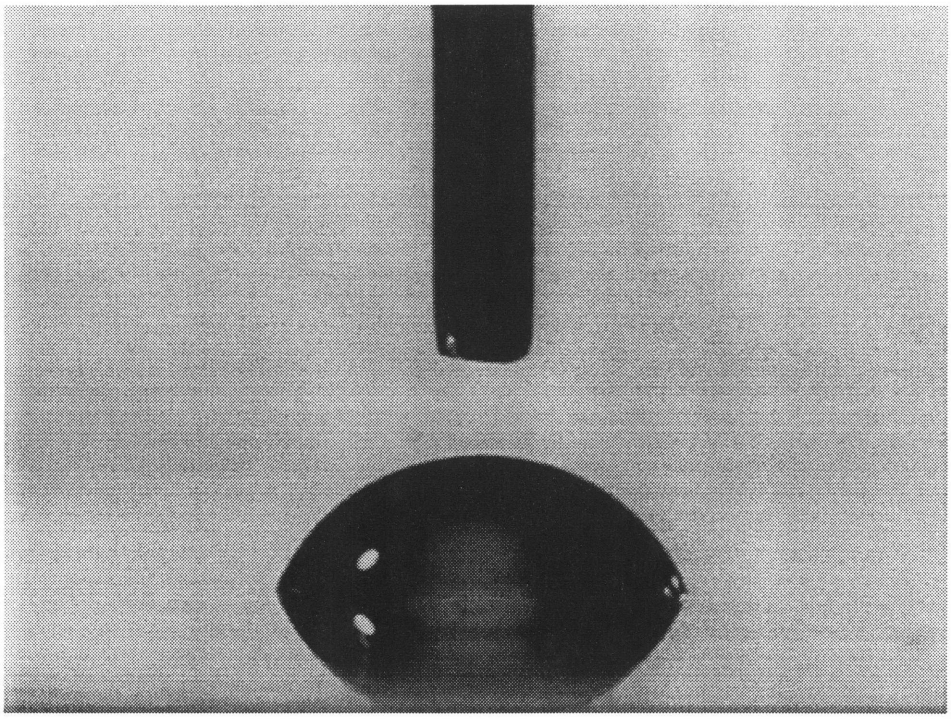

(a)

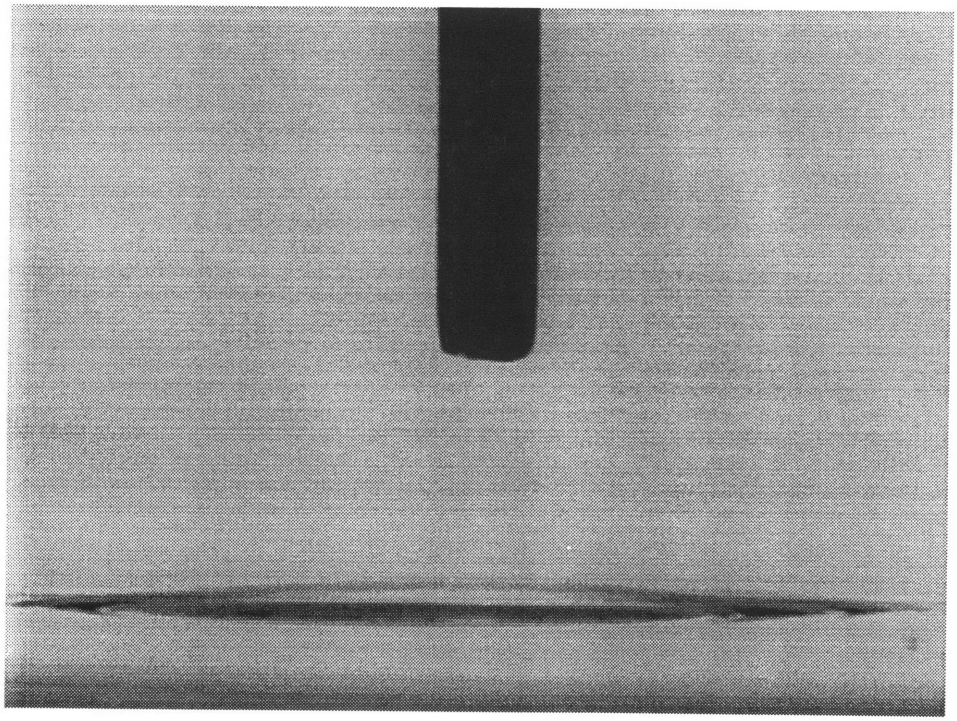

(b)

Figure 3.4. Contact angles of (a) hydrophobic slide glass and (b) 1 bilayer of PAH/PAA on hydrophobic slide glass with PAA as outermost layer.

It is also observed that PAH layers in the PAH/PTAA system have higher contact angles than the PAH layer in PAH/PAA system. The different wettabilities of the PTAA layer and the PAA layer apparently affected the contact angles of PAH layers in the PAH/PAA and PAH/PTAA multilayer films. The influence of the underneath layer on the wettability of outermost layers suggests that layers are interdiffused up to some level, though the layer-by-layer wettability dependence is still observed. The contact angles of PAH/PAA samples have shown the strong dependence on the processing method. The automatic dipping methods did not apply the blow drying station between dippings, instead, three water rinsings were applied. The thickness data show that the thickness per bilayer of hand-dipped samples was about 33 Å, while the auto-dipped samples was about 42 Å. It might be that the auto-dipping processing helped to keep the swelling of polyions to enhance the amount of adsorption and soaking in water bin for 10 minutes which, in turn, helped the ionized PAA layers to increase the number of sites, even though the number of charges on the surface were titrated again with the pH of PAH solution when the samples were dipped.

Figure 3.4 shows the pictures of water droplets on one bilayer of PAH and PAA and on a hydrophobic slide glass. Only 1 bilayer, which had about 40 Å thickness, successfully produced a completely wettable surface. As long as the bottom layer generates sufficient positive charges on a surface, the completely wettable surface will be obtained by the technique.

3.3 Acid-Base Interaction in Wetting

The completely wettable surfaces were produced by the carboxylic acid groups on the surface. Those groups in polyions can be interconverted from CO_2H to CO_2^- by changing the pH of the solutions. If there is an acid-base reaction on the surface, the additional work goes to increase the wettability of the surface. Whitesides et al intensively studied the interphase of self-assembled monolayer (SAM) structures of their films with titration contact angles [3.32 - 3.34]. By placing water drops of different pH on the surface, we can measure the pK_a value of the carboxylic acid groups on the sample with the PAA as the outermost layer. Because the

transformation from neutral to charged groups is more difficult in the interphase region, higher pK_a values in the solid state than those in the solution state were generally observed using this contact angle titration method. If the pH of the water drops is higher than the pK_a, we expect the acid-base interaction at the surface. One of the interesting results of the study is that the higher concentration of carboxylic acid groups on the surface decreased the actual pK_a value at the surface. This implies

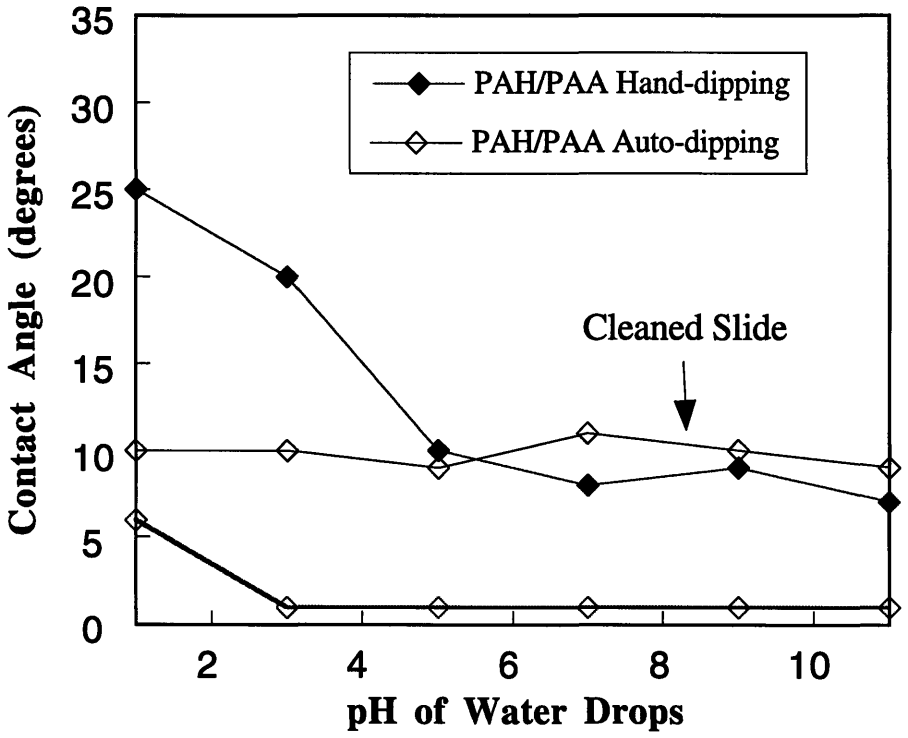

Figure 3.5. Contact angle titrations of 3 bilayers of PAH/PAA with PAA as outermost layers

that the transition of titration of contact angles was decreased with increase of the amount of carboxylic groups on the surface. Even though the carboxylate form (COO^-) induced more hydrophilic character, a high density of unconverted -COOH groups also can work to make the surface hydrophilic sites [3.35]. The lower pH (strong acid) cannot convert the number of the carboxylic groups and therefore interacts less with water drops on the surface. Using contact angle

titration, contact angles of 3 bilayers of PAH and PAA, fabricated by both hand-dipping and auto-dipping, were measured with drops ranging in pH from 1 to 11. Figure 3.5 shows that acidic water (pH $\leq$ 3) produced higher contact angles than neutral and basic water. When the contact angle was lower than 10°, there was almost no dependence on the pH of the drops except for the pH 1 drop [3.33]. Our results are comparable to the results of Whitesides et al where the surfaces are perfectly covered by SAM structure with the carboxylic groups. From these results, it can be concluded that the completely wettable surfaces were obtained primarily by the high density of carboxylic groups on the surface and not from the work of acid-base conversion.

3.4 Fabrication of Completely Wettable Surface

Several different cationic polyelectrolytes, such as PEI, PADA and PAH were used for building up multilayer films. If the polycation is deposited strongly on the surface, the next layer is attached to the positive charges of the layer. As long as the first polycationic layer deposits a sufficient number of charged sites on the surface, the outermost layer will deposit the same amount and thereby change the wettability of the surface. Completely wettable surfaces were obtained independent of the polycations. PEI and PADA both provided a sufficient number of charged groups on the surface.

One and three bilayers of PAH/PAA were built up on hydrophilic, hydrophobic and treated substrates. Because the treated substrate is positively charged, the PAA was the first layer on the substrates. The 1 bilayer and 3 bilayer films of the three different substrates exhibited a completely wettable surface regardless of the nature of the substrates.

The stabilities of the completely wettable surfaces were monitored by placing the PAH/PAA samples in the air and in a 90°C oven. Figure 3.6 shows the aging of the contact angles of 3 bilayers of PAH/PAA on hydrophilic and hydrophobic substrates with time. The PAA layers retained their wettability at room temperature for more than 1 month but started to lose some of their hydrophilic character after 2 months. Figure 3.7 shows that the contact angle of the

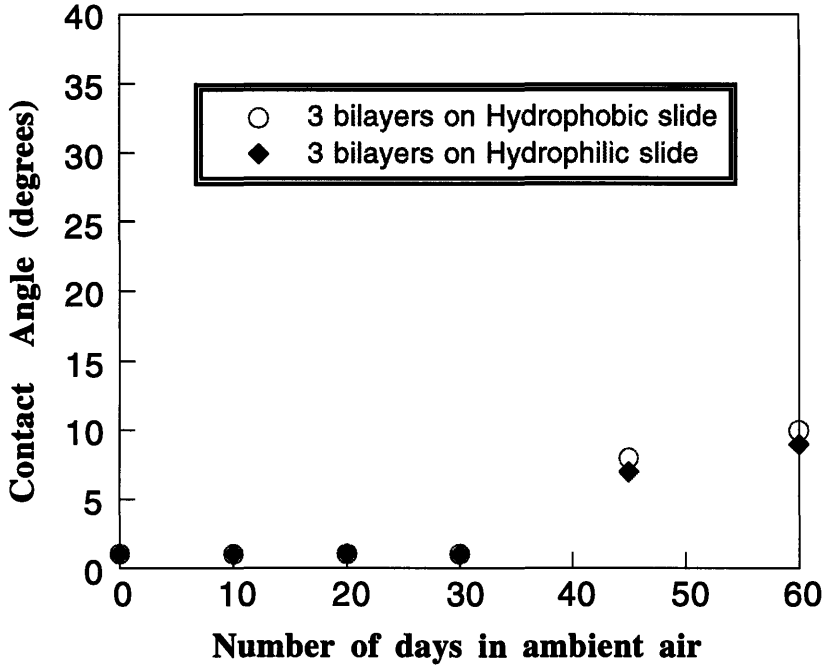

Figure 3.6. Aging effect on contact angles of PAH/PAA layers in the air.

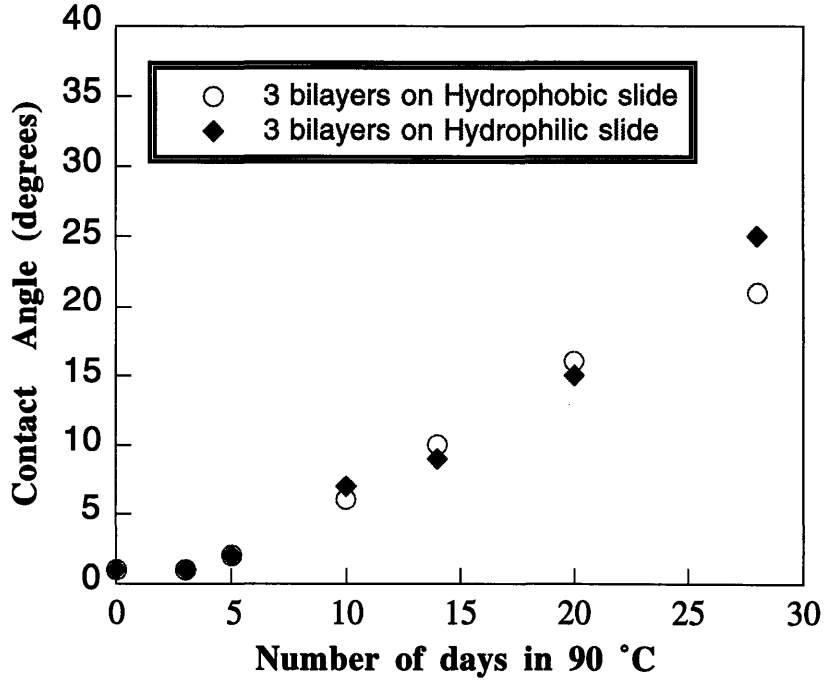

Figure 3.7. Aging effect on contact angles of PAH/PAA layers at 90 °C.

completely wettable surface, exposed to a 90°C static oven, retained its hydrophilicity for more than 1 week. Compared with modified surfaces using different conventional techniques, the layer-by-layer deposited films show excellent stability. The plasma treated polymer surface does not last more than a few days due to the reorientation of the polymer chains at the interface [3.36].

The PAH/PAA films with PAA as the outermost layer have a high density of carboxylic groups at the surface. The reorientation of the polymer chains at the surface, therefore, may not influence the wettability of PAH/PAA layers as much as in the plasma treatment. The adsorption of particles, such as dust as well as oxygen and the interdiffusion of the carboxylic acid groups decrease the hydrophilic nature of the PAH/PAA surfaces. The completely wettable surfaces are high energy surfaces that adsorbs contaminants from the air.

From previous work in our group and others, it is known that the layer thickness of the adsorbed polyelectrolyte can be manipulated by the ionic strength and concentration of the dipping solutions. The structure of the layers and the level of interdiffusion were studied by analyzing the surface properties of the multilayer films. Based on the theory and experimental results of a single layer polyelectrolyte adsorption on a charged surface, the adsorption behavior in multilayer film buildup was tried to be understood. For this study, several sets of PAH/PAA layers were made with different sets of solution conditions, which produced various thicknesses per bilayer and degrees of oscillation of the contact angles.

4. PAH / PAA Multilayer Film Fabrication

The automatic dipping method was used to build up a number of PAH/PAA layers on hydrophilic slides. The linear growth of these films with various dipping conditions was measured primarily by profilometry and confirmed through ellipsometry measurements of the films on a silicon wafer. During adsorption, the charges of the deposited polyelectrolytes limit the adsorption of additional polyions through electro-static repulsion at the interface. Figure 3.8 displays the

linear growth of PAH/PAA multilayer films up to 30 bilayers at various pH, ionic strength, and concentrations of PAH and PAA solutions.

To understand the contribution of each layer to the thickness per bilayer of the PAH/PAA samples, the thickness increment after each layer was measured on a silicon wafer by ellipsometry. The thickness per bilayer and the incremental thicknesses are summarized in Table 3.2. The results show that various dipping conditions produced different ratios of the PAH and PAA layers. When the polyelectrolyte is likely to deposit as a loopy coil, a relatively thick layer will be developed. On the other hand, when the polyelectrolyte is deposited as an extended chain, a thin layer will be obtained. PAH, with pH 2.5 and 10^{-2} M, and PAA, with pH 2.5 and 10^{-2} M, produced a linear thickness of about 42 Å where the layer of PAA was about 29 Å and the PAH layer was only about 13 Å layer. The addition of a divalent salt, $MgCl_2$, at a concentration of 0.4 M in the PAH solution produced about 58 Å per bilayer by increasing the thickness contribution of the PAH layers.

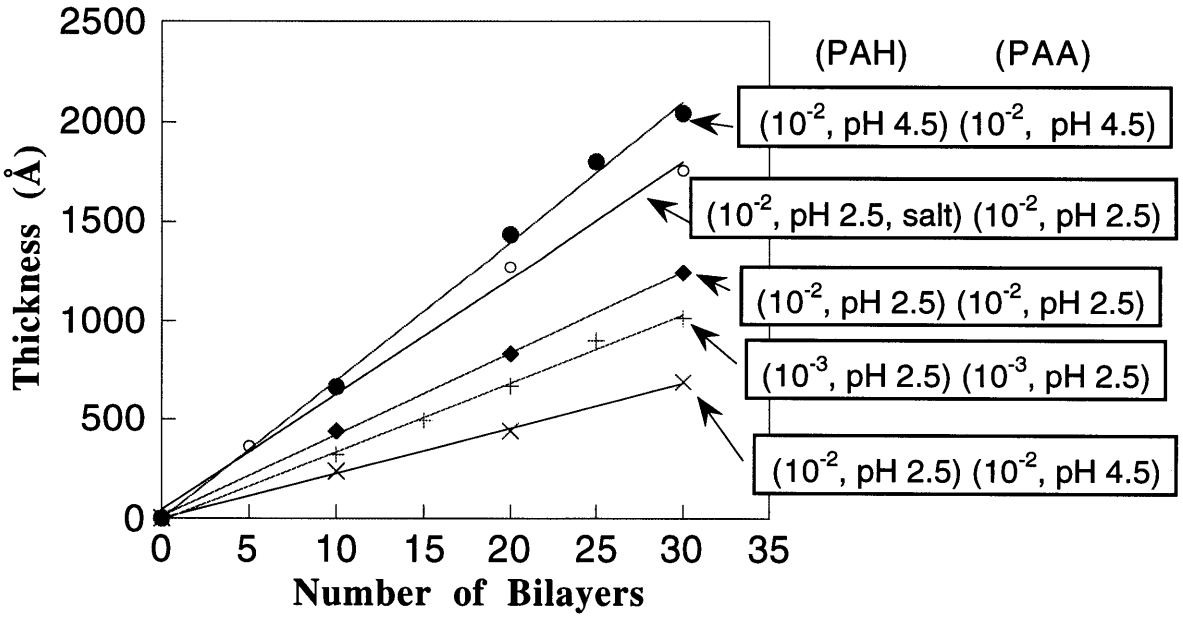

Figure 3.8. Linear growth of several sequentially adsorbed PAH/PAA films. Note that the first parenthesis shows the condition (concentration, pH) of PAH solution and the second parenthesis shows the condition of PAA solution.

PAH, with pH 4.5 and 10^{-2} M, and PAA, with a pH 4.5 and 10^{-2} M, produced even thicker layers (about 65 Å) with 47 Å contributed by the PAH and 18 Å contributed by the PAA. Compared to the PAA solution with a pH 2.5, the pH 4.5 of PAA solution produced a thin layer with a more extended chain conformation. The thickest layer in the PAH/PAA systems was 72 Å per bilayer and was obtained with the combination of PAH at a pH of 4.5 and 10^{-2} M and PAA at a pH of 2.5 and 10^{-2} M. This made thick layers of both PAH and PAA, but the film growth turned nonlinear after 10 bilayers. The thinnest layer in the PAH/PAA systems, 29 Å per bilayer, was produced by the condition of PAH with a pH of 2.5 and 10^{-2} M and PAA with a pH of 4.5 and 10^{-2} M. The lower concentration of PAH and PAA solutions with 10^{-3} M produced 32 Å per bilayer.

In Table 3.2, we can see that a pH of 2.5 for the PAA solution produced about 30 Å while a pH of 4.5 of PAA produced about 16 Å regardless of the PAH solution conditions. The

Table 3.2. Layer thickness of PAH/PAA with different solution conditions (*** no data generated).

Condition of PAH Solution	Condition of PAA Solution	PAH layer contribution to bilayer	PAA layer contribution to bilayer	Total Thickness per bilayer
10^{-2} M, pH 2.5	10^{-2} M, pH 2.5	13 ± 2 Å	29 ± 2 Å	42 ± 3 Å
10^{-2} M, pH 2.5 ($MgCl_2$ 0.4 M)	10^{-2} M, pH 2.5	28 ± 3 Å	30 ± 3 Å	58 ± 4 Å
10^{-2} M, pH 4.5	10^{-2} M, pH 2.5	39 ± 3 Å	33 ± 2 Å	72 ± 3 Å
10^{-2} M, pH 4.5	10^{-2} M, pH 4.5	47 ± 2 Å	18 ± 2 Å	65 ± 3 Å
10^{-2} M, pH 2.5	10^{-2} M, pH 4.5	14 ± 3 Å	15 ± 3 Å	29 ± 3 Å
10^{-3} M, pH 2.5	10^{-3} M, pH 2.5	***	***	32 ± 2 Å

same trend was observed in the thickness data for a pH of 2.5 and 4.5 for the PAH solution. The thickness of PAH layers fabricated at the pH 2.5 was about 15 Å and that fabricated at the pH 4.5 was in the range of 40 Å. These results suggest that the thickness of previously deposited layers in the PAH/PAA systems may not affect the additional layer thickness of the oppositely charged layers. This phenomena will be discussed in the discussion section in greater detail.

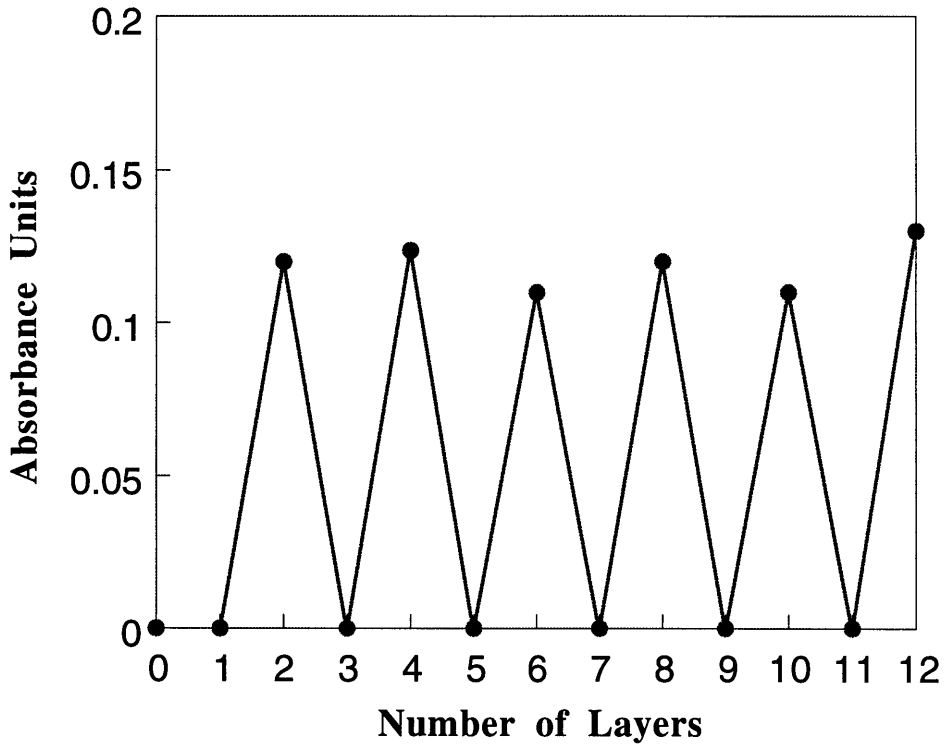

Figure 3.9. The amount of methylene blue dye adsorption onto PAH/PAA layers fabricated by pH 2.5, 10^{-2} M of PAH with $MgCl_2$ 0.4 M and pH 2.5, 10^{-2} M of PAA solutions.

A simple dying technique was introduced to give a relative measure of the amount of carboxylic acid groups on the surface. By dying the adsorbed layers with positively charged methylene blue, the intensity of the methylene blue absorption indirectly indicates the amount of negative charge on the surface. Because the dye molecule may, however, diffuse into the

multilayer films, the methylene blue dipping time was controlled to be rather short. The consecutive layers from 7 through 10 were dipped into the methylene blue dye solution for 10 minutes. Methylene blue did not detectably adsorb onto a bare glass slide. For the odd numbered layers, PAH is the outermost layer, if it covers the previous layer completely, the positive charges of the methylene blue will be repelled by the positive charges of the PAH. Figure 3.9 shows the relative amount of the dye adsorbed onto multilayers produced with a pH of 2.5 of 10^{-2} M PAH solution with 0.4 M $MgCl_2$ and with a pH 2.5 of 10^{-2} M PAA solution. Like the contact angle oscillation, the amount of methylene blue adsorption systematically varied with the outermost layer. The amount of dye adsorbed at the different conditions are summarized in Table 3.3.

In Table 3.3, some cases show the positively charged methylene blue dye does adsorb onto the polycationic (PAH) layers. This tends to indicate that there were some negatively charged species on the surface which promoted dye adsorption. By comparing this result to the thickness data, methylene blue was adsorbed onto the PAH layers, when the PAH forms rather thin layers.

Table 3.3. UV/Vis intensity of methylene blue absorbance peaks (at 600 nm).

Condition of PAH Solution	Condition of PAA Solution	7 layers	8 layers	9 layers	10 layers
10^{-2} M, pH 2.5	10^{-2} M, pH 2.5	0.021	0.147	0.0298	0.1369
10^{-2} M, pH 2.5 ($MgCl_2$ 0.4 M)	10^{-2} M, pH 2.5	< 0.001	0.12	< 0.001	0.11
10^{-2} M, pH 4.5	10^{-2} M, pH 2.5	< 0.001	0.068	< 0.001	0.0644
10^{-2} M, pH 4.5	10^{-2} M, pH 4.5	< 0.001	0.019	< 0.001	0.018
10^{-2} M, pH 2.5	10^{-2} M, pH 4.5	0.0041	0.0093	0.0047	0.010
10^{-3} M, pH 2.5	10^{-3} M, pH 2.5	0.0169	0.081	0.025	0.0851

This indicates that thick layers of PAH limit the access of negative charges to the surface. The largest amount of dye adsorption for an even number of layers was for the one made with a pH of 2.5 for the PAA solution, while the least amount of dye adsorption for an even number of layers was for the one made with a pH of 4.5 for the PAH solution. We can use this technique to estimate the level of interpenentration between layers as well as the amount of carboxylic acid groups on the surface.

In the previous section, the number of carboxylic acid groups primarily affected the wettability of the PAH/PAA multilayer films. By comparing the methylene blue adsorption with the layer-by-layer contact angles, information about the interdiffusion of the layers will be obtained. The various conditions generated different layer thicknesses of PAH/PAA multilayer films. The surface properties of various PAH/PAA systems are possibly explained as layer diffusions by comparing with the thickness data and the amount of methylene blue adsorption in the layer-by-layer manner.

5. Contact Angles of PAH / PAA multilayer films

5.1 Salt Effect

Multilayers of PAH and PAA on hydrophilic slides were fabricated with a pH of 2.5 and 10^{-2} M for both solutions. The contact angles for films containing from 1 to 12 layers are shown in Figure 3.10. The films with an even number of layers produced completely wettable surfaces, while the contact angle of the films with PAH as the outermost layer was about 25 - 27 degrees. The thickness per bilayer of the films was in the 41 Å range where an average layer increment was 29 Å for PAA and 12 Å for PAH. An even number of layers generated completely wettable surfaces and the highest methylene blue adsorption. Methylene blue also adsorbed onto the cationic outermost layer (PAH), which suggests that this thin PAH layer did not block the adsorption of methylene blue completely.

The contact angles of PAH/PAA multilayers on hydrophilic and hydrophobic slide substrates, with a pH of 2.5 and 10^{-2} M for both PAH and PAA solutions, are shown in Figure 3.3 and Figure 3.10. The same repeated oscillation of the contact angle by the even-odd pattern was observed regardless of the wettability of the bare substrates. The different hydrophilicity of the surfaces does not influence the wettability of the multilayer films if the first layer attaches to the surface to render sufficient positive charges.

When 0.4 M of $MgCl_2$ was added to PAH solution with a pH of 2.5, the added ionic strength increased the thickness of the bilayer to about 58 Å, which was thicker than the sample fabricated without salt by 17 Å. Figure 3.10 shows an increased oscillation of the contact angle with added ionic strength in the PAH solution. The PAH layers with salt have higher contact angles than the PAH layers formed without salt in the solution. In the methylene blue adsorption,

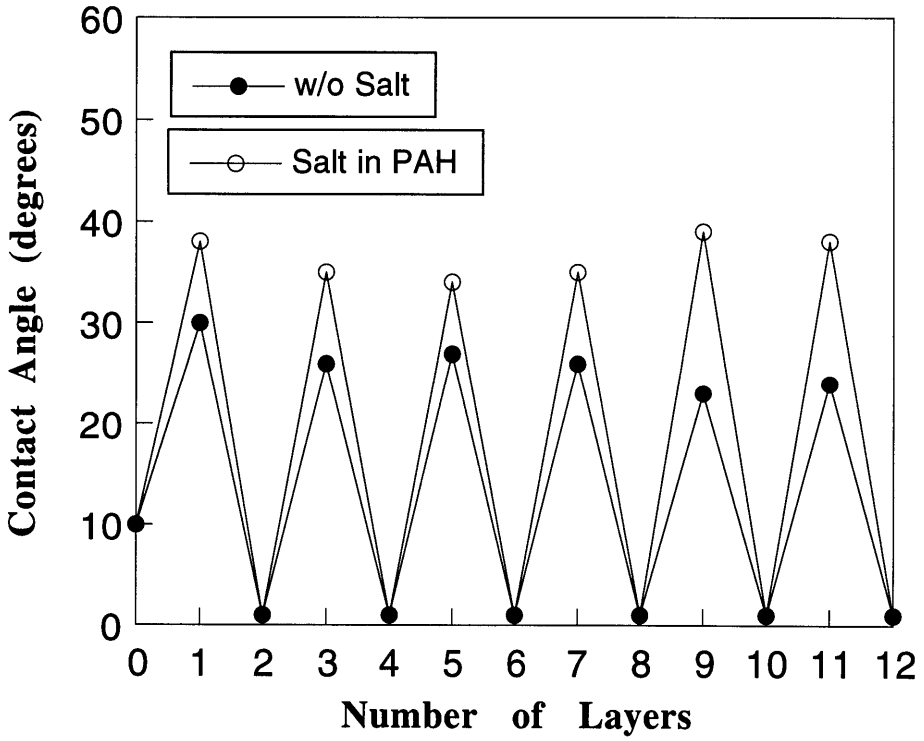

Figure 3.10. Salt in PAH solution effect on contact angles of PAH/PAA layers fabricated by pH 2.5, 10^{-2} M of solutions.

the even numbered layers attracted a lesser amount of dye, but, the odd numbered layers did not attract the methylene blue. The thicker polycationic layer may cover the polyanionic layer more fully and therefore reduce the amount of carboxylic acid groups on the surface with PAH as the outermost layer.

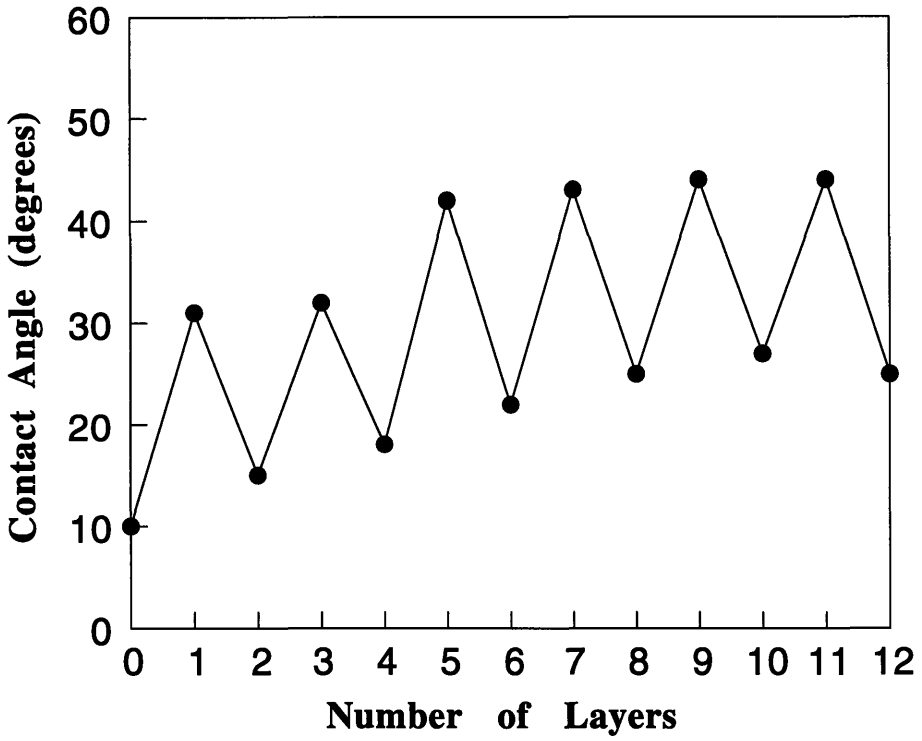

Figure 3.11. Contact angles of PAH/PAA layers fabricated by both 10^{-2} M, pH 4.5 solutions.

5.2 Solution pH Effect

We further examined effects of varying the solution pH on the PAH/PAA multilayer films. A pH of 4.5 and 10^{-2} M of both PAH and PAA solutions produced the multilayer films ranging from 1 to 12 layers. As compared to the films made with a pH of 2.5 for both solutions, Figure 3.11 shows that the oscillation of the contact angle in the PAH/PAA layers moved to higher values, while the amount of oscillation between an odd and even number of layers did not maintain

constant for each bilayer. The thickness of the PAH layer increased from 12 to 47 Å by changing the pH of PAH solution from 2.5 to 4.5. The PAA layers did not produce completely wettable surfaces. Compared with the PAA layer fabricated in a pH 2.5 solution, the layer thickness decreased from about 30 to 15 Å and the methylene blue adsorption also decreased drastically. A different pH of the solutions changes the adsorption behavior of the PAH and PAA layers and therefore the thickness of the PAH and PAA layers were modified. The combinations of the different pH solutions were used to produce the different thicknesses of PAH and PAA. A pH of 2.5 for the PAH solution and a pH of 4.5 for the PAA solution formed thin layers, while a pH 4.5 for the PAH solution and a pH of 2.5 for the PAA solution formed thicker layers.

Figure 3.12 shows the contact angle of PAH/PAA layers fabricated with a pH of 2.5 for

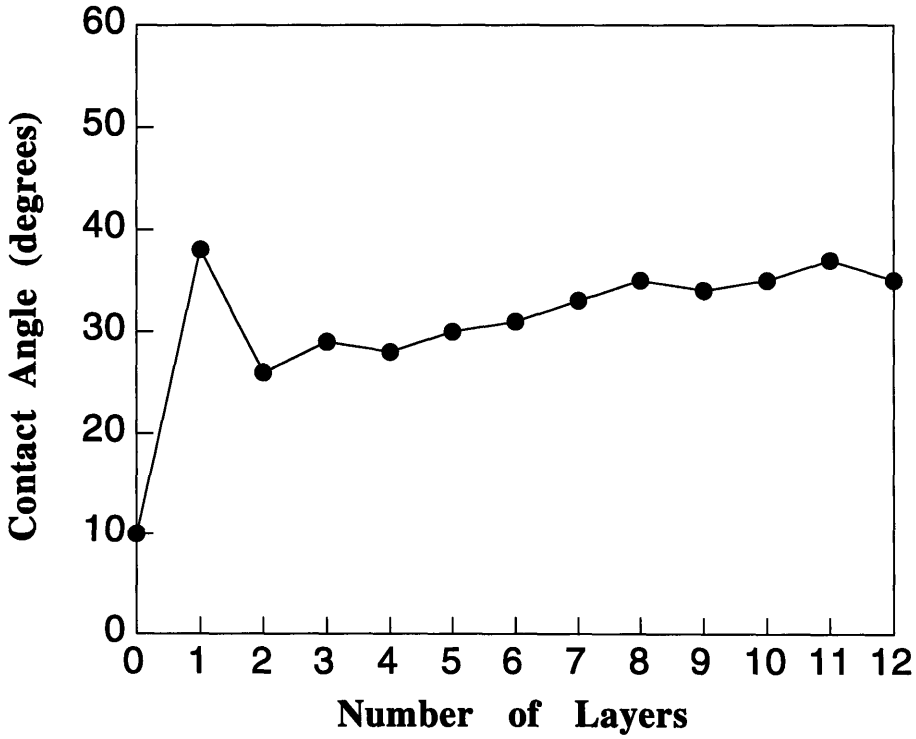

Figure 3.12. Contact angles of PAH / PAA layers fabricated by pH 2.5, 10^{-2} M of PAH and pH 4.5, 10^{-2} M of PAA solutions.

the PAH solution and a pH of 4.5 for the PAA solution. The oscillation in contact angles was not obtained at this condition and the thickness per bilayer was about 29 Å. The disappearance of the contact angle oscillation suggests that each layer was not fully separate enough to generate different wettable surface at the level of the resolution of contact angle measurements. The resolution of contact angles was known within 10 Å. In Table 3.3, the methylene blue deposited onto the PAH and PAA layers, while PAA layers incurred more dye adsorption.

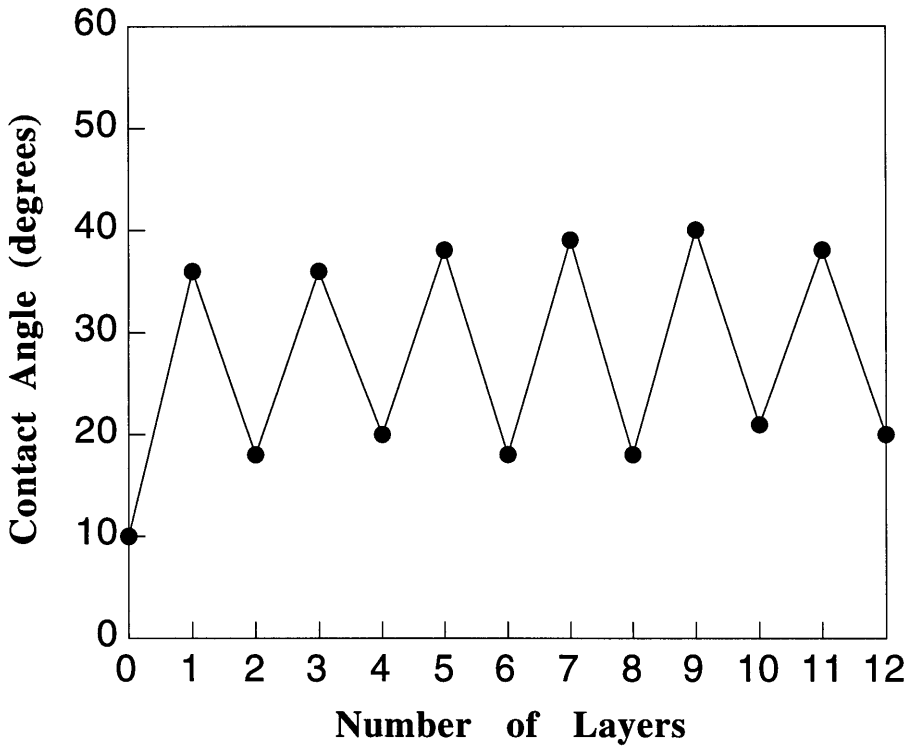

Figure 3.13. Contact angles of PAH / PAA fabricated by pH 4.5, 10^{-2} M of PAH and pH 2.5, 10^{-2} M of PAA solutions.

A pH of 4.5 for the PAH and a pH of 2.5 for the PAA solution were used to form thick PAH/PAA multilayer films. Figure 3.13 shows that a strong oscillation of the contact angles were regained, but the PAA layers did not produce completely wettable surfaces under these conditions. The thickness per bilayer of this film was about 72 Å. It is believed that the thicker layer of PAH

penetrated more into the PAA layer to produce less hydrophilic surfaces. The methylene blue only adsorbed onto the PAA layers and not onto the PAH layers. The relative thickness of each layer strongly affected the surface properties of outermost layers.

Several researchers including our group, have demonstrated that the ionic strength of the dipping solutions influences the layer thicknesses of the multilayer films. In addition, in weak polyelectrolytes like PAA, the pH of the dipping solutions also affected the layer thickness. In the strong polyelectrolytes, which are relatively insensitive to the pH, the importance of the pH of the dipping solutions is less.

For the above contact angle data of the PAH/PAA layers, a concentration of 10^{-2} M dipping solutions were used. However, the next section discusses concentration effects on the PAH/PAA system.

5.3 Concentration Effect

A concentration of 10^{-3} M for the PAH and PAA dipping solutions, which is ten times more dilute than the previous experiments, was used to form multilayer films as shown in Figure 3.14. This figure shows that the contact angles varied from 10-12° to 28-34° where an even number of layers did not generate fully wettable surfaces. The average thickness per bilayer made under the conditions of pH 2.5 and 10^{-3} M for PAH and PAA was about 32 Å. This indicates that the number of carboxylic acid groups on the surface decreased when a lower concentration of the solutions was used. The low concentration of the polyions decreased the amount of surface coverage at first layers and decreased the polyion adsorptions. The methylene blue adsorption data shows a very similar pattern to the pH 2.5 of 10^{-2} M PAA and PAH solutions, but, the adsorption was decreased. This is due to the fact that the thin PAH layer could not block the previous PAA layer from attracting the methylene blue dye.

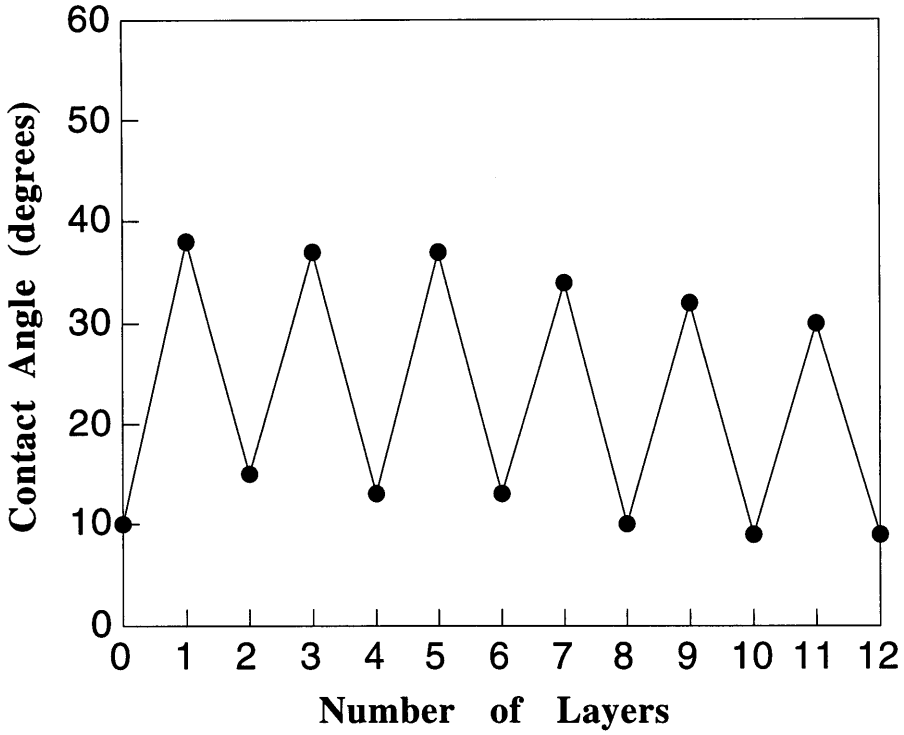

Figure 3.14. Contact angles of PAH / PAA fabricated by pH 2.5, 10^{-3} M of PAH and PAA solutions.

5.4 Infrared Spectra of PAH/PAA Films

Two samples of 5 bilayer PAH/PAA films were prepared on ZnSe plates with a pH of 2.5 of PAH and PAA solutions and with a pH 4.5 of those solutions. The films were rinsed with deionized water for 1 minute before infrared spectroscopy measurement. Figure 3.15 displays the infrared spectra of 5 bilayers for those two cases. Comparison of the infrared spectra of the two samples (pH 2.5 and pH 4.5 solutions) show an apparent difference in the peaks at 1560 and 1700 cm^{-1}. For the sample made with a solution of pH of 4.5, most of the carboxylic acid groups existed as the carboxylate form ($-COO^-$) (1560 cm^{-1}), while for that made with the pH 2.5 solution, most of carboxylic acid groups existed as free acid (-COOH) (1700 cm^{-1}). The differing number of charge segments in the PAA chain affects the structure of the adsorbed PAA layers.

The high concentration of carboxylate groups confirms that the pK_a value of the PAA polymer is around 4. This infrared spectra shows that the pH of 4.5 of both solutions has a higher charge density of the PAA chain. Another interesting observation is that despite reports that carboxylate form (pH 4.5) on the surface induces a stronger interaction with water than the free carboxylic acid form (pH 2.5), a pH of 2.5 for both solutions formed more wettable surfaces

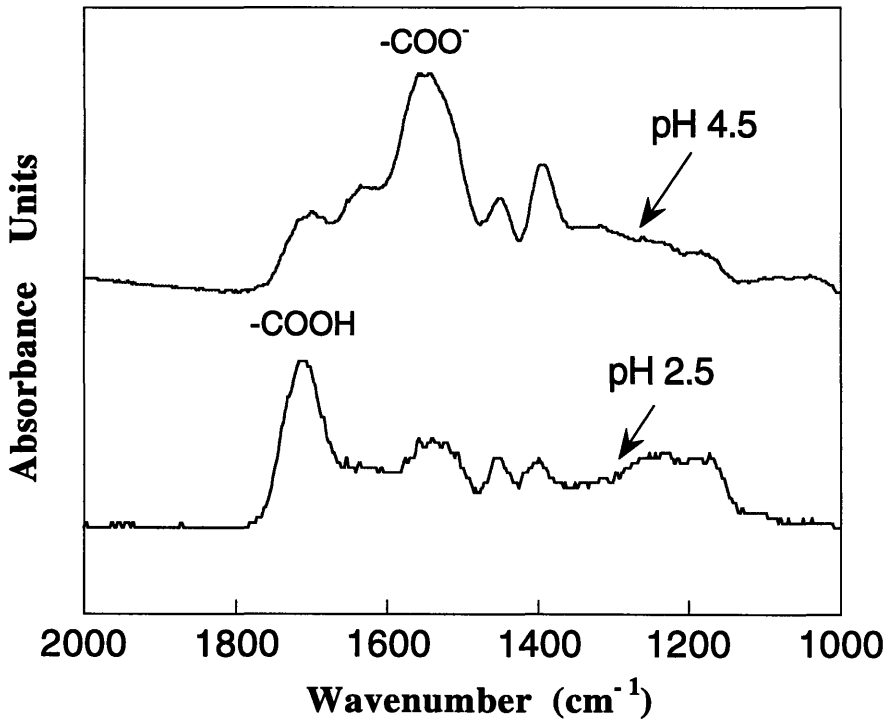

Figure 3.15. Infrared spectra of PAH / PAA films on ZnSe.

through carboxylic acid groups than a pH of 4.5. This means that a high density of less wettable carboxylic acid sites at the interface successfully produced completely wettable surfaces.

Table 3.4 shows the relative intensity of the infrared peaks at 1560 cm^{-1} and 1700 cm^{-1} of the PAH/PAA films as a function of time. The samples were prepared with a pH of 2.5 for the solutions and the spectrum contained a large peak at around 1700 cm^{-1} and smaller peak at around

1560 cm^{-1}. The 1560 cm^{-1} peak, which corresponds to the carboxylate form, intensified with time. A distinct difference in the as prepared and the 1 month old sample was observed. This can be assumed that unbound carboxylic acid groups in the PAH outermost layer reconstructed to form ionic linkages with the oppositely charged amine groups or were just titrated at interface in air. The contact angles of PAH/PAA films were measured after 1 month and the effect of aging the samples was studied.

Table 3.4. Relative amount of Infrared peaks at 1560 and 1700 cm^{-1}.

Days in the air	1560 cm^{-1}	1700 cm^{-1}
As prepared	33 %	67 %
14 days	53 %	47 %
28 days	62 %	38 %

5.5 Aging Behavior of PAH/PAA Multilayer Films

Samples with the number of PAH/PAA layers ranging from 1 to 12 were stored in a plastic case under air which was the same as that for the film on ZnSe. The contact angle of the samples was measured over a period of 1 month.

Figure 3.16 shows the contact angles of the as prepared samples as well as the samples stored for 1 month. The oscillation in the contact angle was still observed and the wettability of the even numbered layers did not change over 1 month. However, the contact angle of the films with an odd numbered of layers increased after storage. This increase implies either that the density of unbound carboxylic acid at the PAH outermost layers decreased through the increase of bound sites or the deposition of more contaminants from the air onto unstable amine groups of PAH layers. The amine groups on the surface are known to have a stronger tendency to interact with

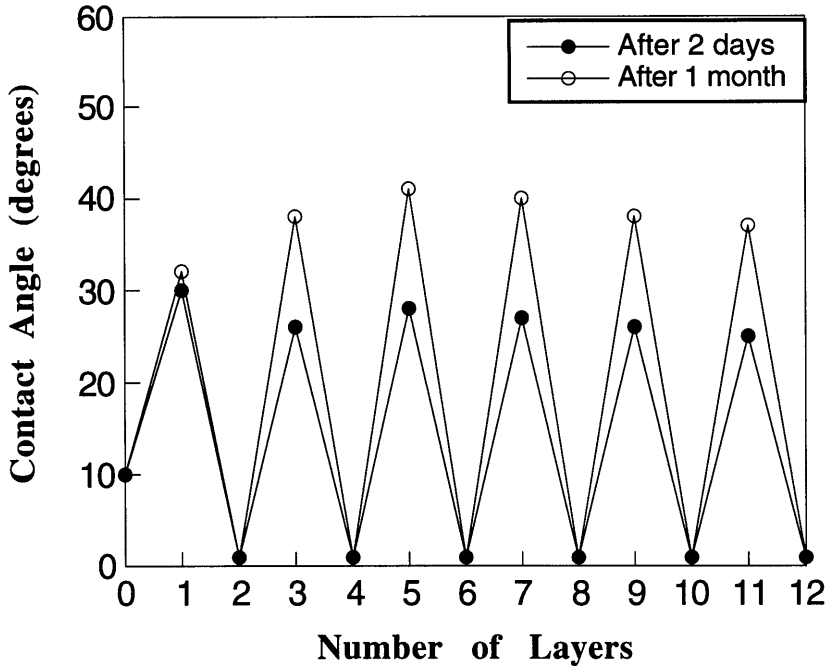

Figure 3.16. Aging effects on contact angles of PAH/PAA multilayer films fabricated by pH 2.5, 10^{-2} M of PAH and pH 2.5, 10^{-2} M of PAA.

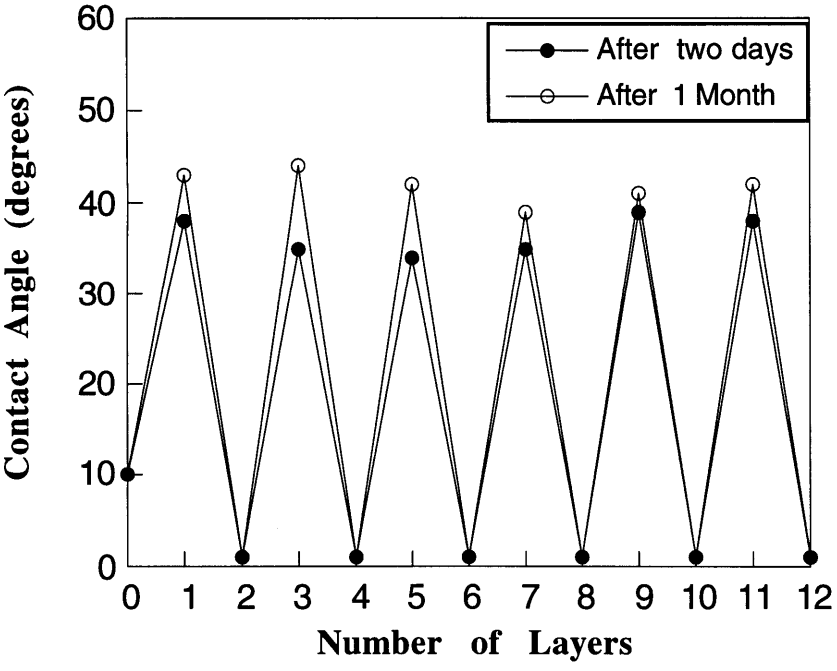

Figure 3.17. Aging effects on contact angles of PAH/PAA multilayer films fabricated by pH 2.5, 10^{-2} M of PAH with $MgCl_2$ 0.4 M and pH 2.5, 10^{-2} M of PAA solutions.

particles or gases in the air than the carboxylic acid groups [3.37]. Figure 3.16 shows the case of a thicker PAH layer which already has a reduced amount of carboxylic acid groups on the surface. The contact angle of the PAH layers increase by a small amount up to 45 - 50° after 1 month.

6. Discussion

In the layer-by-layer sequential adsorption technique, the level of interlayer interpenentration and the layer structure in the multilayer films are still not clearly understood. In order to study the structure, various layer structures using the PAH/PAA system were produced. The adsorption behavior of the PAH and PAA was examined by analyzing the surface properties. Contact angle measurements and methylene blue adsorption were performed to monitor the level of interdiffusion and amount of negative charges on the surface. The wettability of each layer was sensitive to the chemical structure of the polyelectrolytes and the level of interpenentration of each layer. The methylene blue was strongly adsorbed onto the negative charges on the surface. To compare the amount of the methylene blue adsorption with wettability, the peak intensity of the UV/Vis spectra was used to determine the amount of methylene blue adsorption on the surface.

First, the mechanism of how the layer-by-layer deposition technique generates completely wettable surfaces in the PAH/PAA system will be discussed. I propose a model (depicted in Figure 3.18) of producing completely wettable surfaces, which is explained as follows. When a polyion adsorbs onto a charged surface, some of its charges are not bound to the opposite charges on the surfaces but remain unbound. During the deposition, the outermost layer, which may develop a loose and swollen form due to the solubility of the unbound polyion segments, are ready to bind to oppositely charged polyions. A drying station induces the collapse of the loose and swollen layer to a densified surface layer structure. The adsorbed structures, which are classified in terms of trains, loops and tails, can highly influence the layer thickness and the level of layer interdiffusion after drying. If the outermost layer has high density of loops and tails, it will likely

cover the previous layers rather completely. This model suggests that although two layers may interdiffuse, the surface can still be dominated by the outermost layer through the collapse of this layer.

A pH of 2.5 for the PAH solution formed a thin and extended chain (train) structure layer, but many unbound charged sites still remained on the PAH layer. A pH of 2.5 for the PAA solution was adsorbed onto the already deposited PAH layer with loops and tails. The loopy and thick PAA layer produced a completely wettable surface. On the other hand, a pH of 4.5 for the PAH solution formed a thick PAH layer, while a pH of 4.5 for the PAA solution produced thin and extended PAA layers. The thin and extended structure of the PAA layer might be heavily interdiffused with the thick PAH layer which consequently produced a less wettable surface. As discussed previously, different hydrophilicities originated from the number of carboxylic acid

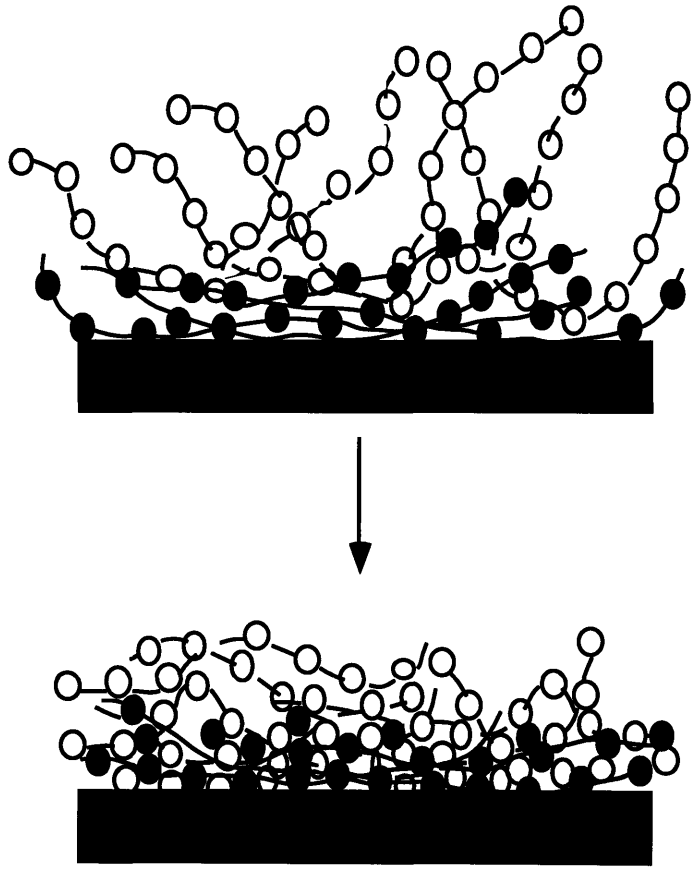

Figure 3.18. A proposed model of the layer-by-layer deposition.

groups on the surface and therefore not from the different hydrophilicities of the carboxylate and free carboxylic acid groups. We can guess that the thin, extended chain configuration of the PAA layer did not fully cover the previous PAH layer and it deposited much less carboxylic acid groups on the surface, while the thick and loopy structure of the PAA outermost layers produced a stable and completely wettable surface (The completely wettable surface was found to be stable for more than 4 months in the controlled environment.). The high density of carboxylic acid groups on the surface maintained the hydrophilicity even though some of charged groups became buried in the layers of PAH and PAA.

The different solution pH generated either thin or thick layers of PAH and PAA in the layer-by-layer deposition process. The layer thickness dependence on pH of the dipping solution is possibly explained based on a theory of polyelectrolyte adsorption and the experimental results of a monolayer adsorption onto charged surfaces.

The amount of segmental repulsion in the polymer chain, the number and strength of the interaction sites, and the screening of charges determine the behavior of polyion adsorption [3.38]. For flexible polymer chains with weak acid groups, such as PMA and PAA, the solution pH affects not only the dissociation of the carboxylic acid groups in the polyelectrolytes in solution but also the charge densities of adsorbed PAA or PMA layers at the interface. In Figure 3.15., the infrared data shows that for a pH of 4.5 in the PAA solution, many of the groups are in their carboxylate form. When the pH of the PAA solution is higher than the pK_a value of 4, most of functional groups are ionized and have a high level of repulsion between segments as well as between the already deposited PAA chains and the PAA chains in solution. At this high level of dissociation, the extended chain shape of the PAA layer will likely form a thin layer. When the pH is lower than the pK_a value of the PAA, the chain has a low charge density. The low level of segmental repulsion in the polyelectrolytes and the screening of the same charges between the deposited polyions and polyions in solution will produce a thick and loopy structure. The incremental thickness data in Table 3.2 shows that a pH of 2.5 for the PAA solution produced a thick layer while a pH of 4.5 for PAA solution produced a thin layer.

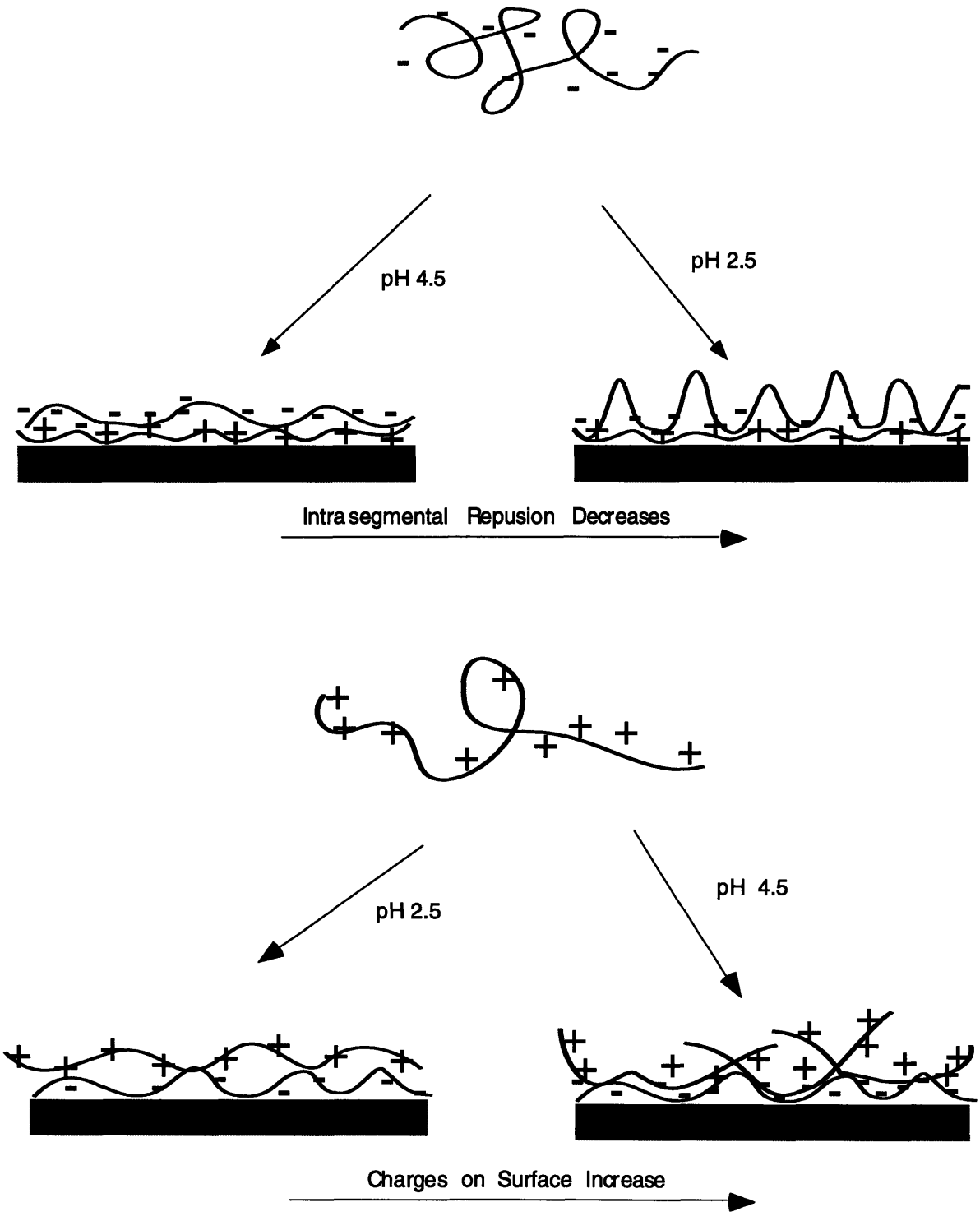

Figure 3.19. Mechanism of PAH/PAA Layer adsorption.

A pH of 2.5 or pH 4.5 of the PAH, which has a pK_a value of about 10, causes the amine groups to become fully charged and to have strong repulsive forces between the segments. The intrasegmental repulsive forces in PAH effectively do not change over the pH range from 2.5 to 4.5. However, the thickness of the PAH layer varies from about 10 Å to 40 Å by changing the pH from 2.5 to 4.5. The highly charged PAH layer adsorbs due to electro-sorption between the carboxylic acid groups of the PAA layers and the amine groups of the PAH. The charge compensation between the amine groups and the carboxylic acid groups are the main forces which induced the adsorption of the PAH layer. The degree of ionization of the carboxylic acid groups of the already deposited PAA layers are influenced by the solution pH of PAH. If the pH is above the pK_a, many carboxylic acid groups are dissociated which increases the interaction sites on the surface. This enhances the adsorption amounts of a fully charged PAH layer. Other studies have shown that the amount of a strong polycation adsorption is likely dependent upon the opposite charge density of the surface [3.39]. We believe that an increase in the number of interaction sites can enhance the amount of polycation adsorbed.

In summary, the charge density of the surface determines the amount of PAH adsorbed while the amount of segmental repulsion in the PAH effectively remains constant. On the other hand, the amount of intrasegmental repulsion determines the amount of PAA adsorbed while the charge density of the already deposited PAH layer remains constant. This mechanism is depicted in Figure 3.19 for each case.

PAH with a pH of 2.5 and PAA with a pH of 2.5 generate a thin, extended chain of PAH and a thick, loopy chain of PAA. Some of methylene blue adsorbed on the PAH outermost layer and small oscillation of contact angles with even-odd pattern were observed in the thick layer of PAA and thin layer of PAH. When salt was added to the PAH solution, the oscillation of the contact angle was enhanced and methylene blue did not adsorb onto the film with PAH as the outermost layer. The thick PAH layer blocked the influence of the previous PAA layers. A similar behavior was observed in the recent results by the McCarthy group [3.40]. In the reference, by adding $MnCl_2$ to both PAH and SPS solutions, they have shown an increase in the level of

oscillation of the contact angle. The loop structures of polyelectrolytes generated the less interpenentrated layer structure on the surface.

A pH of 4.5 in both the PAH and PAA solutions formed a thick PAH layer and a thin PAA layer. The thin layer of PAA decreased the hydrophilic property of PAA outermost layers and the thick layer of PAH increased the hydrophobic property of PAH outermost layers. The methylene blue adsorption on the PAA layers with a pH of 4.5 was 10 times less than that for the PAA layer fabricated with a pH of 2.5. The methylene blue did not deposit onto the PAH surface, due to the complete coverage of the PAA layers by the PAH outermost layer, and a higher contact angle of the PAH layer (about 43°) was obtained. The enhanced interpenentration by the thick PAH layer decreased the density of carboxylic acid groups on the outermost PAA layer. By controlling the pH for the PAH and PAA solutions, we can fabricate extended chain conformations as well as coiled conformations for both the PAH and PAA layers.

The thin and extended chain conformation of both PAH and PAA made with a pH of 2.5 for the PAH and a pH of 4.5 for the PAA solutions, does not produce an oscillation of the contact angle due to the high interdiffusion of the two layers. After deposition, the layers are not separated well enough to be able to observe the contact angle dependence of the layers. The methylene blue adsorbed both onto the PAA and PAH outermost layers. The loopy structure for both the PAH and PAA, made with a pH of 4.5 for the PAH and a pH of 2.5 for the PAA retained the oscillation in the contact angle as well as the selective adsorption of methylene blue.

The proposed mechanism based on the charged polyion adsorption successfully explains the interpenentration of two layers and the density of the carboxylic acid groups on the surface. The oscillation of the contact angle in the PAH/PAA system followed the net hydrophilicity of the surface in these multilayer films.

7. Conclusion

I have demonstrated that the layer-by-layer sequential adsorption method is a simple way to modify surface properties. The oscillation of the contact angle in the even-odd fashion, and the selective adsorption of methylene blue dye indicated that the surface properties were dominated by the outermost layer. The property of outermost layer, in turn, was controlled by the layer thickness and the structure of the multilayer film. The ionic strength and pH of the dipping solutions controlled the structure of the layers in terms of tails, loops and trains. The layer-by-layer deposition technique successfully achieved molecular level controlled multilayer films.

REFERENCES

[3.1] Schrader, E.; Loeb, G. I. "Modern Approach to Wettability"; Plenum Press: New York, 1992.

[3.2] Koberstein, J. T. *Mat. Res. Soc. Bull.,* **1996**, *21*, 19.

[3.3] Briggs, D.; Kendall, C. R. *Int. J. Adhesion Adhesives* **1982**, *2*, 13.

[3.4] Kaplan, S. L.; Rose, P. W. *Plastics Eng.* **1988**, *44*, 77.

[3.5] Ratner, B. D. in "Biomaterials: Interfacial Phenomena and Applications, Chap. 2"; Cooper, S. L. and Peppas, N. A. Eds.; *Advances in Chemistry,* 199; American Chemical Society: Washington, 1982.

[3.6] Briggs, D. in "Practical Surface Analysis by Auger and X-ray Photoelectron Spectroscopy"; Briggs, D. and Seah, M. P. Eds.; John Wiley: Chichester, 1983, p383.

[3.7] Pochan, J. M.; Cerenser, L. J.; Elman, J. F. *Polymer* **1986**, *27*, 1058.

[3.8] Boegin, H. V. "Plasma Sciennce and Technology"; Cornell University Press: Ithaca, 1982.

[3.9] Briggs, D.; Rance, D. G.; Dendall, C. R.; Blythe, A. R. *Polymer* **1980**, *21*, 895.

[3.10] Morra, M.; Occhiello, E.; Garbassi, F. *J. Colloid Interface Sci.* **1984**, *132*, 504.

[3.11] Grisser, H. J.; Youxian, D.; Hugher, A. E.; Genegenbach, T. R.; Mau, W. H. *Langmuir* **1991**, *7*, 2484.

[3.12] Bee, T. G.; Cross, E. M.; Dias, A. J.; Lee, K.; Shoichet, M. S.; McCarthy, T. J. in "Contact Angle, Wettability and Adhesion"; Mittal, K. L. Ed.; VSP: Utrecht, 1993, p561.

[3.13] Rasmussen, J. R.; Stedronsky, E. R.; Whitesides, G. M. *J. Am. Chem. Soc.* **1977**, *99*, 4736.

[3.14] Gibson, H. W.; Bailey, F. C. *Macromolecules* **1988**, *13*, 34.

[3.15] Sudarshan, T. S. "Surface Modification Technologies: An Engineer's Guide"; Marcel Dekker: New York, 1989.

[3.16] Maroudas, N. G. *Nature* **1974**, *254*, 695.

[3.17] Friedrich, C.; Lauprette, F.; Noel, C.; Monnerie, L. *Macromolecules* **1980**, *13*, 1625.

[3.18] Young, T. *Phil. Trans. Roy. Soc.* London, **1805**, *95*, 65.

[3.19] Good, R. J. in "Contact Angle, Wettability and Adhesion"; Mittal, K. L. Ed.; VSP: Utrecht, 1993, p3.

[3.20] Zisman, W. A. in "Contact Angle, Wettability, and Adhesion."; Advance in Chemistry Series 43; American Chemical society: Washington D.C, 1964, p57.

[3.21] Israelchvili, N.; Gee, M. L. *Langmuir* **1989**, *5*, 288.

[3.22] Van Oss, J.; Good, R. J.; Chaudhury, M. K. *Langmuir* **1988**, *4*, 884.

[3.23] Lee, L.-H. *Langmuir* **1996**, *12*, 1681.

[3.24] Fowkes, M.; Mostaf, M. A. *IEC Prod. Res. Dev.* **1985**, *24,* 369.

[3.25] Ko, Y. C.; Ratner, B. D.; Hoffman, A. S. *J. Colloid Interface Sci.* **1981**, *82*, 25.

[3.26] Bain, C. D.; Whitesides, G. M. *Langmuir* **1989**, *5*, 1370.

[3.27] Van Oss, C. J.; Chaudhury, M. K.; Good, R. J. *Chem. Rev.* **1988**, *88*, 927.

[3.28] Wenzel, N. *Ind. Eng. Chem.* **1936**, *28*, 988.

[3.29] Good, R. J. *J. Am. Chem. Soc.* **1953**, *74*, 5041.

[3.30] Bartell, E.; Shepard, J. W. *J. Phys. Chem.* **1953**, *57*, 211.

[3.31] Drelich, J.; Miller, J. D. *J. Colloid Interface Sci.* **1994**, *164*, 252.

[3.32] Wasserman, R.; Tao, Y.-T.; Whitesides, G. M. *Langmuir* **1989**, *5*, 1074.

[3.33] Whitesides, G. M.; Biebuych, H. A.; Fokers, J. P.; Prome, K. L. in "Acid-Base Interaction"; Mittal, K. L. and Anderson , H. R. Jr. Eds.; VSP: Utrecht, 1991, p291.

[3.34] Ferguson, G. S.; Whitesides, G. M. in "Modern Approaches to Wettability: Theory and Applictions"; Schrader, M. E. and Loeb, G. Eds.; Plenum Press: New York, 1992, p143.

[3.35] Holmes-Farley, S. R.; Reamey, R. H.; McCarthy, T. J.; Deutch, J.; Whitesides, G. M. *Langmuir* **1985**, *1*, 725.

[3.36] Xie, X.; Gengenbach, T. R.; Griesser, H. J. in "Contact Angle, Wettability and Adhesion"; Mittal, K. L. Ed.; VSP: Utrecht, 1993, p509.

[3.37] Gaines, G. L. Jr *Nature* **1982**, *298*, 5.

[3.38] Fleer, G. J.; Cohen Stuart, M. A.; Scheutjens, J. M. H. M.; Cosgrove, T.; Vincent, B. "Polymer at Interface"; Chapman & Hall: Cambridge University Press, 1993.

[3.39] Tanaka, H.; Ödberg, L.: Wágner, L.; Lindström, T. *J. Colloid Interface Sci.* **1990**, *134*, 219.

[3.40] Chen, W.; McCarthy, T. J. *Macromolecules* **1997**, *30*, 78.

CHAPTER 4

MULTILAYERS OF FUNCTIONAL DYE MOLECULES AND POLYELECTROLYTES

1. Introduction

Organic dye molecules have shown great potential for applications in electronics and optics [4.1 - 4.3]. However, they are not easily manipulated into thin layer films (μm) without extensive chemical modification of the dye molecule due to their propensity to aggregate and crystallize. The industrial applications of dye molecules are restricted by the processing techniques used for an organic thin film fabrication.

The layer-by-layer deposition technique for fabricating an organic thin film has worked with a wide variety of functional materials. Using this relatively simple approach, our group has demonstrated that layer-by-layer deposited multilayers can be used to modify surfaces [4.4], to create electrically conducting thin films [4.5 - 4.6] and to fabricate light-emitting devices [4.7]. This approach works with a wide variety of polycations and polyanions, making it possible to fabricate complex multilayer heterostructures with properties that are tunable at the molecular level.

In order to extend the versatility of this new layer-by-layer processing method, the possibility of assembling polyelectrolytes and functional organic dyes was examined. Decher et al and others [4.8 - 4.10] have fabricated multilayers from bolaform type materials (molecules with a rigid core connected to ionic end groups by extended alkyl chains) and suitable polyelectrolytes. However, this approach requires the synthesis of molecules with specially tailored molecular architectures. This chapter will describe the

incorporation of small dye molecules into the multilayer films which have only a few charges in the chemical structure. In this process, the electrostatic forces established between ionic dye molecules and oppositely charged polymers are used to build multilayers. The ionic attractions promote strong interlayer adhesion and a uniform and linear multilayer deposition process. With the correct combination of an ionic dye and a polyelectrolyte, it is possible to use these dye-based bilayer systems to construct any number of different multilayer heterostructures.

As dye molecules are linked by only a few ionic groups, the interactions between the polyelectrolyte and dye layers are much weaker than between polyelectrolyte layers. The desorption of adsorbed small dye molecules in the oppositely charged polyions was, sometimes, observed due to the weak interactions. To form uniform multilayered films by layer-by-layer deposition, appropriate pH and salt content of dipping solutions should be used. This is necessary to prevent the dye molecules from coming off in the oppositely charged polyelectrolyte solutions. The fundamentals of dye multilayer films and several examples of functional multilayer films will also be discussed in this chapter.

2. Structural Aspects of Dye Multilayer Film

The sites and number of ionic groups in a functional dye determine whether or not it will be possible to fabricate multilayer structures. Ionic groups in a chemical structure can dissolve the dye molecules in water and create attractive forces between the layers. The strong interactive forces in a polyelectrolyte allow the small dye molecules to be incorporated into multilayer films. The cationic or anionic functional dye molecules, themselves, did not produce the multilayer films. The polyelectrolytes used in the study were shown in Figure 4.1.

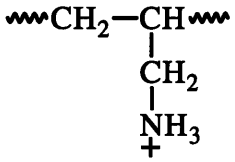

Poly(allylaminehydrochloride) (PAH)

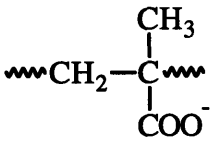

Poly(methacrylic acid) (PMA)

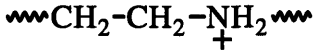

Poly(ethyleneimine) (PEI)

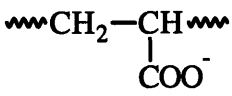

Poly(acrylic acid) (PAA)

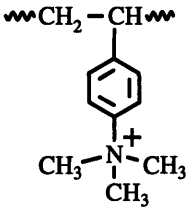

Poly(benzyltrimethylAmoniumtrichloride) (PVBT)

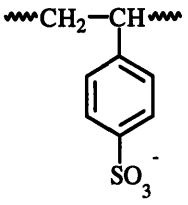

Poly(sulfonated styrene) (SPS)

Figure 4.1. Chemical structures of used polyelectrolytes.

2.1 Fluorescein Complexion Multilayer Film

A single charged dye, such as methylene blue and 8-anilino-1-naphthalene was found to adsorb onto an oppositely charged surface, but multilayer films based on the

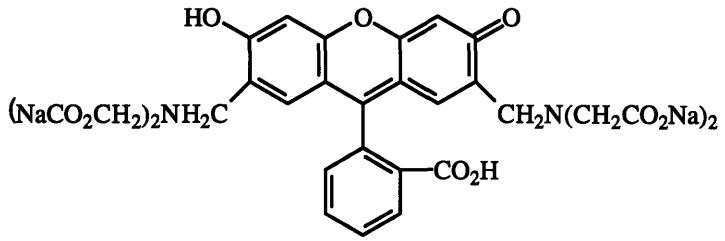

Figure 4.2. Chemical structure of fluorescent complexion dye.

material were not able to be held together. To build up multilayer films through the layer-by-layer deposition, the charges of the outermost layer should be converted to make an oppositely charged layer. In principle, more than two charge groups are required to hold two adjacent layers together. For example, the alternate dippings of $5 \cdot 10^{-3}$ M fluorescein complexion solution and a pH 3.5 of $5 \cdot 10^{-3}$ M poly(allylamine hydrochloride) (PAH) produced uniform multilayer films. The chemical structure of fluorescein complexion was shown in Figure 4.2. The molecule has five carboxylic acid groups. Figure 4.3 shows the linear correlation of UV/Vis spectra of fluorescent complexion with number of bilayers. This result demonstrated that the simple alternate dippings of a functional dye molecule and a polyelectrolyte can form heterostructural multilayer films.

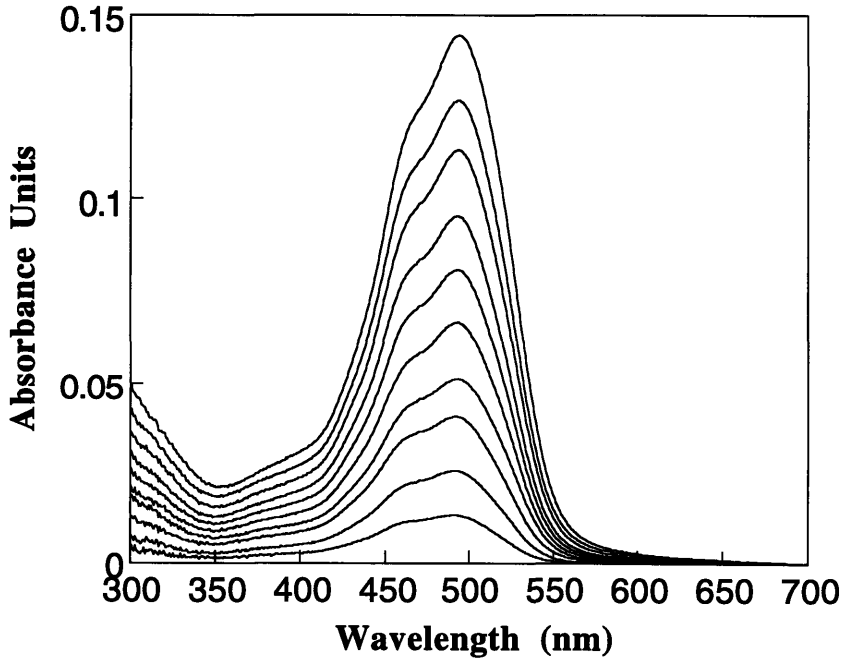

Figure 4.3. Linear deposition of fluorescein complexion/PAH films.

2.2 Bordeaux R and Crystal Violet Dyes

When a polyelectrolyte deposits onto a surface, loops and tails of the polyelectrolyte structure form unbounded charge sites for dye layer adsorption. The deposited dye layer acts as an adsorption site to hold the oppositely charged polyelectrolyte layer, together. To confirm that the dye layers are linked by two adjacent layers, Crystal Violet and Bordeaux R dye multilayer films were studied. Those have identical molecules except at the sites of the charge groups in the dye molecule (Figure 4.4). Only Bordeaux R produced linear growth of a film with PAH (10^{-2} M, pH 3.5), but Crystal Violet was not

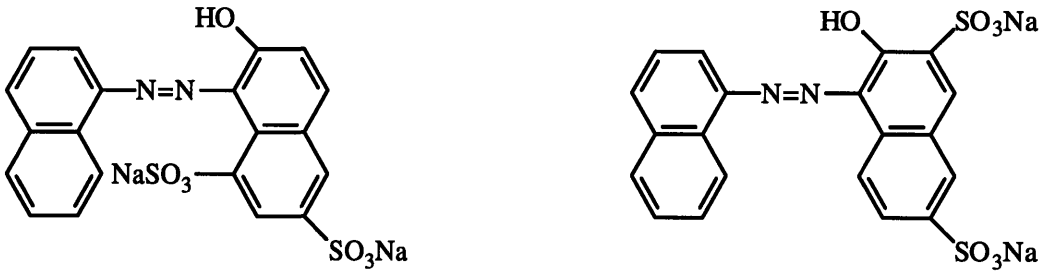

(a) (b)

Figure 4.4. Chemical structures of (a) Crystal Violet and (b) Bordeaux R.

suitable for multilayer formation. In Bordeaux R, the charge sites are separated enough so that they can be shared between adjacent layers to form multilayer films. In Crystal Violet, the charge sites are not separate. Figure 4.5 shows the UV/Vis absorbance of layer films from 1 to 10 bilayers of Bordeaux R and PAH. The small dyes like Bordeux R successfully formed a multilayer film sharing charges with two adjacent layers. The structural factors, such as a number of charges, charge sites in a molecule and types of ionic charges affect the adsorption of small dye molecules.

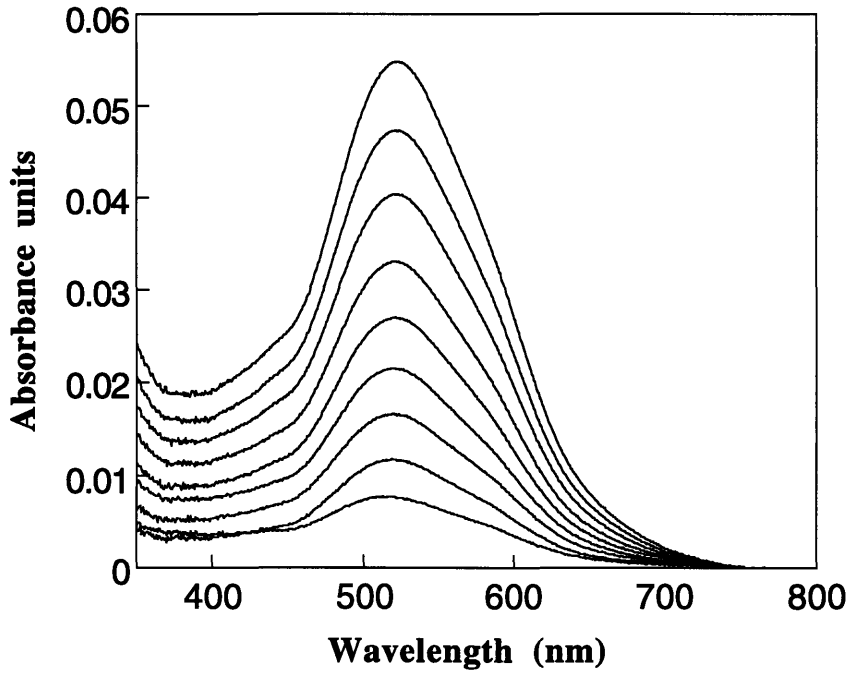

Figure 4.5. Linear deposition of Bordeaux R and PAH film.

3. Functionalized Multilayer Films

3.1 pH indicating Azo dye Film

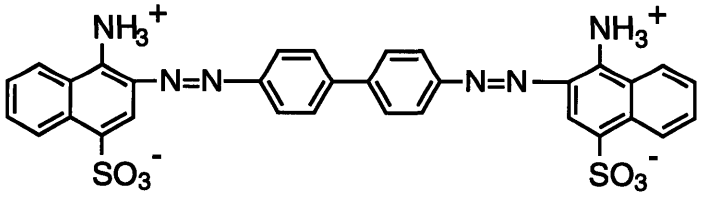

Figure 4.6. Chemical structure of Congo red dye.

Congo red dye (shown in Figure 4.6) contains azo groups that allow the color of the dye to be modified when the pH of the solution is changed [4.11]. Congo red is known as a amphoteric molecule because it has two cationic charges (amine groups) and two negative charges (sulfonic acid groups) in the molecules.

Figure 4.7 shows how the visible absorption of a multilayer thin film varies with increasing numbers of deposited congo red/polyelectrolyte layers. The linear growth observed with this dye system is identical to the behavior of well connected dye molecules.

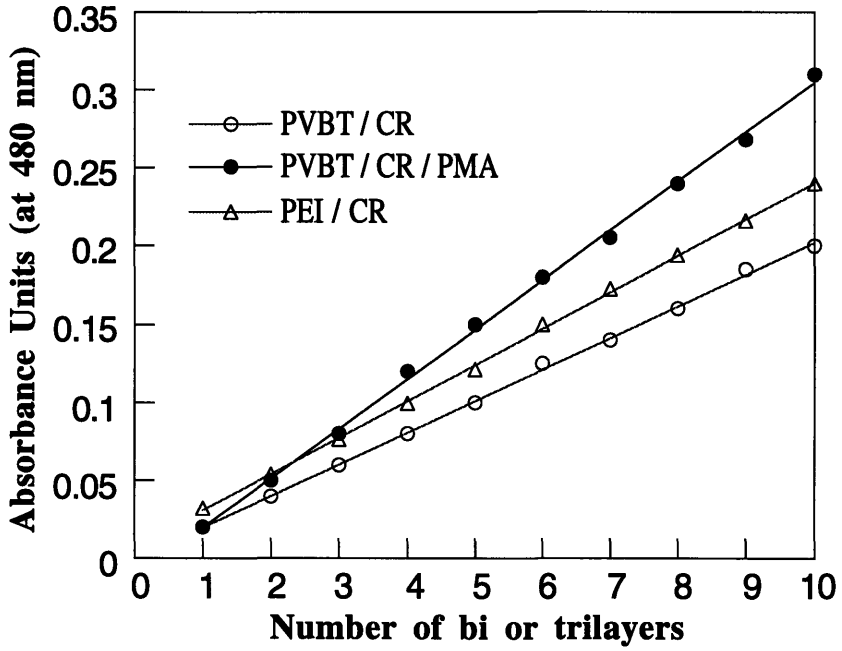

Figure 4.7. Amounts of UV/Vis absorption of Congo red dye/polyelectrolytes.

This also shows that a reproducible amount of dye is deposited during each bilayer (or trilayer) cycle. In Figure 4.7, the amphoteric nature of the Congo red dye makes it possible to fabricate multilayer thin films from either dye/polycation bilayers or from polycation/dye/polyanion trilayers. The alternate dippings of a pH 4.5 of 10^{-2} M poly(vinylbenzylbutyltrimethylamonium) (PVBT) and congo red dye with 0.01 weight percent solution utilized the sulfonic acid groups in the dye, while the poly(methacrylic acid) (PMA) with pH 4.5 and 10^{-2} M used the amine groups of Congo red to build up multilayer films. The trilayer system formed interaction sites with both amine and sulfonic

acid groups in the Congo red dye. In fact, the amount of dye adsorbed per complete dipping cycle (bilayer or trilayer) was seen to be the greatest when a trilayer system was used to build the film, suggesting that the increase of interaction sites occurs when the Congo red dye is sandwiched in between two polymers of opposite charge. In the trilayer system, the two consecutive polyelectrolyte layers adsorbed before the Congo red dye was deposited onto the charged surface. The bottom two layers increased charge sites for dye adsorption and also enhanced the interlayer attractions with the dye molecules.

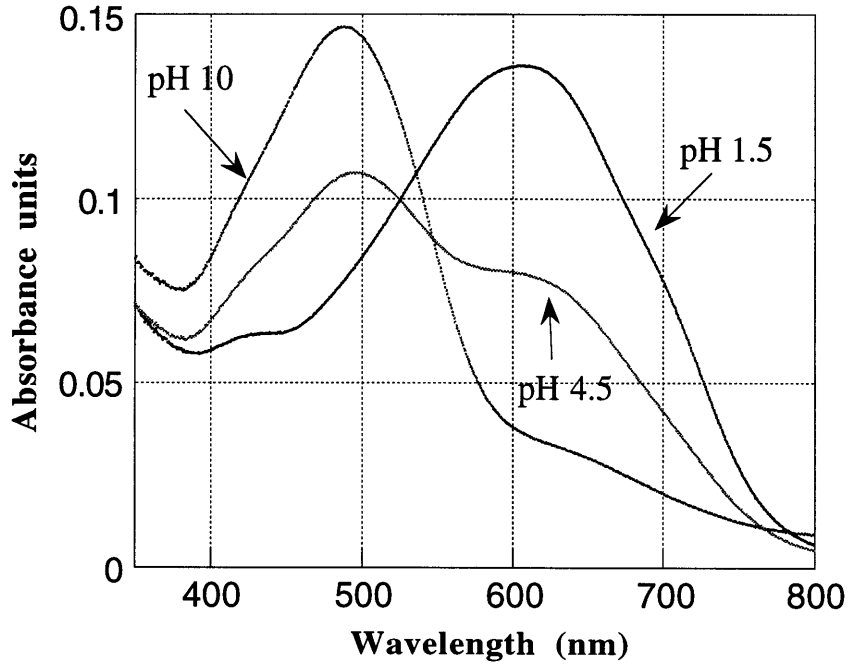

Figure 4.8. pH color change of a PAH/Congo red dye multilayer film.

Since the Congo red dye is a pH indicator dye, it is possible to deposit multilayer thin films of this material onto various substrates and vessels thereby creating glassware with a pH sensitive coating. Figure 4.8 displays the UV/Vis spectra of a glass slide coated with 10 (Congo red/PAH) bilayers recorded after exposure to different pH levels. The multilayer coating was seen to change color from blue to red as the pH changes from low to high pH. At an intermediate pH of 4.5, both absorbing states of the dye are clearly

evident. It should also be noted that, unlike simple dye layers directly adsorbed to glass, the multilayer films are remarkably robust, and can be cycled from very low to very high pH many times without any loss of dye due to desorption. These results indicate that the adsorbed layers are strong enough to maintain the multilayer structure over a wide pH range.

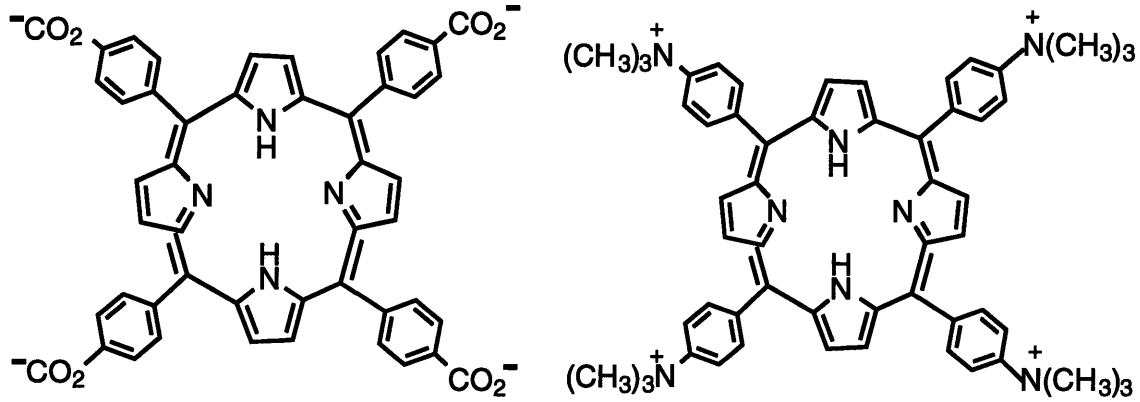

a) Anionic porphyrin dye b) Cationic porphyrin dye

Figure 4.9. Chemical structures of porphyrin dyes.

3.2 Porphyrin dye Multilayer Films

Porphyrin dyes are well known for their interesting electrical and optical properties and have been considered for such applications as nonlinear optics, optical data storage, and electrochromic devices [4.12 - 4.13]. Porphyrin dyes (shown in Figure 4.9) with charge groups were used for a multilayer film. Figure 4.10 shows that it is possible to use the layer-by-layer deposition process to fabricate multilayer thin films with either cationic or anionic porphyrin dyes. In both cases, it can be seen that a linear deposition process is observed when the porphyrin dye is deposited layer-by-layer with a polymer of

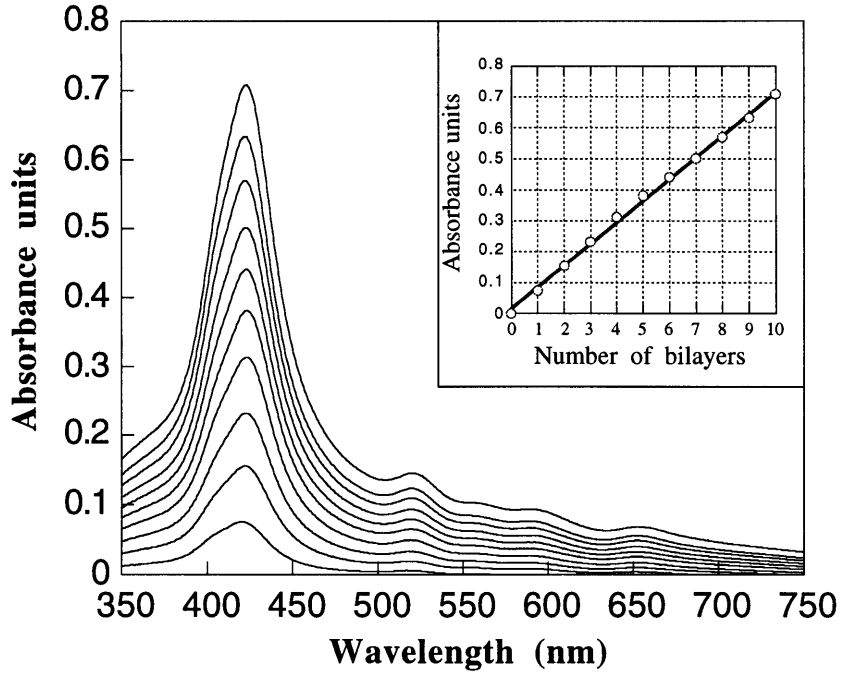

(a)

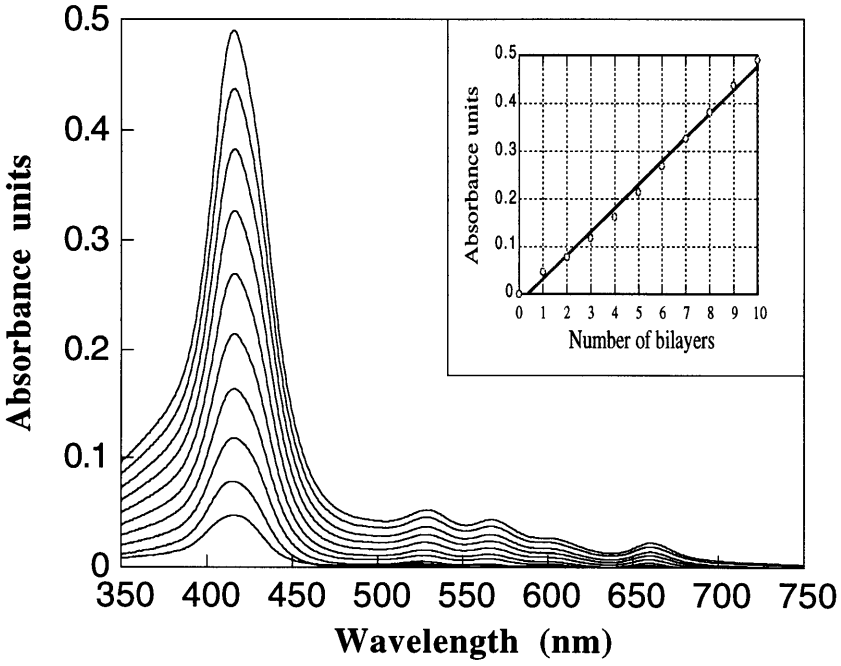

(b)

Figure 4.10. Layer-by-layer growth of (a) a cationic porphyrin dye/PMA multilayer and (b) an anionic porphyrin dye/PEI multilayer. Insets show the absorbance versus number of bilayers plots for these two systems measured at 428nm.

the opposite charge. The anionic porphyrin has a carboxylic acid group which is a weak acid. To keep the charges of the carboxylic acid groups of the anionic porphyrin dyes, both the 10^{-3} M anionic porphyrin and the $5 \cdot 10^{-3}$ M of poly(ethyleneimine) (PEI) solutions were adjusted to a pH of 7. Alternate dippings of pH 4.5 of $5 \cdot 10^{-3}$ M PMA and 10^{-3} M cationic porphyrin dyes formed the multilayer films. Figure 4.9 shows the UV/Vis spectra of multilayers consisting of 1-10 bilayers of cationic porphyrin, PMA, anionic porphyrin, and PEI. As it is the case, the films obtained by this approach was very uniform and had excellent optical quality.

Because of the planar structures, the porphyrin dyes have oriented chromophore. The ratio of absorbance of the sample for polarized radiation parallel (r_P) to the axis direction and perpendicular (r_S) to the axis direction indicated the degree of the orientation. The quantity $D = r_P / r_S$ is called *dichroic ratio* to the angle of a radiation of polarized light. If there is no preferred orientation of the dye molecules, different orientations of polarized lights do not generate different spectra. The dichroic ratio increases with the degree of orientation of the chromophore. The normal and 45° degree radiation angles were used to

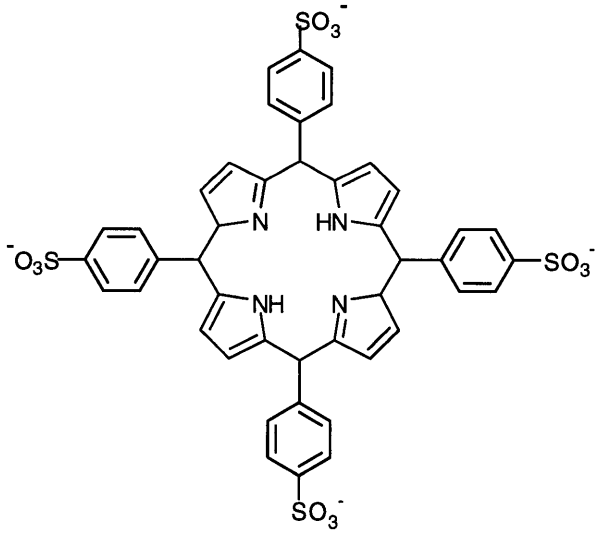

Figure 4.11. Chemical structure of tetraphenyl porphine tetrasulfonic acid, tetrasodium salt.

measure the dichroic ratio of UV/Vis spectra peak of the films. The Dichroic ratio at the normal radiation of the 10 bilayers of cationic porphyrin/PMA and anionic porphyrin/PEI films were 0.98 and 1.00, while that at the 45° radiation angle of those films were 1.07 and 1.05. The results indicate that the preferential orientation of the dye molecules were hardly observed in the films, therefore, the dye molecule was randomly oriented in the thin film structure.

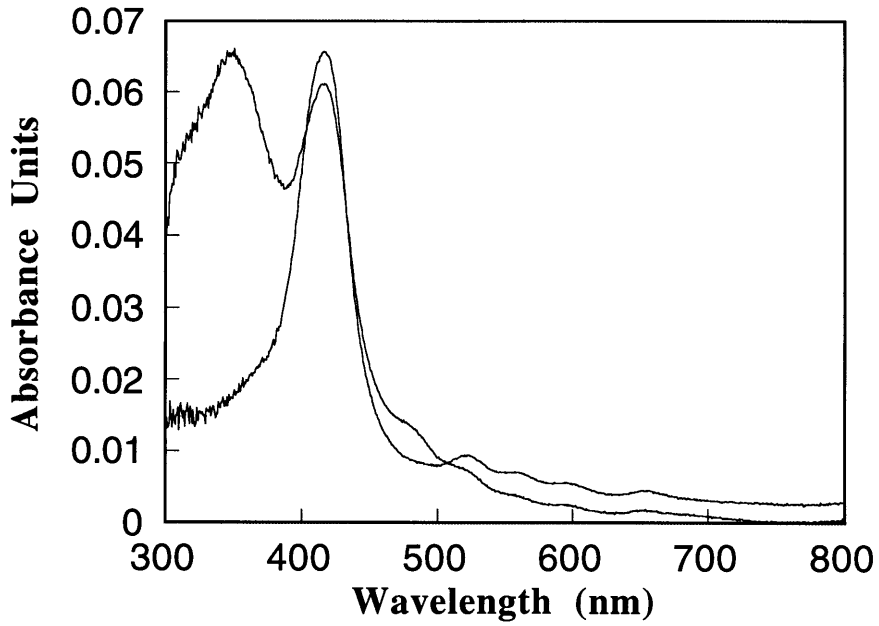

Figure 4.12. UV/vis spectra of anionic porphyrin/PAH multilayer film (420 nm peak) and with iron in the ring (370 nm peak).

An anionic porphyrin dye with four sulfonic acid groups (structure in Figure 4.11) also formed a clear multilayer film with PAH. The films were made from solutions of pH 4.5 of 10^{-2} M PAH and 10^{-3} M porphyrin dye. After the deposition of 10 bilayers on the glass slide, the PAH/porphyrin dye film was dipped into the $FeCl_3$ solution to incorporate Fe molecules into the porphyrin rings. Figure 4.12 shows that an additional

peak was observed at 370 nm after the iron was successfully incorporated into the ring of the porphyrin molecules. Like this kind of behavior, the layer-by-layer deposited film shows a novel possibility to generate sensor applications.

3.3 Infrared Absorbing Dye Multilayer Film

The near infrared region covers the wavelengths from 700 to 2000 nm. The 750-1300 nm region is particularly important, partially because semiconductor lasers such as gallium-aluminum-arsenide (GaAlAs) lasers use those wavelengths [4.14]. The deposition technique makes it possible to build a multilayer thin film which specifically absorbs in this region (the chemical structure of the infrared absorbing dye (IR dye) is shown in Figure 4.13). The absorption intensity of this thin film can be controlled by changing the number of bilayers. Figure 4.14 shows the visible spectrum of a multilayer thin film with

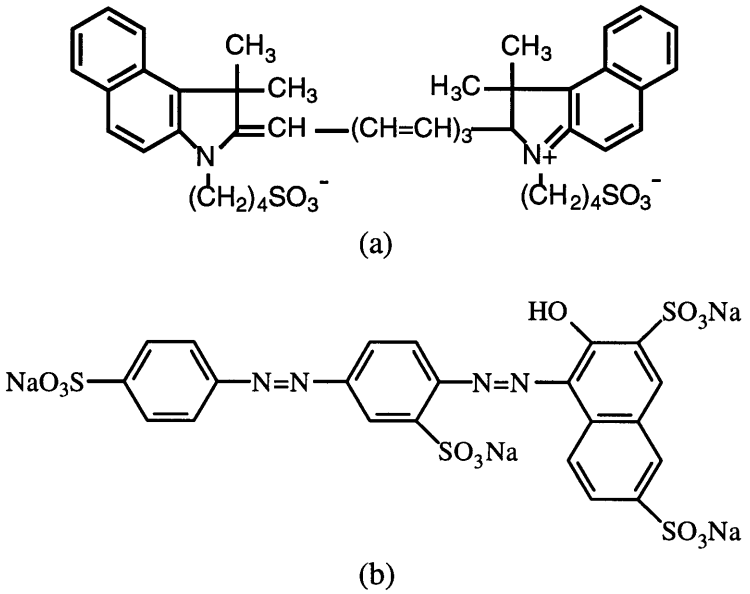

Figure 4.13. Chemical structure of (a) Infrared absorbing dye (IR dye) and (b) Ponceau S dye.

increasing numbers of deposited dye/PAH bilayers. This technique is also able to create multilayer heterostructures comprised of several dye bilayers that absorb in different spectral regions.

This hetero-structured films can produce a color filter which can be tuned by simply changing the number and type of dye/polymer bilayers added to the heterostructure.

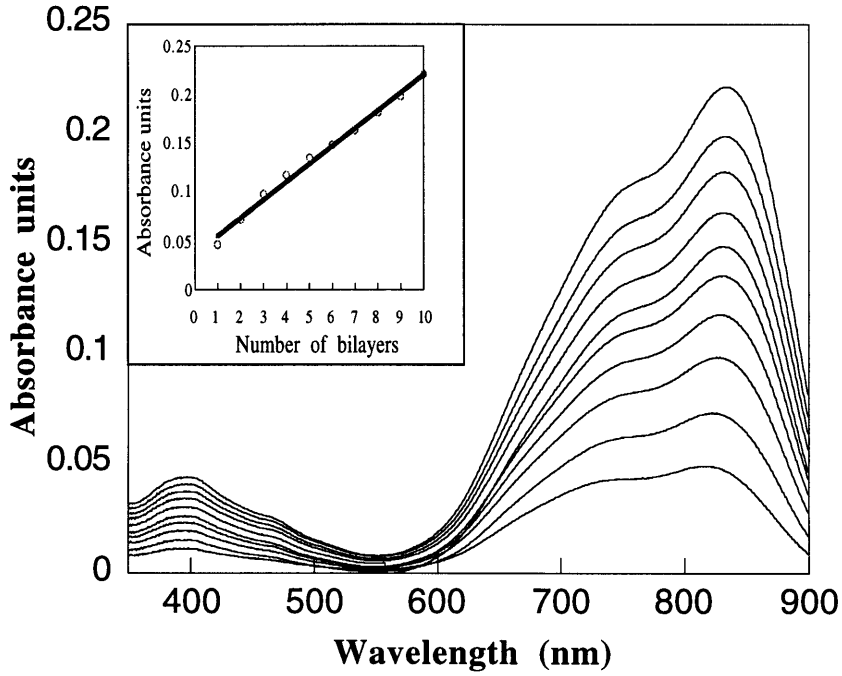

Figure 4.14. Linear growth of infrared absorbing dye/PAH multilayer.

To demonstrate the ability to make thin film heterostructures from functional dye molecules, a multilayer thin film containing two different negatively charged dyes; Ponceau S and IR dye (the chemical structures are shown in Figure 4.13) were fabricated. These dyes were deposited layer-by-layer as adsorbed layers alternating with the cationic polyelectrolyte, PAH. The resultant linear deposition process was easily monitored though UV/Vis measurements of the Ponceau S absorption band (λ_{max} = 506 nm) and the IR dye absorption band (λ_{max} = 810 nm). Twenty layer films were prepared by alternate dipping

of PAH and each dye molecule. The final structure of the multilayer film was (|PAH|Ponceau S|PAH|Infrared dye 125|)$_5$. Figure 4.15 shows the UV/Vis spectra of a 20 layer film containing 5 layers of each dye molecule. This result suggests that with the correct combination of ionic dyes and polyelectrolytes, it is possible to manipulate multilayers of several dye molecules by the repeated dipping of each dye molecule and a suitable polyelectrolyte.

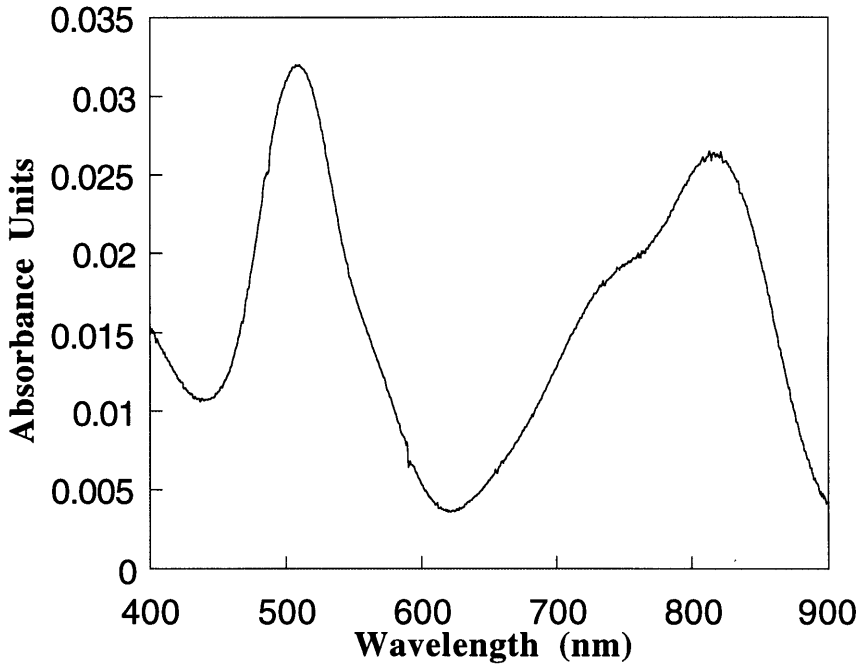

Figure 4.15. UV/vis spectra a multilayer film containing 5 layers of Ponceau S (510 nm) and Infrared dye 125 (810 nm).

4. Ru complex Multilayer Films

The Ruthenium (bipyridine)$_3^{+2}$, [Ru(bpy)$_3$]$^{+2}$ complexes shown in Figure 4.16 are well known for their novel chemiluminescent properties and excellent redox stability [4.15 - 4.16]. The solution states of [Ru(bpy)$_3$]$^{+2}$ have been heavily examined by many researchers. However, the solid state is not easily obtained due to poor film forming

properties. Since the molecule does not have two separate charges to hold adjacent layers, the multilayer film cannot be formed through layer-by-layer deposition technique. We therefore synthesized the tris(bathophenanthroline disulfonate ruthenium), sulfonated $[Ru(phen')_3]^{+2}$ shown in Figure 4.16 [4.17 - 4.18]. Since this new ruthenium dye contains six sulfonate groups, it is water soluble, does not readily crystallize and can be multilayer deposited with various polycations. This reduced the crystallinity of the whole complex in the solid state and made it soluble in polar solvents such as water, methanol and dimethylsulfoxide. This enabled us to make good quality thin films by spin-coating and also allowed us to build multilayer light emitting devices by the layer-by-layer deposition technique.

A polymer $[Ru(bpy)_3]^{+2}$ (poly($[Ru(pby)_3]^{+2}$)ester) was prepared to enhance the Ru polypyridyl complex adsorption in the multilayer films. Refer to chapter 2 for details describing the structure and synthesis routes. The device behavior based on sulfonated $[Ru(phen')_3]^{+2}$ and poly($[Ru(pby)_3]^{+2}$) ester will be discussed in chapter 5.

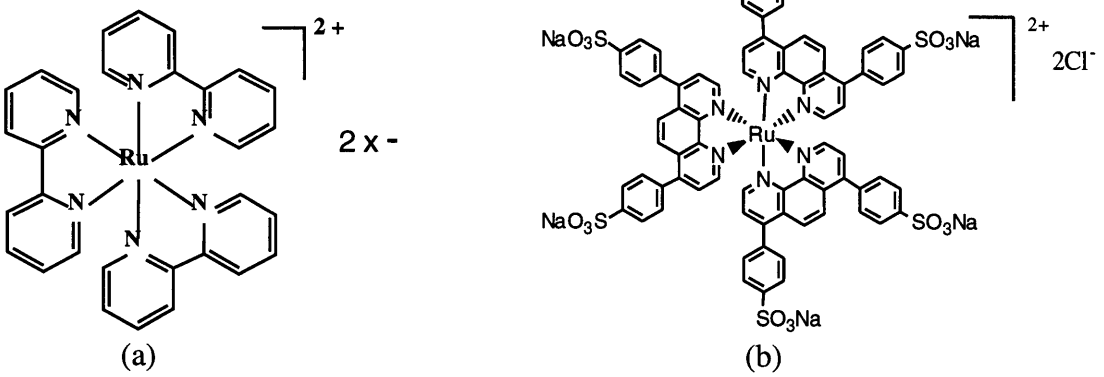

(a) (b)

Figure 4.16. The chemical structures of (a) $[Ru(bpy)_3]^{+2}$ and (b) sulfonated $[Ru(phen')_3]^{+2}$.

4.1. Sulfonated $[Ru(phen')_3]^{+2}$ / Polyelectrolyte Multilayer Film

The layer-by-layer deposited multilayer films were produced by alternate dipping of polycations such as PAH and the sulfonated $[Ru(phen')_3]^{+2}$ solution. Solutions, 10^{-3} M of $[Ru(phen')_3]^{+2}$ and $5 \cdot 10^{-3}$ M of PAH were prepared for the $[Ru(phen')_3]^{+2}$/PAH multilayer films through the automatic dipping method. Table 4.1 displays the intensity of UV/Vis spectra of 5 and 10 bilayers of sulfonated $[Ru(phen')_3]^{+2}$/PAH when pH of those dipping solutions were adjusted to be 2.5 and 4.5. The first two cases in Table 4.1 show the peak intensity of the sulfonated $[Ru(phen')_3]^{+2}$ adsorption in 5 and 10 bilayers on the glass slides without the first bilayer of PEI/SPS on the substrate. The PEI/SPS bilayer is often used to generate the ionic charges on the surface of hydrophilic glass. The latter two cases in Table 4.1 shows the sulfonated $[Ru(phen')_3]^{+2}$ adsorption on the substrates with the addition of a PEI/SPS layer. The pH of the dipping solutions did not change the adsorption of $[Ru(phen')_3]^{+2}$. In Table 4.1, it can be seen that the dye adsorption initially increased with the presence of the PEI/SPS layers, however the adsorption of 10 bilayers was not dependent on the bottom PEI/SPS layers. The sulfonic acid groups of $[Ru(phen')_3]^{+2}$ and amine groups of PAH are strong acids and bases. As a result, the pH

Table 4.1. Intensity of UV/Vis absorbance peaks of PAH/$[Ru(phen')_3]^{+2}$ films.

	5 bilayers	10 bilayers
PAH (pH 2.5) w/o PEI/SPS	0.018	0.053
PAH (pH 4.5) w/o PEI/SPS	0.019	0.052
PAH (pH 2.5) with PEI/SPS	0.03	0.051
PAH (pH 4.5) with PEI/SPS	0.027	0.056

of solutions does not affect charge densities of the PAH in the solutions and the outermost layers.

Thickness per bilayer of the sulfonated $[Ru(phen')_3]^{+2}$ and PAH was about 15 Å. The PEI and PADA polycations also successfully formed multilayer films with sulfonated $[Ru(phen')_3]^{+2}$. Most of the sulfonated $[Ru(phen')_3]^{+2}$ multilayer films, however, turned into non-uniform films after 35 bilayers were deposited. It is thought that the interaction of $[Ru(phen')_3]^{+2}$ and polyelectrolytes were weak due to the low number of charge sites and positive charges of Ru metal in the chemical structure. To increase the strength between layers and the stability of layer deposition, we introduced polymer type $[Ru(bpy)_3]^{+2}$.

4.2 Poly($[Ru(bpy)_3]^{+2}$) ester / Polyelectrolyte Multilayer Film

Both sulfonated poly(styrene) (SPS) and poly(acrylic acid) (PAA) were introduced to build up multilayer films of the poly($[Ru(bpy)_3]^{+2}$)ester. The positively charged poly($[Ru(bpy)_3]^{+2}$)ester are oligomer structure type materials, which we assume have about 3 - 4 repeat units in the polymer chain. A solution of pH 3.5 of 10^{-2} M SPS and the pH 3.5 of 10^{-2} M poly($[Ru(bpy)_3]^{+2}$)ester were used to fabricate the multilayered film. The sulfonic acids in SPS are fully charged at pH 3.5 and have a high charge density. This creates strong intrasegmental forces. Under those conditions, SPS formed thin and extended chains with a thickness per bilayer of about 25 Å. The carboxylic acid groups in PAA are partially charged at pH 3.5 and thereby the intrasegmental repulsion forces in the polymer chain are screened. The looped and coiled structure of a PAA layer was expected at a pH of 3.5. The thickness per bilayer of poly($[Ru(bpy)_3]^{+2}$)ester/PAA was about 60 Å. Figure 4.17 shows the UV/Vis absorption of 20 bilayers of the poly($[Ru(bpy)_3]^{+2}$)ester/PAA and the poly($[Ru(bpy)_3]^{+2}$)ester/SPS multilayer films. The amount of poly($[Ru(bpy)_3]^{+2}$)ester adsorption by the SPS layer is less than half of the dye adsorption through a PAA layer. These thick and loopy layer structures enhanced the dye adsorption.

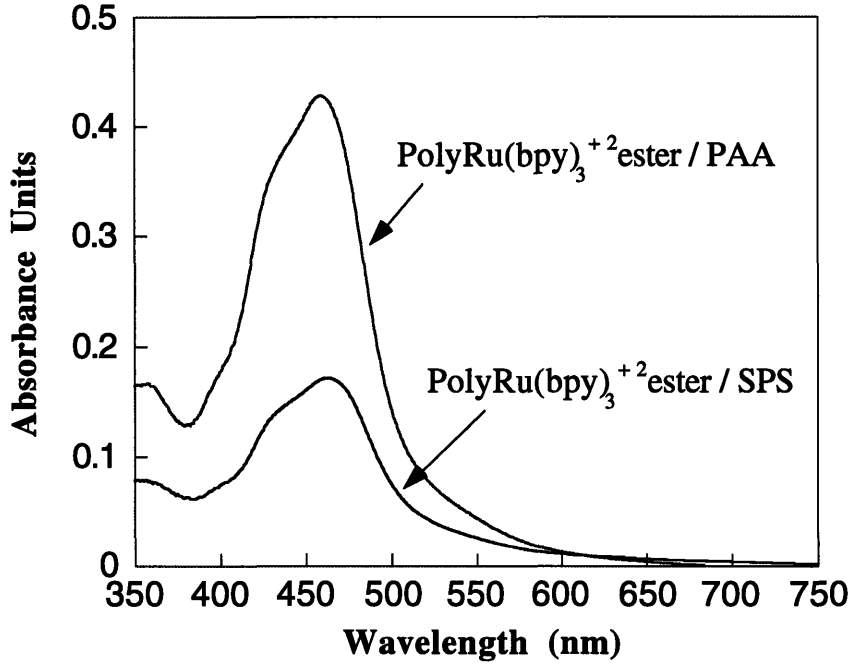

Figure 4.17. UV/Vis absorption of the poly($[Ru(bpy)_3]^{+2}$)ester/PAA and the poly($[Ru(bpy)_3]^{+2}$)ester/SPS films (20 bilayers)

4.3 Sulfonated $[Ru(phen')_3]^{+2}$ / Poly($[Ru(bpy)_3]^{+2}$)ester Film

The negatively charged sulfonated $[Ru(phen')_3]^{+2}$ and the positively charged poly($[Ru(bpy)_3]^{+2}$) ester can be bounded in order to hold the adjacent two layers to build up multilayer films. The bottom layers of the multilayer films were composed with PAH (pH 4.5, 10^{-2} M) and SPS (pH 4.5, 10^{-2} M) deposited onto the glass slide first.

By continuous dippings of $5 \cdot 10^{-3}$ M of cationic poly($[Ru(bpy)_3]^{+2}$)ester and anionic sulfonated $[Ru(phen')_3]^{+2}$, the totally ruthenium complex based films were fabricated. In Figure 4.18, again, the pH of the dipping solutions did not influence the adsorption of the Ru polypyridyl complexes. The sulfonic acid groups and bipyridyl groups do not change their charge densities as the solution pH is changed. Figure 4.19 shows the linear growth of multilayer films of sulfonated $[Ru(phen')_3]^{+2}$ and

poly($[Ru(bpy)_3]^{+2}$) ester. The small molecular weight of poly($[Ru(bpy)_3]^{+2}$) ester incorporated the limited amount of sulfonated Ru complexes. Thickness per bilayer was about 6 Å.

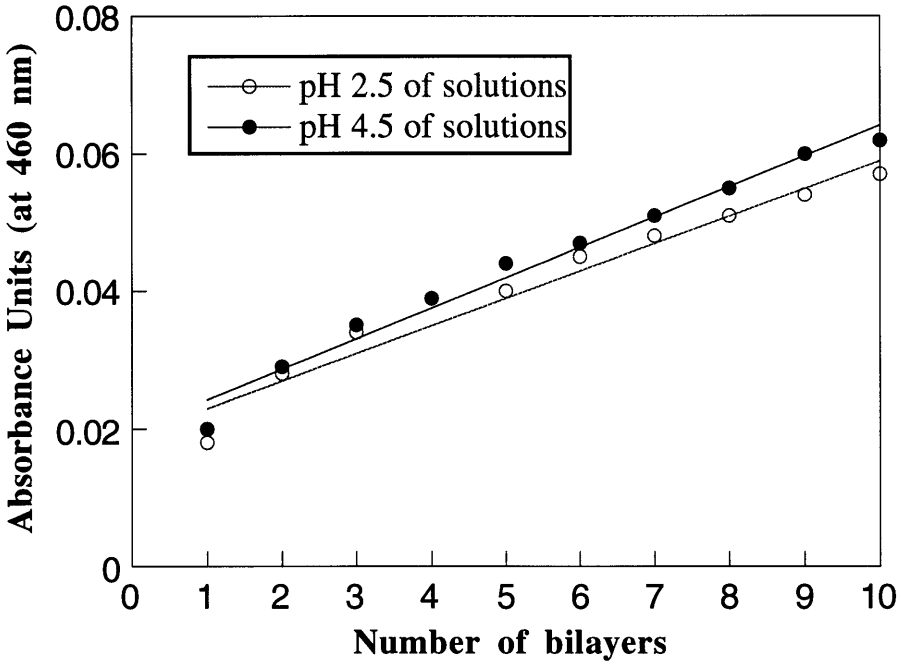

Figure 4.18. The amount of Ru complex adsorption at pH 2.5 and pH 4.5 of $[Ru(phen')_3]^{+2}$ and poly($[Ru(bpy)_3]^{+2}$)ester solutions.

The poly($[Ru(bpy)_3]^{+2}$) ester and sulfonated $[Ru(phen')_3]^{+2}$ system were applied as probe layers in Tunneling Electron Microscopy (TEM). The electron charge density of the layer makes it possible to detect the poly($[Ru(bpy)_3]^{+2}$) ester/$[Ru(phen')_3]^{+2}$ layers in the vinyl polyelectrolyte layers. The cross-sectional image of the multilayer films had strong contrast in the normal direction where poly($[Ru(bpy)_3]^{+2}$) ester/$[Ru(phen')_3]^{+2}$ layers were contained in the multilayer film.

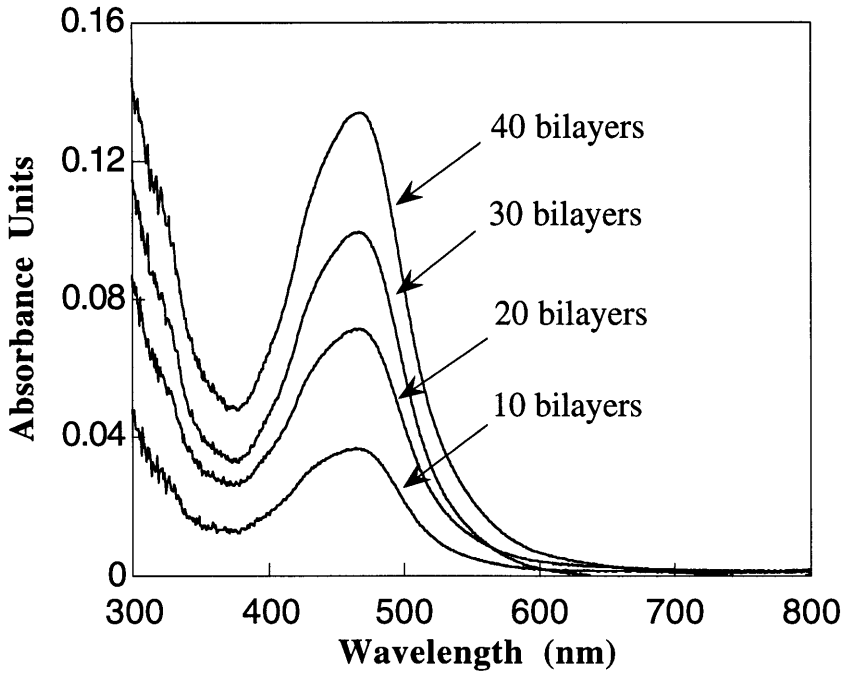

Figure 4.19. UV/Vis absorbance of sulfonated $[Ru(phen')_3]^{+2}$ and poly($[Ru(bpy)_3]^{+2}$) ester films.

5. Conclusion

Several functional dye molecules were successfully incorporated into the layer-by-layer deposited multilayer films. The structural requirement was simply two separate charges to hold two adjacent layers together. It was demonstrated that heterostructures with various materials can be formed by controlling the order of dippings.

REFERENCES

[4.1] Waring, D. R.; Hallas, G. "The Chemistry and Application of Dyes"; Plenum Press: New York, 1990.

[4.2] Gregory, P. "High-Technology Applications of Organic Colorants"; Plenum Press: New York, 1991.

[4.3] Ulman, A. "An Introduction to Untrathin Organic Thin Films from Langmuir-Blodgett to Self-Assembly"; Academic Press: San Diego, 1991.

[4.4] Yoo, D.; Rubner, M. F. *SPE Prodeedings*, Boston, MA, **1995**, 2568.

[4.5] Cheung, J. H.; Fou, A. C.; Rubner, M. F. *Thin Solid Films* **1994**, *244,* 985.

[4.6] Ferreira, M.; Cheung, J. H.; Rubner, M. F. *Thin Solid Films* **1994**, *244*, 806.

[4.7] Fou, A. C.; Onitsuka, O.; Ferreira, M.; Rubner, M. F.; Hsieh, B. R. *J. Appl. Phys.* **1996**, *79*, 1.

[4.8] Decher, G.; Hong, J. D. *Ber. Bunsenges. Phys. Chem.* **1991**, *95*, 1430.

[4.9] Decher, G.; Hong, J. D. *Thin Solid Films* **1992**, *210/211*, 831.

[4.10] Mao,G.; Tsao, Y.; Tirrell, M.; Ted Davis, H.; Hessel, V.; Ringsdorf, H. *Langmuir* **1993**, *9*, 3463.

[4.11] Bányai, É. in "Indcator"; Bishop, E. Ed.; Pergamon Press: Oxford, 1972, p65.

[4.12] Kampas, F. J.; Yamashita, K.; Fajer, J. *Nature* **1980**, *284*, 40.

[4.13] Hanack, M.; Lang, M. *Adv. Mater.* **1994**, *6*, 819.

[4.14] Gordon, P. F.; Gregory, P. "Organic Chemisty in Color"; Springer-Verlag: Berlin, 1983.

[4.15] Roundhill, D. M. "Photochemistry and Photo-physics of Metal Complexes, Chap. 5"; Plenum Press: New York, 1994.

[4.16] Balzani, V.; Bolletta, F.; Gandolfi, M. T.; Maestri, M. *Topics in Current Chemistry* **1978**, 75, 1.

[4.17] Yoo, D.; Lee, J-K.; Rubner, M. F. *Mat. Res. Soc. Symp. Proc.* **1996**, *413*, 395.

[4.18] Lee, J.-K.; Yoo, D.; Handy, E. S.; Rubner, M. F. *Appl. Phys. Lett.* **1996**, *69*, 1686.

[4.19] Radzilowski, L. *Private Communication.*

CHAPTER 5

NOVEL RUTHENIUM POLYPYRIDYL COMPLEXES FOR LIGHT EMITTING DEVICES

1. Introduction

1.1 Organic Light Emitting Devices

Organic-based light emitting devices (LEDs) have attracted much attention in the last several years because of their potential applications in large area, flat and flexible displays that can emit a full range of colors [for review papers on organic LEDs, see 5.1 - 5.6]. The use of polymers and small organic molecules as active materials in LEDs holds the promise of fabricating stable and relatively inexpensive large area displays. Some organic LEDs are reported to show more than 4% internal quantum efficiency and to have operating lifetimes up to 10,000 hours [5.7]. The brightness of these type organic LEDs reached more than 10,000 cd/m^2 in the best cases [5.8], which is about 100 times brighter than the cathode ray tube (CRT) computer screen. Although such displays still should be improved in several respects for commercial applications, development of this field has produced great improvements in a relatively short period of time. Industrialization may be possible within a few years.

Several methods based on inorganic materials are currently applied for producing electroluminescent devices [5.9], which are (1) III-V semiconductor p-n junctions, (2) fluorescent ion doped semiconductor thin film devices, and (3) semiconductor powder devices. As the p-n junction types are the most common method in semiconductor LEDs

and have some similarities to organic LEDs, the brief description of the mechanism of this p-n type devices will be useful [5.10]. In III-V semiconductor LED devices, control of doping level of the two adjacent materials, which are interconnected and acted as positive and negative electrodes, produce well defined band gap between them. When a voltage is applied by electrodes, the negative and positive charges meet at the junction of the two materials and produce light the color of which is determined by the band-gap of the two materials. Because the semiconductor LEDs are fabricated based on a single crystal form of two materials, the size of an LED is limited by the size of the single crystal. A big wafer of single crystal form of gallium arsenide is not produced yet. The brittleness of semiconducting materials also makes it impossible to form flexible LEDs.

In the organic-based LEDs, there are no limitations in fabricating the various shapes, sizes and even flexible displays, where well-defined interfaces and crystal structures are not needed due to the amorphous nature of organic emitters. The fabrication methods for the organic LEDs are cheaper by decreasing the processing steps and be easier by the amorphous nature. In terms of emitted colors, organic LEDs can easily produce full-color emissions through the use of several emitting materials and mixing emitters with other organic dopants. The low cost, full-color emission and possible application to large and flexible displays make the organic LEDs very attractive to many researchers. Organic LEDs, however, still need more environmental stability and better operation efficiency for display applications. These LEDs are going to be commercialized in near future as soon as more stable and efficient emitters are developed through a processing method to form uniform and well-ordered thin films.

Numerous organic materials have been reported as having electroluminescent properties. The organic emitters are categorized generally as small dye molecules and conjugated polymers. A small dye molecule like an aluminum complex, aluminum tris(8-hydroxyquinoline) (Alq_3), has been used frequently as an emitter material especially with the vacuum deposition technique [5.11 - 5.19] or spin-cast films with polymer binders

[5.20 - 5.22]. Consecutive evaporation forms multi-slab structures to enhance the efficiency of the devices. The mixing of Alq_3 with other dopants can be used to generate full colors easily.

The polymer type emitters have attracted much attention, because the polymer structure inhibits the crystallization of a spin-cast form and processing techniques for the polymer LEDs is simper than for the small dye molecular LEDs. Many conjugated polymers such as poly(para-phenylenevinylene) (PPV) or poly(para-phenylene) (PPP) have been used in the LEDs [5.23 - 5.28]. Non-conjugated polymers containing emitters in the chains have shown potential for the application in LEDs [5.29 - 5.30]. The emission from the polymer type emitters is tuned by chemical modification of their conjugation length. The spin-casting method is often used for fabricating LEDs based on the polymer type emitters. This simple technique successfully produces films that are good enough for the LED application. Stability and purification of materials, however, still need improvements for the device applications.

Organic LEDs are fabricated as various structures. The device structures are also important for stable and efficient device behavior. Some structural considerations for fabricating organic LEDs will be discussed in the next section.

1.2 Structure of Organic LEDs

In organic LEDs, the so-called injection-type LEDs, there are three different stages ; charge injection, charge transport and charge recombination for the formation of excitons. The excitons will decay to a ground state and light will be emitted. In the first stage, double charge carriers - electrons, holes - are injected from the cathode and the anode, respectively into the organic layers of the devices. A balanced injection from both sides is a prerequisite for high efficiency. The high work function metals like indium-tin oxide (ITO), Au and Pt can be used as the anode for hole-injection. For LED applications, thin transparent ITO is necessary for the emission of light. The low work function metals, such

as Al, Ca, and Mg are evaporated on the top of the organic thin films for a cathode, facilitating electron injection. The electrodes will modify the characteristics of injection of charge carriers to the thin films. Lower work function electrodes such as Ca and Mg may facilitate electron injection to enhance the efficiency of devices by one or two orders of magnitude, because the electron injection is harder than hole injection in organic materials [5.31 - 5.32]. However, Ca and Mg are extremely unstable in air. Al is preferable for outside device applications.

In the second stage, charge carriers migrate into the devices and excite the emitter materials. The semiconductor LEDs which have a band gap of at least 3 eV, utilize a small number of carriers of a high density of carriers at the interface of the p-n junction, while in organic LEDs, most of carriers for recombination should be injected from the electrodes because of the low density of carriers in the device at the ground state. The mobility of charge carriers and the relative mobilities of holes and electrons influence the efficiency and the brightness of organic LEDs. The organic materials, in general, differ in their abilities to transport electrons and holes.

The simplest type of LEDs is a single-layer-device with one organic emitter layer. The emitter layer transports both electrons and holes in the device. In the single layer device, the electron and hole transport generally are not balanced and recombination is localized at the interface between the emitter layer and electrode metals. This localization may be accompanied by quenching at the interface or damage the interface by heat produced at the recombination. Multilayer-type devices have more than two discrete layers, such as a hole-transport layer and an electron-transport layer, sandwiched between injecting electrodes. Since the hole transport layer blocks electrons and the electron transport layer blocks holes, these multilayer structures increase the efficiency of recombining electrons and holes in the emitter layer. Several researchers reported the increase of efficiency through the use of heterostructures with which it is easier to balance hole and electron transport [5.11, 5.12, 5.13, 5.33 - 5.35]. Aromatic amine based materials are known for

their high hole mobility and hereby frequently are used as a hole transport layer, which has a low ionization potential and small electron affinity associated with a large energy gap [5.36 - 5.37]. Alq_3 is one of the most frequently used electron transport layer materials. Oxadiazole and triazole derivatives are also known as the possible materials for accelerating electron transport [5.38 - 5.39]. The bulky substituent on these materials can deter the formation of species such as exciplexes and charge transfer complexes.

In the third stage, recombination of electrons and holes in the organic layer generates singlet excitons. Those excitons are transferred to more stable states through radiative decay or non-radiative decay. Stable excitons are required to generate high efficiency LED. Among the several proposed materials for LED applications, some materials show excellent redox stability at oxidation or reduction. However, some LED materials showed the irreversible decomposition after the recombination. There are few references on the stability of excited states, but understanding of possible decomposition of excited states will help the design do more efficient devices.

The overall efficiency of organic LEDs is dependent on the balance of charge injection and charge transport in the organic layers. Multilayered structure-type LEDs offer more flexibility in choosing the right materials to control the charge carrier injections and the rate of diffusion of charge carriers. However, there are few fabrication methods for generating multilayer films and these fabrication methods have not been successful in producing well-defined multilayer films. The fabrication method for a multilayer film will be discussed in the next section.

1.3 Fabrication Methods for Organic LEDs

A spin-casting technique and a thermal evaporation technique under vacuum are most-widely applied techniques for fabricating organic LEDs. The spin-casting technique involves placing a small quantity of concentrated solution onto a substrate and rotating the substrate to dry solvent [5.40]. An cast organic thin film is thereby produced on the

substrate. The thickness and the quality of thin films are dependent on the rate of rotation of the substrate and the concentration of the solutions. The spin-casting technique is currently applied for many different commercial products in industry because of its simplicity. Polymer-type emitters such as PPV or PPP, are successfully built into single-layer devices using this technique.

The spin-casting technique, however, has several limitations for application to organic LEDs. The small emitter dye molecules easily crystallize in the solid state and produce non-uniform thin films, when spin-cast onto the ITO. The spin-casting technique has other limitations with regard to preparing multilayer structures. By consecutive spin-casting of several solutions, the multilayer structures may be fabricated. However, during the multiple spin-castings, the solvent used should not dissolve the bottom layers. Also, the additional layer may not form a good interface with the bottom layer. Even though this technique has some limitations, the technique is the most versatile way to fabricate organic thin films.

The other widely-used method for organic LEDs is the vacuum deposition technique. At high vacuum, the organic emitter is slowly evaporated onto the ITO surface. The vacuum deposition technique can be used to form very uniform and very thin layers as it hinders the crystallization of the emitters and the formation of defects in the layers. By evaporating small organic materials in sequence, the multilayer structure with uniform and clean interfaces can be fabricated. The first highly efficient heterostructure-organic LEDs based on Alq_3 emitters were fabricated by the vacuum deposition technique. Some companies already announced plans to commercialize full color LEDs based on Alq_3 through this technique. The technique, however, requires high vacuum and harsh manufacturing conditions for generating the uniform films. This is somewhat contradictory to the promise that the use of organic materials would make it possible to fabricate LEDs via simple methods.

In the previous chapters, the layer-by-layer deposition technique was shown to be a simple and easy way to fabricate a thin heterostructure film. Our group pioneered the use of the layer-by-layer deposition technique for producing organic LEDs. Thickness and architectures of layers are manipulated with ease by this technique. Various layers, such as hole transport layers, electron injection layers, and emitter layers, can be incorporated into a multilayer with molecular controlled system. The layer-by-layer deposition technique does not require the use of toxic solvents for preparing a thin film, which are used for spin-casting of conjugated polymers. The first LED was fabricated by repeated dipping of a precursor form of PPV and poly(methacrylic acid) (PMA) and poly(sulfonate styrene) (SPS) [5.40]. The behavior of these multilayered LEDs has shown a dependence on the oppositely charged polyelectrolytes. The two slabs of PPV/SPS and PPV/PMA greatly enhanced the efficiency of the LED. The multilayer PPV study demonstrated the possibility of using the layer-by-layer deposition technique for building up heterostructure LEDs. Like these PPV based emitting devices, heterostructure multilayer films can be obtained through the technique.

2. Ru Polypyridyl Complexes as Light-Emitting Materials

2.1. Characteristics of Ruthenium Polypyridyl Complexes

Even though the organic emitter materials show full-color emission, including blue, and have higher quantum yields, the lifetime of the devices still does not match that of semiconducting emitters. Poor durability or poor thermal stability of organic LEDs originate from the non-uniform device film quality or instability of the organic emitter materials at the applied voltage. The electrochemical properties of the emitter materials at the excitation transition, which may influence the efficiency and the lifetime of the LED, have been little studied. However, many of these emitter materials exhibit irreversible oxidation or reduction. For example, the cyclic voltammogram of trimer units of PPV in

solution (THF or acetonitrile) has shown irreversible oxidation and the quasi-reversible reduction peaks. Similar irreversible redox processes have been observed in a soluble PPV derivative, alkoxy-substituted PPV [5.41]. On the other hand, Alq_3 is known to exhibit several reversible reduction processes [5.42] which might account for the very stable emitter behavior.

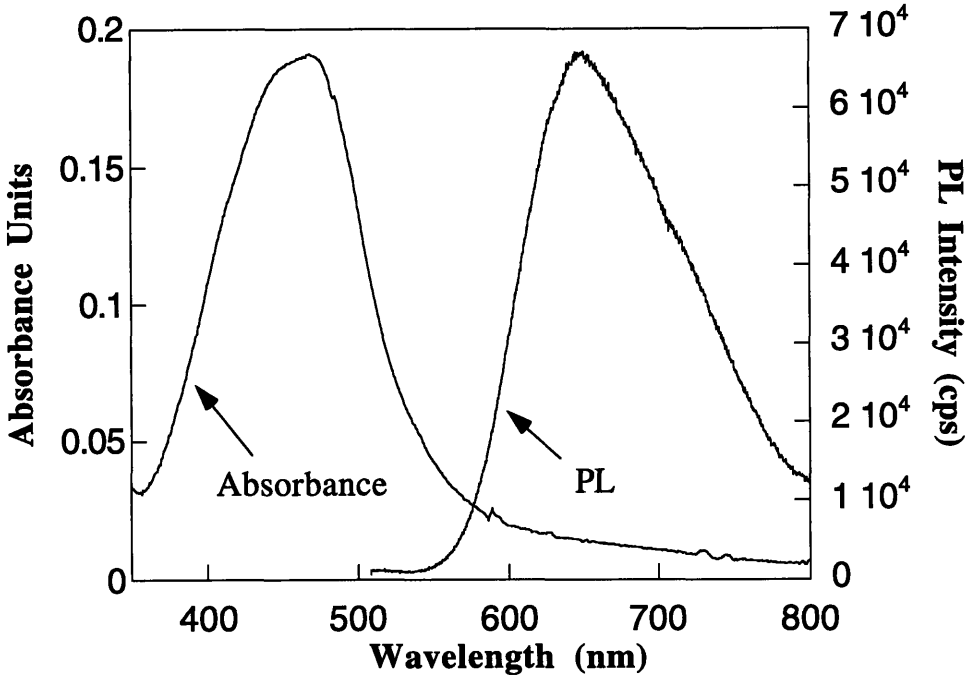

Figure 5.1. Absorbance and photoluminescence (PL) spectra of sulfonated $[Ru(phen')_3]^{+2}$.

Tris-(2,2'-bipyridine)ruthenium(II) $[Ru(bpy)_3]^{+2}$ are well known for their novel chemiluminescent properties and excellent redox stability [5.43 - 5.45]. $[Ru(bpy)_3]^{+2}$ can be oxidized and reduced without decomposition or dissociation of ligands. The excited state has long life time and shows very stable decay to a lower state. To our knowledge, $[Ru(bpy)_3]^{+2}$ has not yet been studied as a possible light emitting material in thin film devices, most likely because of its propensity to crystallize in the solid state. Crystallinity severely hinders the formation of high quality thin films. Our group therefore synthesized

the tris(bathophenanthroline disulfonate ruthenium complex), sulfonated $[Ru(phen')_3]^{+2}$ shown in Figure 2.1 and examined its ability to act as an emitter in LEDs [5.46]. The absorption maximum ($\lambda_{max,ab}$) of this compound is 470 nm as a cast film. Its emission maximum ($\lambda_{max,em}$) is 628 nm.

Figure 5.1 displays the absorbance and photoluminescence spectra of a spin-cast sulfonated $[Ru(phen')_3]^{+2}$ film. The red-orange emission was observed from a single layer of the sulfonated $[Ru(phen')_3]^{+2}$. The sulfonated $[Ru(phen')_3]^{+2}$ produced a good uniform single layer and formed layer-by-layer deposited multilayer films through ionic interactions.

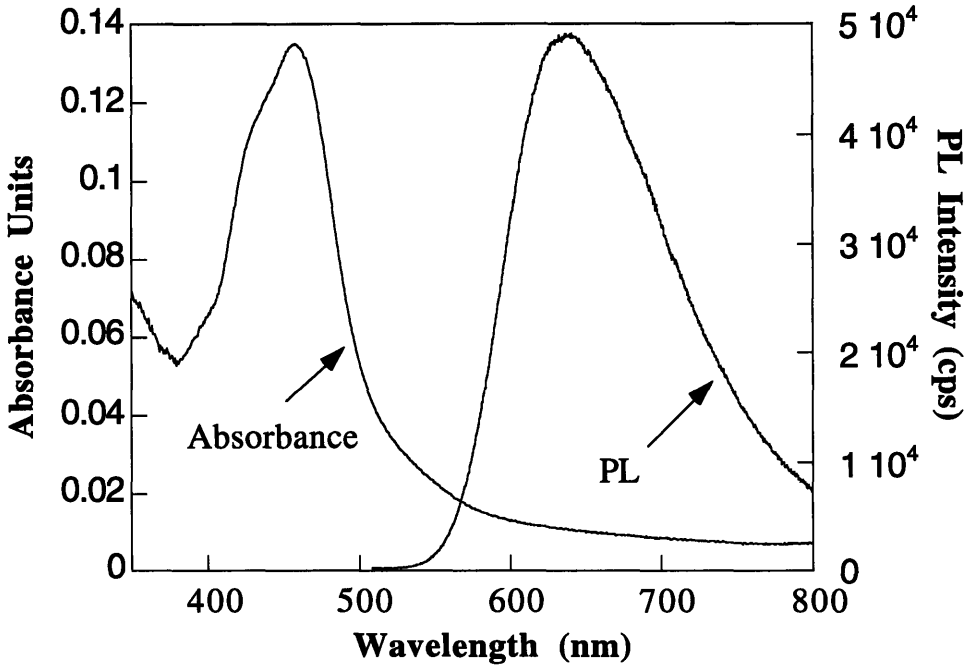

Figure 5.2. Absorbance and photoluminescence (PL) spectra of poly($[Ru(bpy)_3]^{+2}$)ester.

The other Ru polypyridyl complex material, a polymer containing ruthenium (II) tris(bipyridine) complex polymer, poly($[Ru(bpy)_3]^{+2}$)ester was recently prepared and used as an emitter [5.47]. The chemical structure of the polymer was displayed in Figure 2.2.

The stability of electrochemically generated species, such as oxidized Ru(III) and reduced Ru(I) complexes, is expected to enhance the charge-transporting property as well as the probability of creating excited states. The main idea of preparing a poly($[Ru(bpy)_3]^{+2}$)ester is to increase the thin film quality by using high molecular weight materials and to enhance the amount of Ru complex units in the layer-by-layer deposited multilayer films, compared with the $[Ru(phen')_3]^{+2}$. Furthermore, the poly($[Ru(bpy)_3]^{+2}$)ester can be incorporated with a variety of polyanions into the multilayer films and a study made of different polyelectrolyte effects on LEDs.

The absorbance and photoluminescence spectra of poly($[Ru(bpy)_3]^{+2}$)ester are shown in Figure 5.2. The shape and maximum wavelength are almost identical in the sulfonated $[Ru(phen')_3]^{+2}$ and the poly($[Ru(bpy)_3]^{+2}$)ester.

2.2. Single Layer Devices of Sulfonated $[Ru(phen')_3]^{+2}$ and Poly($[Ru(bpy)_3]^{+2}$)ester

Single-layer devices of the sulfonated $[Ru(phen')_3]^{+2}$ dye were prepared by spin-casting. The sulfonated $[Ru(phen')_3]^{+2}$ solution in 2-methoxy ethanol was spun onto glass substrates coated with an ITO conducting layer, followed by evaporation of a 2000 Å aluminum electrode in a vacuum of $5 \cdot 10^{-6}$ Torr. The sulfonated $[Ru(phen')_3]^{+2}$ solution was 5% by weight concentration (0.025g in 0.5 ml solvent). Several drops of the sulfonated $[Ru(phen')_3]^{+2}$ solution covered the 2 cm^2 substrate with 2mm ITO lines. The substrate was spun to dry the sulfonated $[Ru(phen')_3]^{+2}$ solution put onto the ITO. The spin rate of the substrate was 3000 rpm. Typical thickness of the films were measured at 780 Å by profilometry. The single-layer device showed uniform orange emission under forward bias at 6 V, with a luminance of about 1500 nW (Figure 5.3). The intensity of electroluminescence (EL) was proportional to the current and the EL and photoluminescent (PL) spectra were almost the same, indicating the same origin for the emission in EL as in

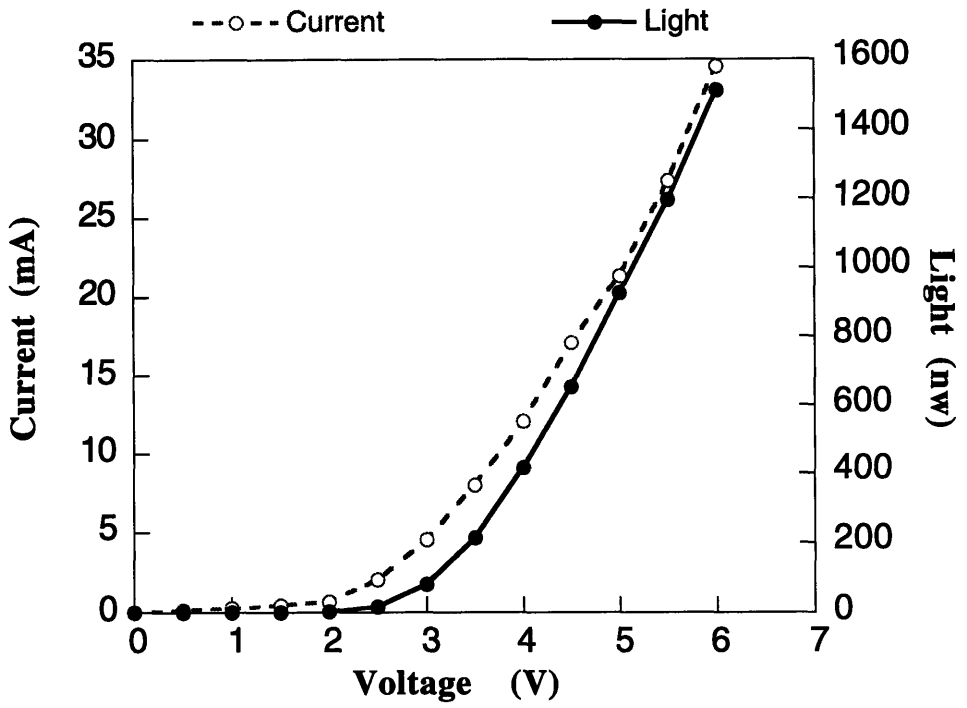

Figure 5.3. Current-voltage and light-voltage behavior of spin-cast sulfonated $[Ru(phen')_3]^{2+}$ device.

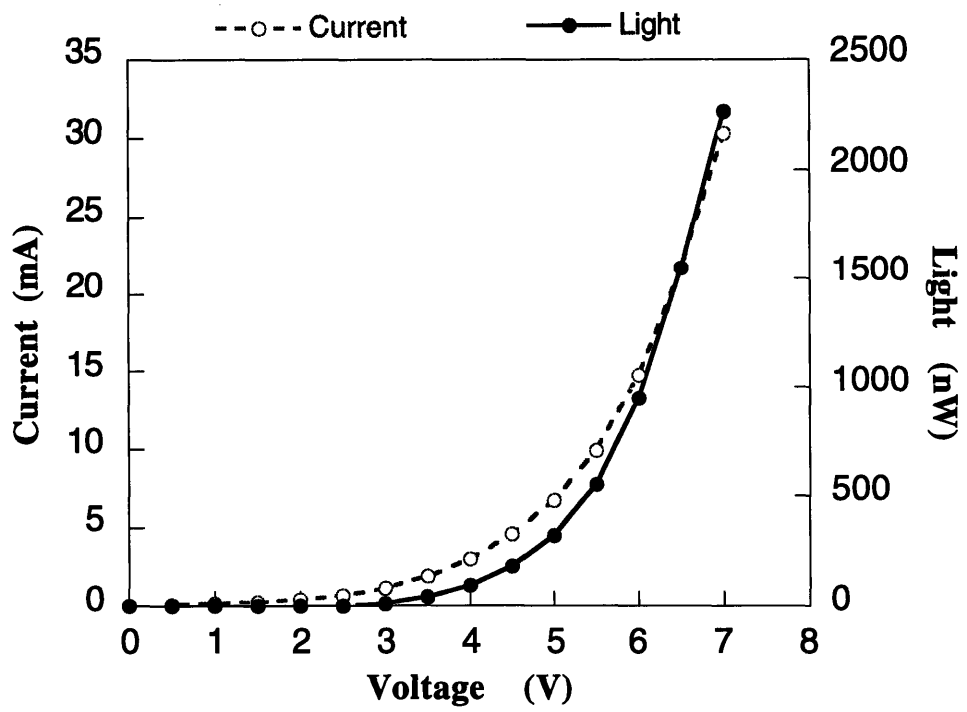

Figure 5.4. Current-voltage and light-voltage behavior of spin-cast poly($[Ru(bpy)_3]^{+2}$)ester device.

PL. Light was not emitted in the reverse bias with ITO as cathode for an electron injection and Al as anode for a hole injection. The turn-on voltage of the device was observed at 2.5 V. The thickness of the sulfonated $[Ru(phen')_3]^{+2}$ layer does not influence the turn-on voltage of the devices.

Single-layer LEDs of a poly($[Ru(bpy)_3]^{+2}$)ester were prepared by spin-casting at similar to the condition for the sulfonated $[Ru(phen')_3]^{+2}$ devices. Figure 5.4 shows typical light-voltage and current-voltage curves for a ITO/poly($[Ru(bpy)_3]^{+2}$)ester/Al device. These single-layer LEDs showed the same color of orange-red emission under forward bias with a maximum luminance of about 80 cd/m^2 (2400 nW) at a current density of 750 mA/cm^2. From these luminance and current density values, the external quantum efficiency of these single-layer devices is calculated to be about 0.02% (photons per electron). Even though high-brightness devices were obtained using the Ru complex type

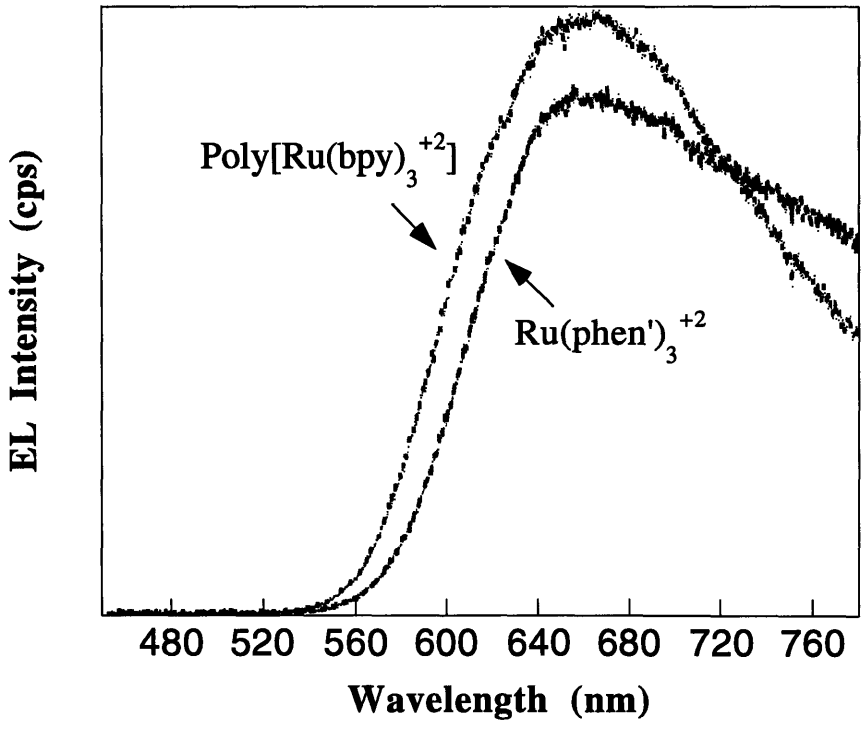

Figure 5.5. EL spectra of sulfonated $[Ru(phen')_3]^{+2}$ and poly($[Ru(bpy)_3]^{+2}$)ester.

devices, the high current of the devices indicates the need for more efficient LEDs. It means that leakage current and unbalanced charge mobility problems persist in the single layered devices. The turn-on voltage of the devices was at 2.5 V, which is the same as that of the single layer devices based on sulfonated $[Ru(phen')_3]^{+2}$.

A comparison of the electroluminescences of the spin-cast of the sulfonated $[Ru(phen')_3]^{2+}$ and the poly($[Ru(bpy)_3]^{2+}$)ester devices is displayed in Figure 5.5. There is only a slight difference observable in the two spectra. Neither devices emitted light at the reverse bias.

The stability of these devices was checked by holding the voltage at 6 V. Figure 5.6 shows the changes of the current and the light intensity of the spin-cast $[Ru(phen')_3]^{+2}$ and poly($[Ru(bpy)_3]^{+2}$)ester devices at 6 V. The devices exhibited relative stable behavior, however, the light intensity dropped below half of the maximum initial value in less than 30 minutes. The current of the poly($[Ru(bpy)_3]^{+2}$)ester devices dropped faster than that of the sulfonated $[Ru(phen')_3]^{+2}$ devices. The sulfonated $[Ru(phen')_3]^{+2}$ single-layer device showed slightly more stable performance than the poly($[Ru(bpy)_3]^{+2}$)ester single-layer device. One of the interesting observations in these devices was so-called charging effects. The current and light intensity of the devices increased for the first two or three minutes (shown in Figure 5.6) before degrading. Our group is still doing research in order to understand the mechanisms of the charging effects of Ru polypyridyl complex based devices, however, we believe this behavior is related with the generation of charged species, such as oxidized forms and reduced forms of the Ru complexes. The Ru complexes take some time to increase the charged species in the devices when the biased voltage is applied. The devices produced the maximum light-out once the density of charge species saturated in the devices. Those behavior is believed to be explained by the mechanism of electrochemiluminescence (ECL). I will discuss a proposed model of Ru

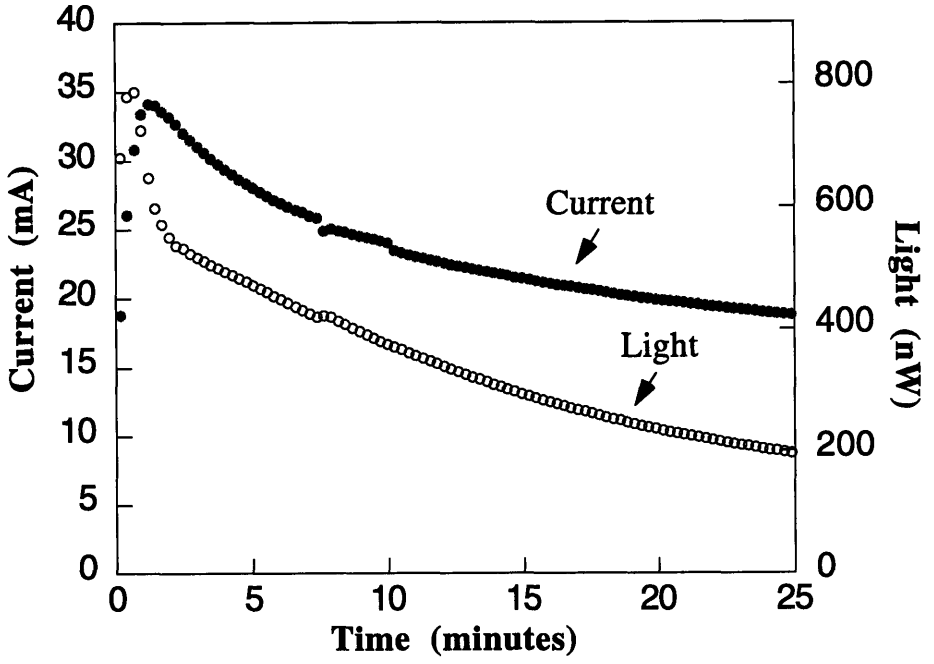

(a)

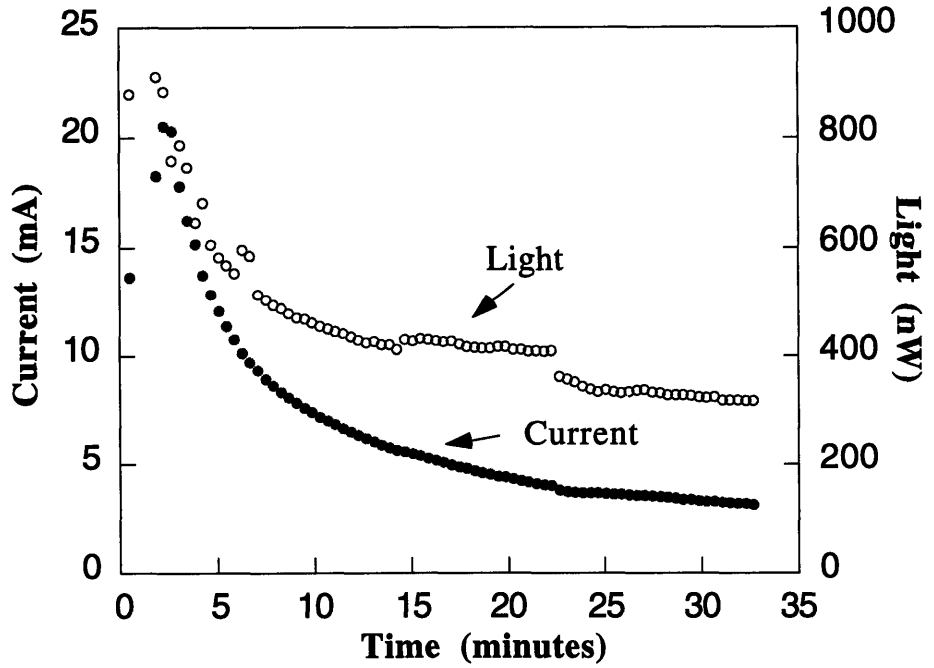

(b)

Figure 5.6. Stability data of (a) $[Ru(phen')_3]^{+2}$ single-layer device and (b) poly($[Ru(bpy)_3]^{+2}$)ester single-layer device at 6 V.

complexes LEDs based on the ECL. The charging behavior in the layer-by-layer deposited devices is going to be discussed in the following sections.

I further investigated for making more efficient and stable devices of the sulfonated $[Ru(phen')_3]^{+2}$ and poly($[Ru(bpy)_3]^{+2}$)ester through the layer-by-layer deposition technique.

3. Sulfonated $[Ru(phen')_3]^{+2}$ and Polyelectrolyte Multilayer Films

A multilayer device was fabricated by alternate dipping of pH 2.5, 10^{-2} M of PEI and the $[Ru(phen')_3]^{+2}$ solution. Thirty bilayer (pair of PEI and $[Ru(phen')_3]^{+2}$ layers) devices, about 50 nm in thickness, were prepared by the layer-by-layer deposition technique on a glass substrate patterned with lines of ITO. This was followed by the

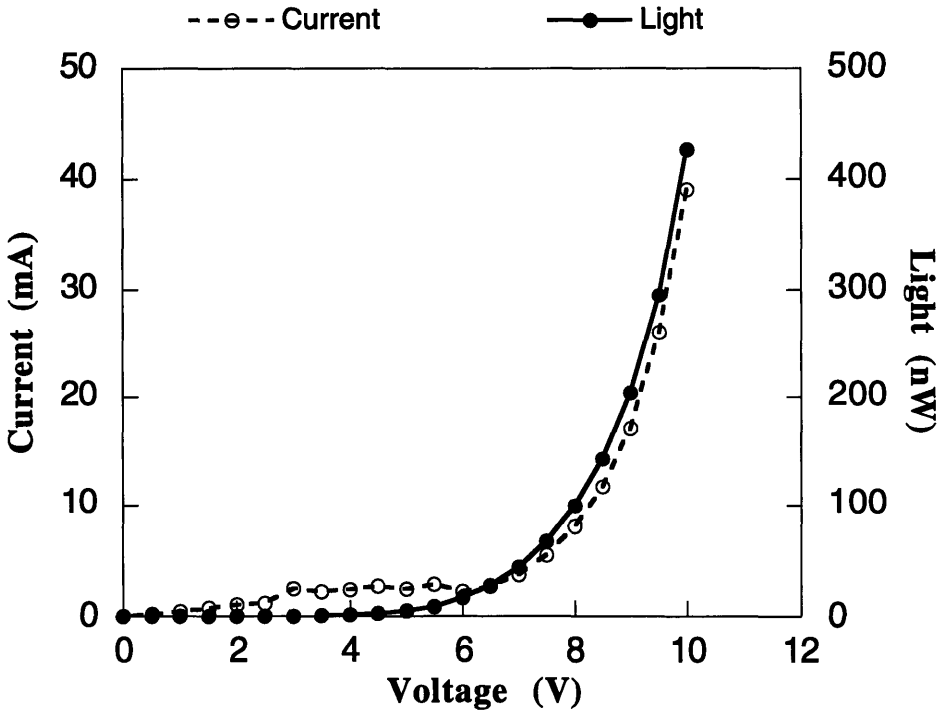

Figure 5.7. Current-voltage and light-voltage curves of PEI/$[Ru(phen')_3]^{+2}$ multilayer film.

evaporation of an aluminum electrode onto the film. This device showed uniform orange emission under forward bias at 10 V and a luminance of 400 nW (Figure 5.7). After inserting insulating layers (PEI) between $[Ru(phen')_3]^{+2}$ layers, the turn-on voltage of the device increased compared to that of the single-layer device. We expected much improved film quality by using the layer-by-layer technique, but the actual film quality was not improved due to the weak interaction between the polyelectrolyte layers and $[Ru(phen')_3]^{+2}$ layers. The nature of the dipping solution for a polyelectrolyte and $[Ru(phen')_3]^{+2}$ strongly affected the film fabrication. The external quantum efficiency of the multilayer device was about 0.004% which was actually lower than that of the single-layer device. The emission of light was not obtained in the reverse bias.

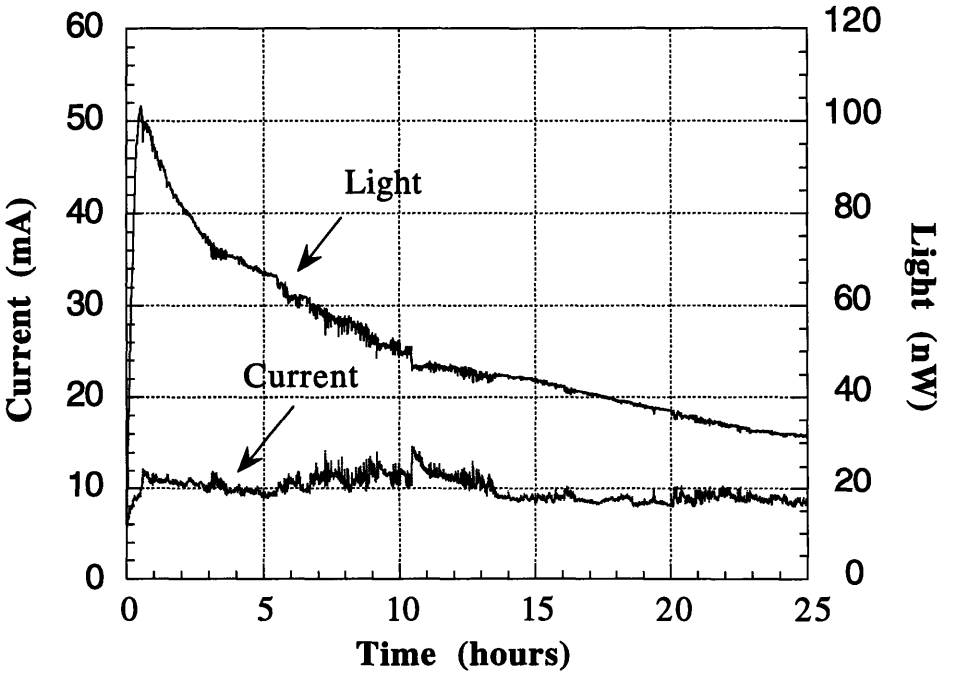

Figure 5.8. Stability of 30 bilayer PEI/$[Ru(phen')_3]^{+2}$ LEDs.

The most interesting feature of this device was its relatively high stability. The stability of the device was checked at 8 V with a luminance of 100 nW. The luminance

actually increased during the first 30 minutes of operation. This phenomena was observed in all cells in the device and is probably due to some charging effects [5.48]. It took longer time to produce maximum light-out than the spin-cast devices. The luminance then decreased slowly over many hours (Figure 5.8). The device kept more than 30% of the original luminance, even after 25 hours of continuous operation. The very stable current (about 10 mA, Figure 5.8) during the entire measurement also indicated the stability of the device.

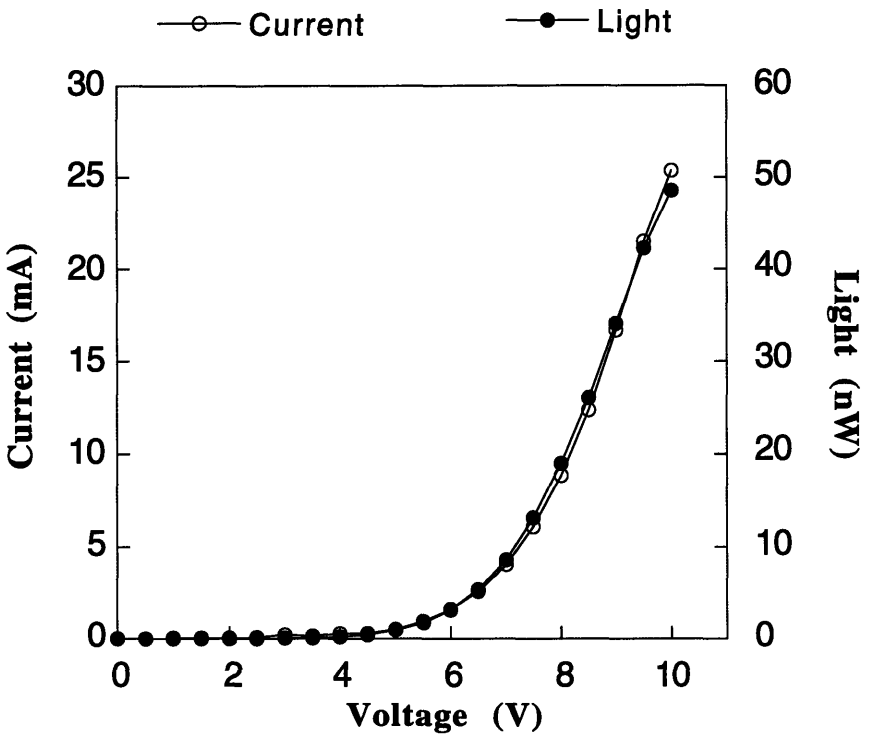

Figure 5.9. Current-voltage and light-voltage curves of PAH /$[Ru(phen')_3]^{+2}$ multilayer film.

Figure 5.9 shows the device behavior of 30 bilayers of PAH and sulfonated $[Ru(phen')_3]^{+2}$. By alternate dipping of 10^{-2} M PAH at pH 2.5 and 10^{-2} M sulfonated $[Ru(phen')_3]^{+2}$ at pH 2.5, a 30-bilayer, about 450 Å thick film was deposited onto ITO and the LED was prepared. The maximum light output was only 50 nW at 10 V and the turn-on voltage of the device was the same as the PEI/$[Ru(phen')_3]^{+2}$ device. The amount

of deposited sulfonated $[Ru(phen')_3]^{+2}$ was almost the same in those two systems. The UV/Vis spectra revealed that the peak intensity of 30 bilayers of $[Ru(phen')_3]^{+2}$/PEI was 0.15 and that of $[Ru(phen')_3]^{+2}$/PAH was 0.13.

The repeated dippings of $[Ru(phen')_3]^{+2}$ and polyelectrolyte solutions could not produced a uniform film of thicker than 35 bilayers. I suspect that the positive charges (+2) of Ru in the sulfonated $[Ru(phen')_3]^{+2}$ may inhibit the interactions with positive polyions, PAH and PEI. To increase the strength between layers for building up thick films and enhance stability of layer deposition, the polymer type of $[Ru(bpy)_3]^{+2}$ emitter was introduced. I further studied the poly($[Ru(bpy)_3]^{+2}$)ester multilayer films to produce LEDs.

4. Poly($[Ru(bpy)_3]^{+2}$)ester and Polyelectrolyte Multilayer Films

The poly($[Ru(bpy)_3]^{+2}$)ester is a water-soluble polycation so it can be self-assembled in a layer-by-layer manner with suitable polyanions such as poly(acrylic acid) (PAA), poly(methacrylic acid), and sulfonated poly(styrene) (SPS). The thickness and composition of bilayer of poly($[Ru(bpy)_3]^{+2}$)ester/anionic polyions can be controlled with the condition of polyion solution.

4.1. Poly($[Ru(bpy)_3]^{+2}$)ester and Poly(acrylic acid) Devices

Layer-by-layer deposited multilayers of the poly($[Ru(bpy)_3]^{+2}$)ester and PAA were fabricated by the automatic dipping method. One bilayer of poly(allylamine hydrochloride) (PAH) and PAA was deposited as a bottom layer onto the ITO substrate to enhance adsorption of the first layer of a poly($[Ru(bpy)_3]^{+2}$)ester. The continuous dipping of pH 3.5, 10^{-2} M of poly($[Ru(bpy)_3]^{+2}$)ester and PAA generated a uniform and a linear growth multilayer film up to 50 bilayers. This multilayer film is composed of the

continuous layers of the poly($[Ru(bpy)_3]^{+2}$)ester and insulating layers (PAA). The thickness-per-bilayer of the poly($[Ru(bpy)_3]^{+2}$)ester/PAA was measured to be approximately 60 Å. At pH 3.5 of the PAA solution, the PAA had a loopy structure and many unbounded sites were left on the outermost layer. Fifteen, twenty five and thirty five bilayers of the poly($[Ru(bpy)_3]^{+2}$) ester and PAA were adsorbed onto the ITO substrates.

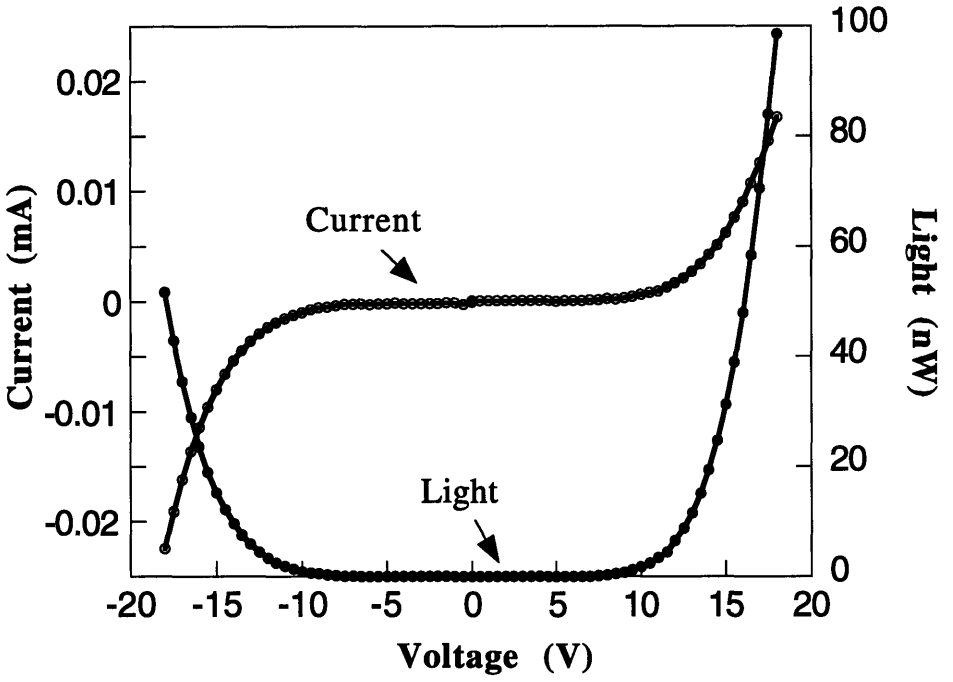

Figure 5.10. Current-voltage and light-voltage curves of poly($[Ru(bpy)_3]^{+2}$) ester/PAA multilayer film.

After annealing them for 10 hours at 110 °C in the vacuum oven, again, about 2000 Å of Al was deposited onto the multilayered films.

Figure 5.10 shows current-voltage and light-voltage curves of 35 bilayers of the poly($[Ru(bpy)_3]^{+2}$)ester and PAA. Each active light emitting cell was scanned multiple times until the light and current versus voltage curves were identical in the upward and downward scans (for further explanation, see chapter 2). The current and light of the

positive voltage data (0 to 18 V) in Figure 5.10 were obtained by applying the voltage in the forward bias multiple times first. Those of the negative voltage data (0 to - 18 V) were generated separately by applying the voltage in the reverse bias multiple times later.

Compared with the spin-cast sample of the poly($[Ru(bpy)_3]^{+2}$)ester, the 35 bilayers of the poly($[Ru(bpy)_3]^{+2}$)ester and PAA showed excellent efficiency, which was about 100 times more efficient. Even though Al was used as a cathode, the external quantum efficiency of the device reached approximately 2%. This behavior of the devices approaches the best device performance reported.

The maximum brightness of the spin-cast device was 120 nW at 18 V. The maximum light of this multilayer device did not reach that of the spin-cast devices, but were still bright enough to see under the fluorescent lamp. It can be seen that the strong increase of the efficiency of the device was due to the increase of the balance of the charge mobilities between reduced and oxidized forms of the poly($[Ru(bpy)_3]^{+2}$) esters. The PAA layers may decrease charge mobilities and increase the possibility of the recombination, or may help to produce high quality films by just decreasing the pin-holes in the device. The insulating PAA layers increased the turn-on voltage of the device and operating voltage. The high operating voltage facilitated the generation of irreversible excited species during the operation. The light intensity dropped less than half of the original light intensity within 10 minutes at 16 V.

The other interesting characteristic was that light was emitted in the reversed bias mode. In the multilayer-deposited device of the poly($[Ru(bpy)_3]^{+2}$)ester and PAA, almost symmetric behavior was observed at forward bias and reverse bias modes. The turn-on voltage of the device was exactly the same at the two electrodes. The efficiency of the forward bias, however, is higher than that in reverse bias. These results indicate that the device behavior does not depend on the work function of metals at the interfaces. The generation of charge species was performed at both electrodes to build up p/n junction type interfaces when the voltage applied. This kind of reversible device performance was

reported in the PPV film. Heeger group introduced the reversible light-emitting electrochemical cells through mixing PPV with poly(ethyleneoxide) (PEO) and salts, while the single layer PPV devices were strongly dependent on the metal electrodes [5.49]. MacDiarmid et al. also reported the AC operating device by coating a conducting polymer on both sides of the emitting materials [5.50].

A. Charging Effect

Charging effect, which is seen in the hysteresis between the upward voltage stroke and downward voltage stroke, implied that the device was enriched with reduced and oxidized forms at the upward voltage stroke and showed better performance at the backward voltage stroke.

The multilayer films of PAA/poly($[Ru(bpy)_3]^{+2}$)ester showed the charging effect when the voltage was applied. The device behavior was examined by applying the voltage in forward bias first and in the reverse bias later without recession or in reverse bias first and in forward bias later. In both cases, the devices exhibited a strong dependence on the previous run. Figure 5.11 shows that current-voltage and light-voltage curves followed the normal device behavior at forward bias and strong charging behavior was observed at the reverse bias. Once the voltage was applied to the device, the oxidized and reduced forms of the poly($[Ru(bpy)_3]^{+2}$)ester were generated at the interfaces of the electrodes and the film. The oxidized or reduced forms of the species at the interface did not convert to the neutral states immediately. When a reverse bias was applied to the device again immediately following forward bias, the charge injection was deterred by remaining reduced or oxidized forms of the poly($[Ru(bpy)_3]^{+2}$)ester at the metal interfaces. The strong charging behavior was observed in the reverse bias in Figure 5.11. Figure 5.11 shows that the device performs better when the voltage was ramped up from - 16 V to 0 V than ramped down from 0 V to -16 V. Figure 5.12 shows the same behavior in the

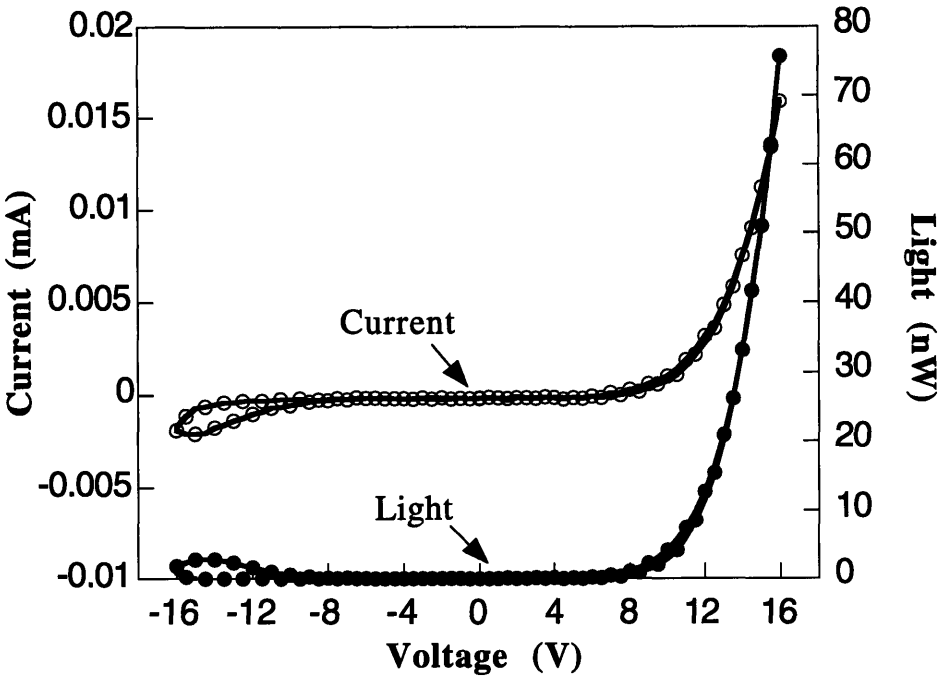

Figure 5.11. Current-voltage and light-voltage curves of PAA/ poly($[Ru(bpy)_3]^{+2}$) ester generated by applying forward bias first.

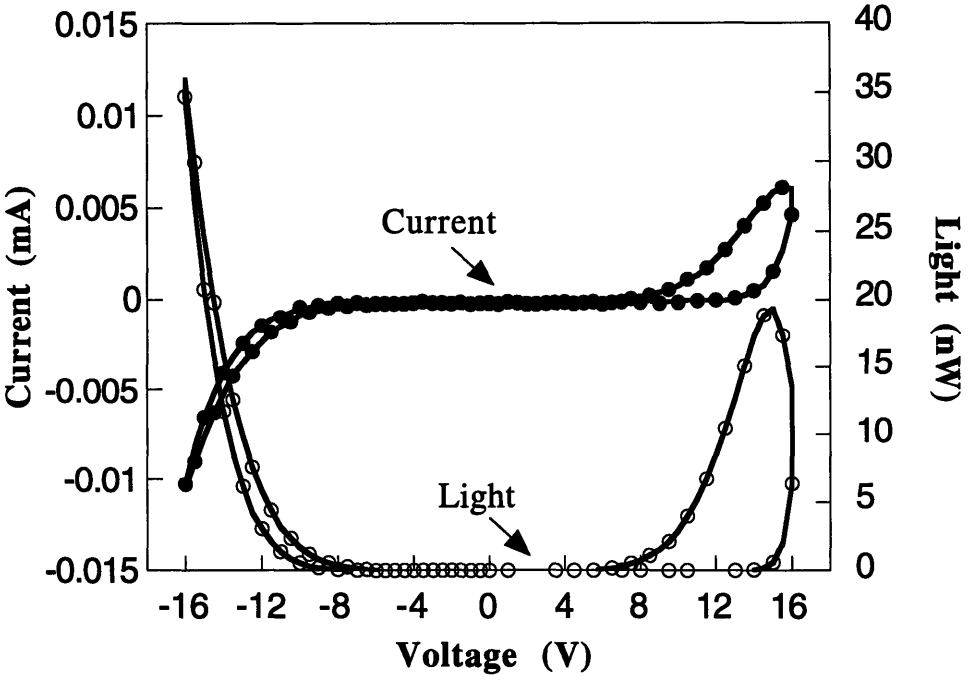

Figure 5.12. Current-voltage and light-voltage curves of PAA/ poly($[Ru(bpy)_3]^{+2}$)ester generated by applying reverse bias first.

opposite direction by applying the reverse bias first and forward bias later. The charging behavior was seen in the forward bias in Figure 5.12.

Similar to the ECL devices, the population of the oxidized and reduced forms generate up to some level before they interact to form the excited state, but this device takes a rather longer time to generate sufficient charge groups for light emission. The charging effects were widely seen in the Ru polypyridyl complexes based devices. In some device performance, it takes minutes at the same voltage to reach the maximum light output.

B. Thickness-Dependence Behavior

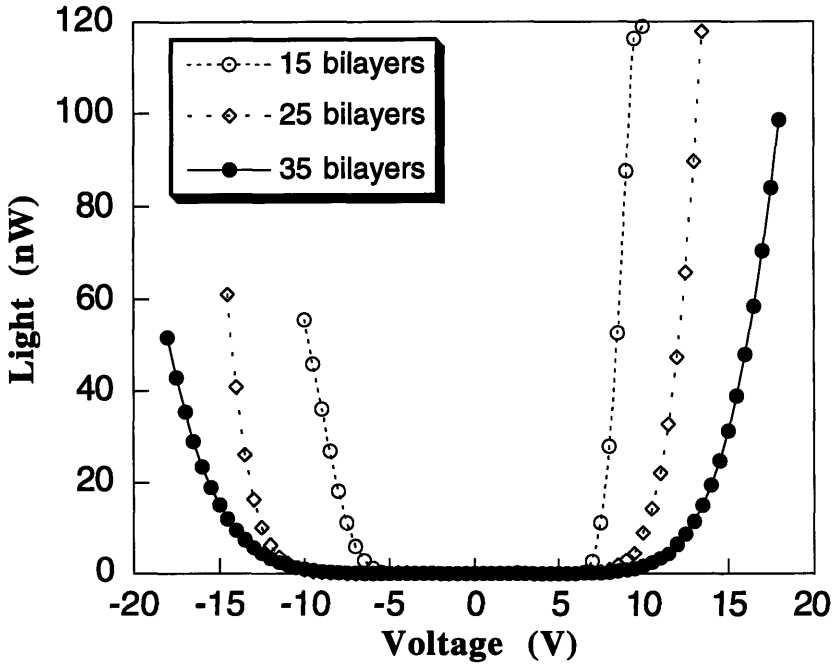

Figure 5.13. Thickness dependence on Light-voltage curves of PAA/poly($[Ru(bpy)_3]^{+2}$)ester.

The dependence of device behavior on thickness of the multilayer poly($[Ru(bpy)_3]^{+2}$)ester and PAA bilayers were studied. The 15, 25 and 35 bilayers of PAA/poly($[Ru(bpy)_3]^{+2}$)ester LEDs were fabricated. Current-voltage and light-voltage

plots were generated by following the same method for generating plots of Figure 5.10. Each device was scanned multiple times for only forward bias until the identical curves in the upward and downward scans measured and later, was done for the reverse bias. The light-voltage curves of forward bias and backward bias were shown together in Figure 5.13.

Figure 5.13 shows that the thinner-layer devices worked at lower turn-on and operating voltage. All three devices exhibited reversible current-voltage and light-voltage curves regardless of the thickness of the devices. The thickness-dependent device performance indicates that the insulating PAA layers decrease the charge mobilities in the devices and that higher voltage are needed to recombine charges to make excited states. This spin-cast devices of the poly($[Ru(bpy)_3]^{+2}$)ester did not show the thickness dependent behavior.

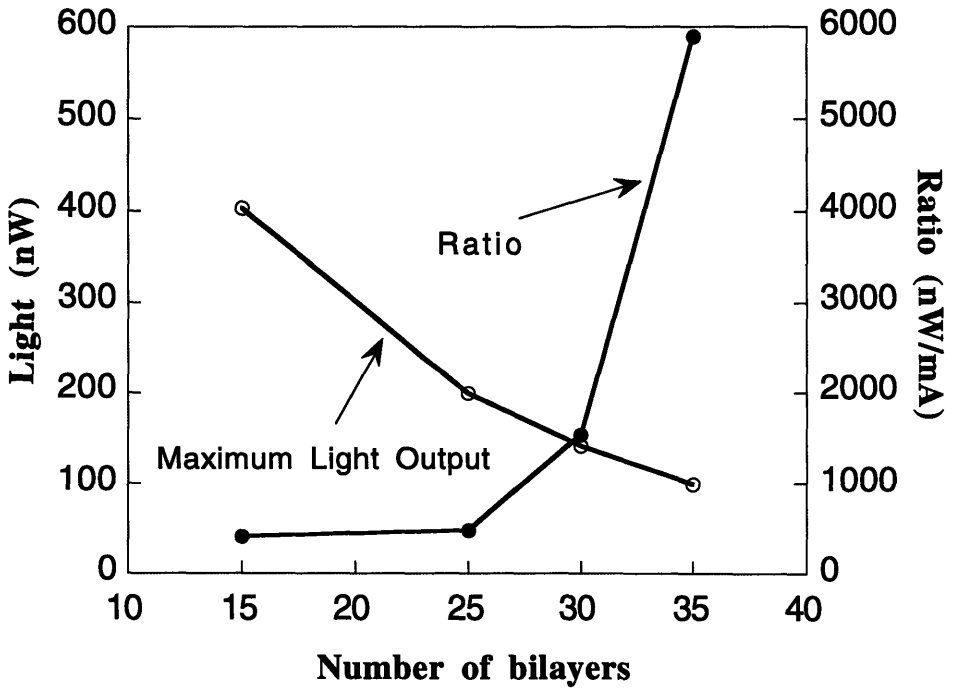

Figure 5.14. Efficiency and maximum light output of 15, 25, 30, 35 bilayers of PAA/poly($[Ru(bpy)_3]^{+2}$)ester devices.

Figure 5.14 displays the maximum light output and light-to-current ratio vs. number of layers. The light-to-current ratio improved about 2 orders of magnitude as the thickness of the device increased from 15 to 35 bilayers, while the maximum light output decreased as the number of layer increased. The PAA layers in the poly($[Ru(bpy)_3]^{+2}$) ester devices successfully lowered the charge mobilities in the system and enhanced the possibility of generating excited states.

4.2. Poly($[Ru(bpy)_3]^{+2}$)ester and Sulfonated poly(styrene) Devices

Fifteen, twenty five, and thirty five bilayers of poly($[Ru(bpy)_3]^{+2}$)ester and poly(sulfonated styrene) (SPS) were fabricated under the same conditions as those used for the poly($[Ru(bpy)_3]^{+2}$)ester/PAA device fabrication. The thickness per bilayer of poly($[Ru(bpy)_3]^{+2}$)ester/SPS was about 25 Å. The poly($[Ru(bpy)_3]^{+2}$)ester/SPS system formed thinner layers and exhibited a lower amount of poly($[Ru(bpy)_3]^{+2}$)ester adsorption in the multilayer film.

Figure 5.15 shows the current-voltage and light-voltage curves of the 25 and 35 bilayers of poly($[Ru(bpy)_3]^{+2}$)ester and SPS devices. The 35-bilayer device also had high turn-on and operating voltages. The thickness dependence of device behavior was also seen in the devices. The quantum efficiency of 35 bilayers of poly($[Ru(bpy)_3]^{+2}$)ester and SPS device was about 0.035% (514 nw/6.5 mA) at 18 V which is lower than that of the poly($[Ru(bpy)_3]^{+2}$)ester/PAA device. However, in the poly($[Ru(bpy)_3]^{+2}$) ester/SPS, it was found that in reverse bias, the devices would not emit light. One of the metal electrodes may work as a quenching site during the operation, because current was still observed at the reverse bias. The 15 bilayers of poly($[Ru(bpy)_3]^{+2}$)ester/SPS exhibited an ohmic behavior. The overall thickness of the 15 bilayer device was about 300 Å, which may be too thin to block some holes in this LED.

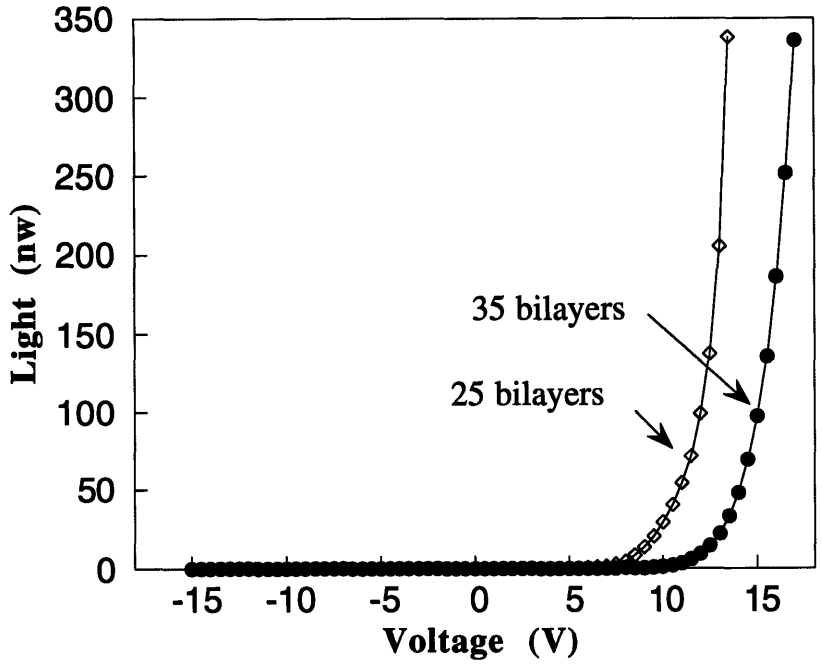

Figure 5.15. Thickness dependence of poly($[Ru(bpy)_3]^{+2}$)ester/SPS multilayer devices.

5. Poly($[Ru(bpy)_3]^{+2}$)ester and Sulfonated $[Ru(phen')_3]^{+2}$ Devices

Thirty, forty, and fifty bilayer films of poly($[Ru(bpy)_3]^{+2}$)ester and $[Ru(phen')_3]^{+2}$ were fabricated on the ITO. By continuous dippings of pH 4.5 of $5 \cdot 10^{-3}$ M of cationic poly($[Ru(bpy)_3]^{+2}$) ester and anionic sulfonated $[Ru(phen')_3]^{+2}$, the totally ruthenium complex based films were fabricated. The thickness-per-bilayer was only 6 Å.

The devices are much thinner than the previous polyelectrolytes and poly($[Ru(bpy)_3]^{+2}$)ester or sulfonated $[Ru(phen')_3]^{+2}$ devices. Ohmic behavior, usually seen with poor film quality, was observed in 30 and 40 bilayer devices. Only 50 bilayers of poly($[Ru(bpy)_3]^{+2}$)ester/$[Ru(phen')_3]^{+2}$ emitted some light at high voltage. Figure 5.16 shows the current-voltage and light-voltage curves of 50 bilayers of poly($[Ru(bpy)_3]^{+2}$)

ester/Ru(phen')$_3^{+2}$ LED. The interesting thing in the device behavior was the high turn-on voltage. Compared with the spin-cast device of Ru polypyridyl complex based emitters, the layer-by-layer deposited Ru-based device required nearly 10 V to start emitting light.

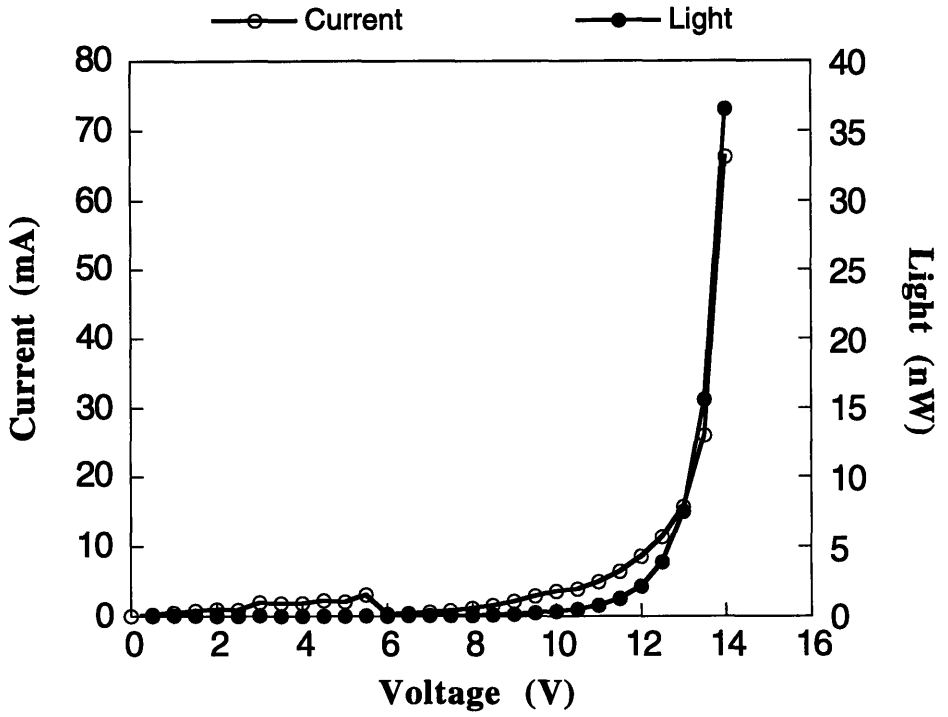

Figure 5.16. Current-voltage and light-voltage curves of poly([Ru(bpy)$_3$]$^{+2}$) ester/[Ru(phen')$_3$]$^{+2}$ LED.

6. Discussion of Ru complexes Based LEDs

ECL cells of the Ru complexes in liquid states have been investigated for many years. Chemical, electrochemical, photochemical stability of Ru complexes attracted much attention as an emitter for ECL cells. Typically, in a solution state, electrogenerated oxidized and reduced forms of the Ru complexes react to form an excited state for light emission. With the help of coreactant in the cell, the generation of the excited states is possible only for the annihilation reaction between the coreactant and either the oxidized or the reduced form.

An ideal solid state ECL device has distinctive features over the conventional organic light emitting devices. (1) The turn-on voltage is independent of film thickness. (2) The turn-on voltage is equal to the band gap of the emitter. (3) The turn-on voltage is independent of electrode metals. (4) The device is operated equally well in forward bias and reverse bias. The main reason of those behavior is that the charge injection of the device is facilitated by charge compensating counterions at the electrodes. Accumulation of couterions at the electrodes lower the charge injection barriers. Once the reduced and oxidized forms are saturated at the electrodes, the two forms react for generating the excited states in the device. I assume that the same excited state of the poly($[Ru(bpy)_3]^{+2}$)ester and the $[Ru(phen')_3]^{+2}$ in a solution state are generated in the solid state devices. The mobility of charge species and the exact mechanism of the generation of excited states in the solid state are still studied in our group.

There are several problems associated with Ru complex solid state ECL devices. According to the literature, the rates of electron hopping in the Ru complexes are not the same for the reduced and oxidized forms [5.51]. Another previous important observation is that the conductive metal electrode (Al electrode) is prone to quench the excited states of the Ru complexes [5.48, 5.52].

In the spin-cast films of the poly($[Ru(bpy)_3]^{+2}$)ester and the sulfonated $[Ru(phen')_3]^{+2}$, the turn-on voltages of the device were independent of the thickness of layer films. The turn-on voltage was in the range of 2.5 - 3.0 V which is close to the band gap of the Ru complexes. At the reverse bias, however, the spin-cast devices did not emit light. This result suggests that the Ru complex, itself, has unbalanced charge transports or does not have sufficient counterion concentration at the electrodes. I think that due to unbalanced transports of the reduced and the oxidized forms, the metal electrode quenched the light emission in the Ru complex materials.

The reversible light emission was observed at the multilayer of PAA/ poly($[Ru(bpy)_3]^{+2}$)ester, although the forward bias generated a slightly better performance.

The turn-on voltage was the same both at the forward and the reverse bias. The efficiency of the multilayer device was much higher than that of spin-cast single layer device. It is believed that the PAA layers in the device helped to balance the transports of the reduced and oxidized forms by decreasing the mobility of the dominant redox form in the system. The high efficiency may be partly due to much improved film quality with the PAA layers. The devices exhibited strong dependence on the thickness of layers. The higher turn-on voltage was required for the thicker layer device. Compared with the ideal solid state ECL, it can be seen that the transportation of charge species was limited by the insulating PAA layers in the system. The SPS/poly($[Ru(bpy)_3]^{+2}$)ester layers exhibited the similar thickness-dependence in the forward bias, while the light emission was quenched at the reverse bias.

The multilayer devices operated at higher voltage than the spin-cast single layer device. Even the turn-on voltage of the only Ru complex based poly($[Ru(bpy)_3]^{+2}$) ester/$Ru(phen')_3^{+2}$ multilayer device was 8 V. The ionic linkage in the multilayer may deter the transport charge species and require high field to generate the excited states of the Ru complexes.

The reversible light emission and the same turn-on voltage of both the forward bias and reverse bias proved the ECL mechanism in the Ru complex devices. However, the ECL process in the Ru complex devices was limited by the charge transport and the counterion transport. The surrounding layers affected those transports and the quenching at electrodes.

7. Conclusion

I have demonstrated that the novel layer-by-layer deposition technique is a viable way to fabricate organic LED films. The technique allows us to control heterostructures of a multilayer and to build up different combinations of materials with molecular-level

control. The Ru polypyridyl complex based LEDs performed differently according to the fabrication conditions. The layer-by-layer deposition technique was proved to form device-quality films and to achieve high efficiency devices.

REFERENCES

[5.1] Holmes, A. B.; Bradley, D. D. C.; Brown, A. R.; Burn, P. L.; Burroughes, J. H.; Friend, R. H.; Greenham, N. C.; Gymer, R. W.; Halliday, D. A.; Jackson, R. W.; Fraft, A.; Martens, J. H. F.; Pichler, K.; Samuel, I. D. W. *Synthetic Metals* **1993**, *55-57*, 4031.

[5.2] Conwells, E. M.; Stolka, M.; Miller, M. R. *Proc. SPIE* **1993**, 1910.

[5.3] Sheats, J. R.; Antoniadis, H.; Hueschen, M.; Leonard, W.; Miller, J.; Moon, R.; Roitman, D.; Stocking, A. *Science* **1996**, *273*, 884.

[5.4] Bradley, D. D. C. *Synth. Met.* **1993**, *54*, 401.

[5.5] Tang, C. W. *Information Display* **1996**, *10*, 16.

[5.6] Friend, R. H.; Bradley, D. D. C.; Holmes, A. B. *Physics Worrld* **1992**, *November*, 42.

[5.7] Service, R. F. *Science* **1996**, *273*, 878.

[5.8] Murayama, R. *Extended Abstracts (The 54th Autumn Meeting) of the Japan Society of Applied Physics*, **1993**, 1127.

[5.9] Bergh, A. A.; Dean, P. J. "Light Emitting Diodes"; Clarendon Press: Oxford, 1976.

[5.10] Saleh, B. E. A.; Teich, M. C. "Fundamentals of Photonics, Chap. 16."; Wiley-Interscience: New York, 1991.

[5.11] Tang, C. W.; VanSlyke, S. A. *Appl. Phys. Lett.* **1987**, *51*, 913.

[5.12] Tang, C. W.; VanSlyke, S. A.; Chen, C. H. *Jpn. J. Appl. Phys.* **1989**, *65*, 3610.

[5.13] Adachi, C.; Tsutsui, T.; Saito, S. *Appl. Phys. Lett.* **1989**, *55*, 1489.

[5.14] Adachi, C.; Tsutsui, T.; Saito, S. *Appl. Phys. Lett.* **1990**, *56*, 799.

[5.15] Adachi, C.; Tsutsui, T.; Saito, S. *Appl. Phys. Lett.* **1990**, *57*, 531.

[5.16] Kido, J.; Hayase, H.; Hongawa, K.; Nagai, K.; Okuyama, K. *Appl. Phys. Lett.* **1994**, *65*, 2124.

[5.17] Kido, J.; Kimura, M.; Nagai, K. *Science* **1995**, *267*, 1332.

[5.18] Burrows, P. E.; Sapochak, L. S.; McCarty, D. M.; Forrest, S. R.; Thompson, M. E. *Appl. Phys. Lett.* **1994**, *64*, 2718.

[5.19] Burrows, P. E., *Appl. Phys. Lett.* **1994**, *65*, 2308.

[5.20] Mori, Y.; Endo, H.; Hayashi, Y. *Oyo Buturi* **1992**, *61*, 1044.

[5.21] Kido, J.; Kohda, M.; Hongawa, K.; Okuyama, K.; Nagai, K. *Appl. Phys. Lett.* **1992**, *61*, 2627.

[5.22] Kido, J. *Appl. Phys. Lett.* **1994**, *64*, 815.

[5.23] Braun, D.; Heeger, A. J. *Appl. Phys. Lett.* **1991**, *58*,1982.

[5.24] Gustafsson, G.; Cao, Y.; Treacy, G. M.; Klavetter, F.; Colaneri, N.; Heeger, A. J. *Nature* **1992**, *357*, 477.

[5.25] Yu, G.; Zhang, C.; Heeger, A. J. *Appl. Phys. Lett.* **1988**, *53*, 195.

[5.26] Burroughes, J. H.; Bradley, D. D. C.; Brown, A. R.; Marks, R. N.; Machary, K.; Friend, R. H.; Burn, P. L.; Holmes, A. B. *Nature* **1990**, *347*, 539.

[5.27] Burn, P. L.; Holmes, A. B.; Kraft, A.; Bradley, D. D. C.; Friend, R. H.; Gymer, R. W. *Nature* **1992**, *356*, 47.

[5.28] Greenham, N. C.; Moratti, S. C.; Bradley, D. D. C.; Friend, R. H.; Holmes, A. B. *Nature* **1993**, *365*, 628.

[5.29] Kim, Y. H.; Kwon, S. K.; Yoo, D. ; Rubner, M. F. *To be submitted.*

[5.30] Zhang, C.; Von Seggern, H.; Krabel, B.; Schmidt, H.-W.; Heeger, A. J. *Synthetic Metals* **1995**, *72*, 185.

[5.31] Parker, I. D. *J. Appl. Phys.* **1994**, *75*, 1656.

[5.32] Egusa, S.; Miura, A.; Gemma, N.; Azuma, M. *Jpn. J. Appl. Phys.* **1994**, *33*, 2741.

[5.33] Brown, A. R.; Bradley, D. D. C.; Burroughes, J. H.; Friend, R. H.; Grrenham, N. C.; Burn, P. L.; Holmes, A. B.; Kraft, A. *Appl. Phys. Lett.* **1992**, *61*, 2793.

[5.34] Saito, S.; Aminaka, E.; Tsutsui, T.; Era, M. *J. Luminescence* **1994**, *60-61*, 902.

[5.35] Era, M.; Adachi, C.; Tsutsui, T.; Saito, S. *Chem. Phys. Lett.* **1991**, *178*, 488.

[5.36] Tsutsi, T.; Aminaka, E-I.; Fujita, Y.; Hamada, T.; Saito, S. **1993**, *55 - 57*, 4157.

[5.37] Naka, S.; Shinno, K.; Okada, H.; Onnagawa, H.; Miyahita, K. *Jpn. J. App. Phys.* **1994**, *33*, L1772.

[5.38] Strukelj, M.; Papadimitrakopoulos, F.; Miller, T. M.; Rothberg, L. J. *Science* **1995**, *267*, 1969.

[5.39] Kido, J.; Ohtake, C.; Hongawa, K.; Okuyama, K.; Nagai, K. *Jpn. J. Appl. Phys.* **1993**, *32*, L918.

[5.40] Fou, A. C.; Onitsuka, O.; Ferreira, M.; Hsieh, B. R.; Rubner, M. F. *J. Appl. Phys.* **1996**, *79*, 1.

[5.41] Lee, J.-K.; Schorock, R. R.; Baigent, D. R.; Friend, R. H. *Macromolecules* **1995**, *28*, 1996.

[5.42] Dehn, H.; Gritzner, G.; Gutmann, V. *Mikrochim. Acta* **1967**, *3*, 422.

[5.43] Peterson, J. D.; Gahan, S. L.; Ramnussen, S. C.; Rondo, S. E. *Coord. Chem. Rev.* **1994**, *132*, 15.

[5.44] Roundhill, D. M. "Photochemistry and Photophysics of Metal Complexes"; Plenum Press: New York, 1994.

[5.45] Miller, C. J.; McCord, P.; Bard, A. J. *J. Am. Chem. Soc.* **1991**, *7*, 2781.

[5.46] Lee, J.-K.; Yoo, D.; Handy, E. S.; Rubner, M. F. *Appl. Phys. Lett.* **1996**, *69*, 1686.

[5.47] Lee, J.-K.; Yoo, D.; Rubner, M. F. *Submitted in Chem. Mater.* **1997**.

[5.48] Lyons, C.; Rubner, M. F. *To be submitted.*

[5.49] Pei, Q.; Yu, G.; Zhang, C.; Yang, Y.; Heeger, A. J. *Science* **1995**, *269*, 1086.

[5.50] Wang, Y. Z.; Gebler, D. D.; Lin, L. B.; Blatchford, J. W.; Jessen, S. W.; Wang, H. L.; Epstein, A. J. *Appl. Phys. Lett.* **1996**, *68*, 894.

[5.51] Chidsey, C. E.; Feldman, B. J.; Lundgren, C.; Murray, R. W. *Anal. Chem.* **1986**, *118*, 601.

[5.52] Zhang, X.; Bard, A. J. *J. Phys. Chem.* **1982**, *104*, 2641.

CHAPTER 6

Conclusion, Summary, and Future Work

This work has shown that sequential layer-by-layer adsorption is a powerful and versatile technique for development of organic thin films. This technique allows us to precisely control the overall thickness and layer structure in a multilayer film. We can design various heterostructures using many functional materials as building blocks. The simplicity of this technique makes it attractive and economical for industrial applications.

During my thesis work, I expanded the technique successfully to include surface modification and fabrication of light emitting devices. I found that pH, ionic strength, and concentration of the dipping solutions generated different bilayer compositions and structures and thereby influenced the performance of the functional multilayer films. I demonstrated that the technique can be used to incorporate various functional materials, from small dye molecules to Ru complexes, into a multilayer film.

In closing, I will briefly summarize the important contribution I have made for this technique.

1. Summary - Surface Modification

It has been shown that the layer-by-layer sequential adsorption technique can modify various surfaces so that they have very different properties. Specific surface characteristics can be added to the heterostructure by controlling the functional groups that are incorporated into the outermost layer. Modified surfaces produced with the bilayer

scheme were quite stable. They maintained their modified surface properties even when immersed in a liquid. For example, completely wettable surfaces were produced with thick layers of PAA and thin layers of PAH. These surface properties were maintained for more than one month.

2. Summary - Control of Layer Structure

The net charge densities of a polyelectrolyte chain and a charged surface are controlled by changing the pH and ionic strength of dipping solutions. When a polyelectrolyte is highly charged, it adsorbed as thin, extended-chain layer structure. However, a polyelectrolyte that is less charged and is screened by high ionic strength, will adsorb in a thick, loopy layer structure. Previous studies using the sequential adsorption technique only discussed the effect of ionic strength on the thickness of an adsorbed layer. I found that the bilayer thickness and composition also can be controlled by the pH of the dipping solutions. In this work, weak polyelectrolytes were used for the first time in multilayer films. Thus, I was able to observe the effect of the solution pH on the structure of the adsorbed layer. A pH of 2.5 for PAA solution formed a thick, loopy layer, while a pH of 4.5 for PAA solution formed a thin, extended chain layer.

The solution pH determined the charge density of an adsorbed weak polyelectrolyte. If a polyelectrolyte in solution has fixed charge density, the amount of adsorption increases with the number of charges on a surface. A pH of 4.5 for the PAH dipping solution enhanced the dissociation of carboxylic acid groups of an adsorbed PAA layer and thereby formed a thick PAH layer.

After measuring incremental thickness of PAH/PAA layers, I concluded that the thickness of an adsorbed layer did not affect the thickness of an additional layer. The condition of the dipping solutions primarily determined the thickness of the additional layer.

3. Summary - Small Dye Multilayer Films

I demonstrated that small dye molecules containing at least two separate charges can be incorporated into multilayer films with polyelectrolyte layers. The structure of an adsorbed polyelectrolyte layer determined the amount of small dye adsorption. Previous researchers assumed that multilayer film build-up was not possible due to the small size of typical dye molecules. Instead of small dye molecules, these groups used the bolaform molecules, which have extended chains. The current work described a unique and a simple way to generate multilayers containing small dye molecules.

4. Summary - Light Emitting Device Fabrication

To my knowledge, this work describes the first attempt to fabricate light emitting devices (LEDs) based on Ru complexes. The Ru complex materials are well known for being very stable electrochemiluminescent (ECL) emitters in a liquid state. The spin-cast films of the sulfonated $[Ru(phen')_3]^{+2}$ and poly($[Ru(bpy)_3]^{+2}$)ester exhibited very bright red emission. The multilayer film of the poly($[Ru(bpy)_3]^{+2}$)ester/PAA produced highly efficient and reversible ECL devices. I demonstrated that the technique can be used successfully to fabricate uniform multilayer films for the Ru complex LEDs with molecular level control.

Future Work

1. Surface Modification

Surface properties play a important role in various applications. Desirable surface properties can be generated using the technique by selecting proper materials for the layers. For example, poly(ethyleneoxide), which has excellent resistance to fouling by protein adsorption, can be applied as an outermost layer. The previous results of our group showed that alternate dipping of poly(aniline) and poly(ethyleneoxide) could produce a

multilayer film. Likewise, we can simply change the materials of the outermost layer to modify the system for biological or chemical applications.

2. Solution pH effects on PAH/PAA Layer

I studied several solution conditions for PAH/PAA multilayer film fabrication. The highly extended chain of the PAA layers was obtained at a pH of 4.5 and the loopy chain layers at a pH of 2.5. By adjusting the pH of PAH and PAA solutions to unexplored values, we can see how bilayer thickness and composition vary with solution pH. The additional data of thickness increments at the different solution pH and ionic strength will help us understand the exact mechanism of polyelectrolyte adsorption.

3. Structure of Layer-by-Layer Deposited Multilayer Films

The contact angle data in chapter 3 showed the layer diffusion occurred in the PAH/PAA films. Layer interdiffusion is an important factor to consider when designing functional multilayer films. Depth profiling through secondary-ion mass spectrometry (SIMS) or x-ray photoelectron spectroscopy (XPS) could possibly be used to determine the level of interdiffusion. For electrical devices, charge transport in multilayer films is affected by the level of bilayer interdiffusion. Recent results of cross-section transmission electron microscopy (TEM) showed the distinct contrast of Ru complex layers in the multilayer films. Thus, TEM can be used as an additional tool for the study.

4. Small Dye Molecules in Multilayer Films

By choosing highly extended chain conformations of a polyelectrolyte, we may increase the alignment of dye molecules in the multilayer films. Once we understand how to orient dye molecules in multilayer films, wide applications for optics may be possible using the layer-by-layer adsorption technique.

By simply adding some charge groups into a functional dye molecule, it may be possible to build up a multilayer film containing the molecule. Thus, charge transport materials, thermochromic materials, and electrochromic materials may be incorporated into a multilayer film.

5. PAA/Poly($[Ru(bpy)_3]^{+2}$)ester Multilayer Light Emitting Devices

I demonstrated that pH, ionic strength, and concentration of dipping solutions affected layer thickness of a multilayer film. I used a single pH of 3.5 for the poly($[Ru(bpy)_3]^{+2}$)ester and PAA solutions for device applications. The device performance can be maximized by controlling the PAA layer contribution to the bilayer composition. It will be interesting to see how much the device performance is modified by changing the bilayer composition of the poly($[Ru(bpy)_3]^{+2}$)ester/PAA system.

6. Mechanism of Ru complexes based Light Emitting Devices

An understanding of charge transport mechanisms and excited state formation in the Ru complex emitters will help us design brighter and more efficient LEDs. I speculated that the mechanism of Ru complex LEDs is based on electrogenerated chemiluminescence. I assumed that the Ru complexes, themselves, have unbalanced charge transport between oxidized and reduced forms and that light emission of Ru complex devices is quenched by a metal electrode (Al). Additional experiments will determine the mechanism underlying the device behaviors.

7. Heterostructure Light Emitting Devices

Heterostructure layers containing hole or electron transport layers enhanced the performance and efficiency of organic LEDs. By inserting hole transport layers or electron transport layers in the Ru complex multilayer films, the efficiency and brightness of the

device will be enhanced. These studies will also help us understand the mechanism of the Ru complex devices.

These are some of the many possible directions for future work.

ACKNOWLEDGMENTS

It has been my good fortune to have worked with, learned from, and enjoyed the companionship of many individuals during my stay at MIT. I would like to take a moment to thank the most immediate few who make my graduate school experience a most valuable one.

First of all, I would like to express sincere thanks to my research supervisor, Prof. Michael Rubner for his guidance, interest, and encouragement not only in regard to the thesis but throughout the various stage of my doctoral program. I also thank my thesis committee, Prof. Edwin Thomas and Prof. Kirk Kolenbrander for their advice and perceptive comments.

Although I can no longer express my thanks, I wish to acknowledge my indebtedness to the late Prof. Wan-Sick Ha, my undergraduate advisor. He provided me with opportunities and experiences that will be invaluable throughout the years. Special thanks also go to Prof. Sangyoung Kim, Prof. Sungil Hong, Prof. Seokwon Ko, Prof. Changkun Choi, and Prof. Wonho Jo for their excellent teaching and encouraging me to study abroad.

There are so many people in the Rubner Research Group who have contributed either directly or indirectly to this thesis. I am thankful to have worked with such as outstanding group of individuals whom I thank for their friendship, support, and assistance. Special thanks to Osamu Onitsuka and Jin-Kye Lee for their constant support and scholarly discussion. I am grateful to Marysilvia Ferreira, Josephine Cheung, Ken Zemach, Augustine Fou, Jeff Baur, Mike Durstock, Erika Abbas, Erik Handy, Aiping Wu and Hedi Mattoussi. Thanks also go to three undergraduates-Sarah O'Connor, Douglas Howie, and Anand Raghunathan-for experimental assistance. I would also like to thank Sandy Schaefer-Ung who has been tremendous supportive in many ways, to me and the entire Research Group.

In addition, there are a number of people from outside of our groups who have helped me through my time here. Special thanks to Janelle Gunther for her kindness and friendship. I am grateful to Byeonghyoek Son, Bashir Dabbousi and Yun-hi Kim for scholarly discussions and fun. Thanks also go to Libby Shaw and Tim McClure for help

with the Central Facilities. I would also like to thank to the 3M company, the NSF, and the MIT center for Materials Science, who provided funding for this work.

My thanks also go to many Korean friends of mine in MIT. Special thanks to member of the MIJI for their kind contributions and discussions. Many friends, within MIT and beyond, have made my stay here an enjoyable one. Heejin, Jaejin, Sanghoon, Sungjin, Taeshin, Seokwon, Ohsung, Youngchang, Hayoung, Sukyoung, Sungwhan, Junbum, Hunwook, Jangsik, Yongchae, Taehwan, Jinsang, Jungsu, and Jaedeok, your friendship I will cherish.

My gratitude must go to my family for their support and belief in me. Special thanks to my parents for their endless love, consistent support, encouragement, and many sacrifices for the last 30 years. How can I ever thank you enough? I am grateful to my sisters, Junghee, Jinhee for their love and belief in me. I would also like to thank the new member of my family: parents-in-law, brother-in-law, Youngseok, and sister-in-law, Jungmo for their kindness. Thanks also go to my grandmother for her constant love. My grandfather not only encouraged me to become a polymer scientist but also inspired me as a respectful mentor. I am thankful to my cousins who stayed in Boston with me, Seungeok, Jungmin, Jaemin, Dongkeun, and Jiwon, for sharing my sorrow and happiness.

Finally, I must thank my wife, Hyunmo for her love and constant support. Without her encouragement and assistance, I could not have finished this thesis. Our four month old son, Ian, encouraged me most during the past three months of writing, although it was hard to manage writing the thesis and taking care of Ian. I hope I could give all my love and support to him as I received from my family. I thank again, my wife for having Ian.

To all these people, as well as to many not mentioned by name, I am profoundly grateful.

To myself I seem to have been only like a boy playing on the seashore, and diverting myself in now and then finding a smoother pebble or a prettier shell than ordinary, whilst the great ocean of truth lay all undiscovered before me.

Issac Newton, English Physicist/Mathematician (1642 - 1727)